Micro-electro-thermo-magnetic Actuators for MEMS Applications

by

Sepehr Forouzanfar

A thesis
presented to the University of Waterloo
in fulfillment of the
thesis requirement for the degree of
Master of Applied Science
in
Systems Design Engineering

Waterloo, Ontario, Canada, 2006

© Sepehr Forouzanfar 2006

I hereby declare that I am the sole author of this thesis. This is a true copy of the thesis, including any required final revisions, as accepted by my examiners.

I understand that my thesis may be made electronically available to the public.

Abstract

This research focuses on developing new techniques and designs for highly controllable microactuating systems with large force-stroke outputs. A fixed-fixed microbeam is the actuating element in the introduced techniques. Either buckling of a microbridge by thermal stress, lateral deflection of a microbridge by electromagnetic force, or combined effects of both can be employed for microactuation. The proposed method here is MicroElectroThermoMagnetic Actuation (METMA), which uses the combined techniques of electrical or electro-thermal driving of a microbridge in the presence of a magnetic field. The electrically controllable magnetic field actuates and controls the electrically or electrothermally driven microstructures. METMA provides control with two electrical inputs, the currents driving the microbridge and the current driving the external magnetic field. This method enables a more controllable actuating system. Different designs of microactuators have been implemented by using MEMS Pro as the design software and MUMPs as the standard MEMS fabrication technology. In these designs, a variety of out-of-plane buckling or displacement of fixed-fixed microbeams have been developed and employed as the actuating elements. This paper also introduces a novel actuating technique for larger displacements that uses a two-layer buckling microbridge actuated by METMA. Heat transfer principles are applied to investigate temperature distribution in a microbeam, electrothermal heating, and the resulting thermoelastic effects. Furthermore, a method for driving microactuators by applying powerful electrical pulses is proposed. The integrated electromagnetic and electrothermal microactuation technique is also studied. A clamped-clamped microbeam carrying electrical current has been modeled and simulated in ANSYS. The simulations include electrothermal, thermoelastic, electromagnetic, and electrothermomagnetic effects. The contributions are highlighted, the results are discussed, the research and design limitations are reported, and future works are proposed.

Acknowledgments

I would like to thank my supervisor, Dr. John Yeow, for his patience, support, and encouragement. I appreciate that he agreed to be my supervisor and allowed me to pursue my research interests. He has effectively spent time on my work, heard my reports, and encouraged me to go forward. I am also grateful to Dr. Eihab M. Abdel-Rahman and Dr. William W. Melek who agreed to be my thesis committee members and review my thesis.

Thanks to my fellow research group members from whom I have received companionship and encouragement. Keith always helped me in solving issues I had with my lab computer including software installation, license requirements, and remote access.

Thanks to Mary McPherson who has taken time to review my thesis and correct my writing.

Dedication

To people who have made significant contributions to civilization and better lives for others, but received nothing in return.

To my father, my mother, and my sister Ashraf.

To my son, Bahman, and my wife, Maria, who patiently tolerated my absence during the time needed for this achievement.

To my friend M. H. Fakhrossae who has always been supportive of me, believed in my capabilities, and encouraged me in my past and present achievements.

Contents

1 Introduction **1**

1.1 Motivation 4

1.2 Research Objectives 5

1.3 Contributions 6

1.4 Outline 7

1.5 Summary 10

2 Literature Review **11**

2.1 Introduction 11

2.2 Scaling Laws and Dimensional Analysis 12

2.3 Thermal, Magnetic, and Thermomagnetic Microactuation 13

2.4 Modeling 16

2.5 Summary 19

3 Microactuation and Scaling Laws **20**

3.1 Introduction 20

3.2 Scaling Laws in Heat Transfer and Thermal Microactuation 23

3.3 Scaling Laws in Elasticity and Strength of Material 27

3.4 Scaling Laws in Magnetic Microactuation 27

3.5 Summary 33

4 Heat Generation and Transfer in a Microbridge **35**
4.1 Introduction 35
4.2 Polysilicon Electrothermal Properties 37
4.3 Steady-state Heat Transfer in a Microbridge 42
4.4 Temperature Distribution in a Microbridge 50
4.5 Summary 53

5 Thermoelastic Actuation **55**
5.1 Introduction 55
5.2 Polysilicon Thermomechanical Properties 57
5.3 Microbridge Deflection Analysis 60
5.4 Thermal Stress and Buckling 63
5.5 Summary 68

6 Magnetoelastic Actuation **69**
6.1 Introduction 69
6.2 Magnetic Force on a Microbridge Carrying an Electrical Current . . 71
6.3 Magnetoelastic Analysis 72
6.4 Driving a Microactuator by Powerful Current Pulses 73
6.5 Summary 74

7 Electro-Thermo-Magnetic Actuation **76**
7.1 Introduction 76
7.2 Thermal Stress and Magnetic Pressure on a Microbridge 77
7.3 Microactuation by a Two-Layer Microbridge 78
7.4 Various Microactuator Designs 80
7.5 Summary 83

8 Results and Discussion **84**
8.1 Introduction . . . 84
8.2 Numerical Computations . . . 85
8.3 Simulations . . . 88
8.4 Discussion . . . 94
8.5 Summary . . . 97

9 Conclusions and Future Works **99**
9.1 Introduction . . . 99
9.2 Contributions . . . 100
9.3 The Limitations in this Research . . . 102
9.4 Future Work . . . 104

Appendices **117**

A **117**
A.1 Derivation of Heat Equation Discussed in Section 4.2 . . . 117
A.2 Designs of Microactuators without a Buckling Microbridge as the Actuating Element . . . 118
A.3 A Typical PolyMUMPs Fabrication Process . . . 119

B **127**
B.1 Animated Simulations in ANSYS, Discussed in Section 8.2 . . . 127

List of Tables

3.1 Scaling Factors for Heat Dissipation 26

3.2 Scaling Factors for Heat Generation and Thermal Capacity 27

3.3 Comparison of Scaled Magnetic and Electrostatic Forces 33

4.1 Parameters in Equation 4.3 for Resistivity of Polysilicon [1], [2] . . . 38

4.2 Single Crystal Silicon Thermal Expansion over Temperature [1] . . . 41

4.3 Electrothermal Specifications of Heavily-Doped Polysilicon 41

4.4 Typical Values of Convective Heat Transfer Coefficient h 49

4.5 Convective Coefficients h for an Infinite Flat Plate at Different Temperatures 50

5.1 Selected Typical Polysilicon Mechanical Properties 60

7.1 Driving Signals for the Micromotor Shown in Figure 7.5 82

8.1 Amplitudes and Loads in the Microbridge in Assumed Average Temperatures Computed from equations 8.9 and 8.10 88

8.2 Maximum Temperature, Displacement, and Force in a Simulated Buckling Microbridge, Actuated Electrothermally 90

List of Figures

4.1 Silicon-Polysilicon Specific Heat Variations over Temperature [1] . . 40

4.2 Resistivity and Thermal Conductivity in MUMPS polysilicon [1], [3] . 42

4.3 Silicon Thermal Expansion Coefficient over Temperature [4], [5] . . . 43

4.4 Microbridge, Joule Effect Heating, and Heat Transfer Modes 44

5.1 Buckling Microbridge Experiences, P, Thermally-induced Axial Force. 61

6.1 A Microbridge Experiences, $q(x)$, Lateral Magnetic Pressure. 72

7.1 Microbridge Experiences Lateral Magnetic Pressure, $q(x)$, and Axial Thermally Induced Load, P 77

7.2 Two-Layer Out-Of-Plane Moving Clamped-Clamped Microbeam . . 79

7.3 One-Degree-of-Freedom (DOF), In-plane Linear Microactuator . . . 80

7.4 Two-DOF, In-plane and Out-Of-Plane, Linear Microactuator 81

7.5 High Torque Bi-directional Multi-turn Micromotor 82

8.1 Displacement of an Electrothermally Actuated Microbridge 89

8.2 Temperature over an Electrothermally Actuated Microbridge 90

8.3 Microbridge Actuated by an Electromagnet Pressure, $IB = -0.0353\ \frac{\mu N}{\mu m}$ 91

8.4 Microbridge Actuated by an Electromagnet Pressure, $IB = -0.137\ \frac{\mu N}{\mu m}$ 92

8.5 Thermomagnetical Actuation at $T_{max} = 445\ ^{\circ}K$ and $IB = 0.001\ \frac{\mu N}{\mu m}$ 93

8.6 Electrothermally Actuated Microbridge at $(T_{max} = 445\ ^{\circ}K)$ 94

8.7 Bimorph Thermal Actuator at $T_{max} = 935.8\ ^{\circ}C$ (ANSYS Tutorial) . 96

A.1 Limited-Angle Rotating Actuator, ±45°, by EFAB Technology . . . 118
A.2 PolyMUMPs Fabrication Process 121
A.3 PolyMUMPs Fabrication Process, Step 1 to Step 4 122
A.4 PolyMUMPs Fabrication Process, Step 5 to Step 8 123
A.5 PolyMUMPs Fabrication Process, Step 9 to Step 11 124
A.6 PolyMUMPs Fabrication Process, Step 12 to Step 14 125
A.7 Part of a Microactuator Design Used to Show the PolyMUMPs Fabrication Process Outlined in Figures, A.2, A.3, A.4, A.5, and A.6 . . 126

Chapter 1

Introduction

The success of MEMS applications in a few commercialized products have confirmed their potential and encouraged people to have high expectations of these miniaturized electromechanical systems. Microelectromechanical systems may be expected to offer the same capabilities as do their macroscale counterparts. However, some familiarity with these micromachines enables one to recognize the extensive limitations that exist in building MEMS. The fabrication limitations create corresponding constraints and rules in a microsystem design. Research on the proposed microactuating technique, METMA, the focus of this thesis, concerns using a microbridge as the actuating element being actuated thermally, magnetically, or thermomagnetically. A microbridge is also called a fixed-fixed, clamped-clamped, both-ends fixed, or fixed-ends microbeam. The motivation for this current research will be better understood after a review of MEMS' landmarks, existing possibilities, limitations, and potential, which are discussed in this chapter.

No independent beginning for MEMS is recognizable if one looks for the foundations that MEMS development is based on. The primary structural material, silicon, and the fabrication process, Surface Micromachining, have their roots in the development of the semiconductor industry, which is still facilitating MEMS advances. The difference is that in the semiconductor industry, the electrical properties of silicon are dominant factors, but the mechanical properties of the structural material are more important in MEMS. Some historical reviews consider the development of Radar and of pure semiconductors in the 1940s, and the famous lecture by Richard P. Feynman, "There's plenty of room at the bottom," in 1959, as the initiating events [6]. After the invention of the planar bath-fabrication process in 1960, a resonant gate transistor was the first bath-fabricated MEMS device produced by Nathanson and his team at Westinghouse in 1964, five years after Feynman's fa-

mous lecture. The developing semiconductor industry has had an essential role in MEMS birth and development. Researchers at Stanford University introduced the first micromachined accelerometer in 1979. The technique of polysilicon surface micromachining was proposed at the University of California, Berkeley, in 1984. The improvements in microscopes and associated technologies, which occurred in the meantime, facilitated the advancement. In the early 2000s, a number of MEMS devices were mass produced and successfully commercialized. Governments in some countries began to raise funds for research supporting development processes.

MEMS fabrication technologies enable people to manufacture mechanical components, the sizes of which are fractions of a human hair's diameter. The possibilities include microfabrication of simple gears, motors, pumps, and integrated components of limited complexity. Depending on the type of microfabrication technology, the manufacturing possibilities are dramatically different. The minimum feature size, the distance between two features, the structural material(s), and/or the number of layers is variable from one technology to another one. The projects achievable in MEMS do not depend only on fabrication, but also on design facilities, modeling, simulation, post assembly, packaging, and experimental tools for testing after fabrication. From the system-engineering point of view, the integration of semiconductor sensing, driving, and controlling elements, along with micromechanical components on the same platform, are important potential in MEMS. This integration is achievable because both technologies, MEMS fabrication and the semiconductor industry, use the same structural material, allowing these two groups of components to be manufactured on the same platform. This valuable advantage provided by MEMS is not seen to such an extent in macroscale systems. Microactuation is also highly attractive because, for example, it can be used as a tool to manipulate nano-dimensional components. Zho et al. have investigated a MEMS-based material testing system designed for nano-objects to be used in Nano-scale tensile testing [7]. Using a MEMS-based system as a measuring, manipulating, or interfacing tool for Nano-scale devices has been of interest to many researchers [8], [9].

Miniaturization of complicated electromechanical systems would require development in both fabrication technologies and microactuation techniques. Fabrication limitations impose direct constraints on MEMS design. For example, minimum feature size and minimum distance between features are two important design rules in a given microfabrication technology. In the design of gear teeth with minimum backlash, these design rules are determining factors. These minimums dictate positional accuracy of a microsystem using these microgears. In fact, the obtainable positional accuracy is very much lower than the relative accuracy in a similar

macroscale system. As another example, in a microfabrication technology, the number of layers that can be fabricated determines whether or not a designer can develop moving joints. For instance, there are only two structural layers that can be used for designing moving components in PolyMUMPs. Design of any moving joints would require at least three such structural layers, which are the minimum required to pivot two in-plane moving arms. Design and fabrication of moving arms are important elements in developing more complex microactuating systems, large-stroke-force microactuators, motion conversion from rotary to linear, or vice versa, and consequently, more functionalities for MEMS. In general, two categories of microfabrication technologies can be considered: the non-standard-customizable technique and standard technique. The customizable methods usually allow some limited modifications in the thickness, structural material, number of layers, and/or fabrication process. Customizable techniques require more time and cost, and are not usually mass producible; however, customizable fabrication techniques allow researchers to adjust the fabrication parameters for the product to be closer to their needs. The standard techniques, including PolyMUMPs, MetalMUMPs, SUMMIT, and EFAB, require extra mandatory design rules. These techniques usually offer fixed parameters, layer thickness, the number of layers, the structural material(s), and the process. In comparison to macroscale, the above–mentioned limitations impose considerable constraints on the development of microscale electromechanical systems. Supported by many years of experience and varieties of methods in fabrication, macroscale electromechanical systems are more widely used and easier and faster to manufacture, and their small– to medium–scale mass production are relatively cheaper. In fact, with the existing capacities in microfabrication, design and fabrication of simple microsystems or microsystems with very limited complexity is achievable. With the above–mentioned difficulties and high cost of microfabrication in general, miniaturization of elctromechanical systems is justified only if it offers added values not provided in a larger-scale solution.

However, being efficient and lacking complexity are not always the most important requirements for a system. MEMS shows a very promising future because there are crucially important applications in which efficiency and complexity of the employed component are not serious issues. Analog Device's MEMS accelerometer was successfully commercialized and used in an automobile airbag system. This MEMS product does not have a high degree of complexity. Its low cost, small size, mass scale manufacturability, and reliability are its benefits for the application. However, developing MEMS fabrication technologies and improving facilities for the design of complex multi-degree-of-freedom microactuators will advance MEMS applications, addressing more needs with these miniaturized systems. In other words, sophisticated microelectromechanical systems can satisfy many more human needs.

Transferring data, taking samples, sensing physical or chemical phenomena, and manipulation in microscale are typical of very attractive potential applications. It is quite reasonable to believe that microsystems can reach a level of sophistication to enable people to acquire data and samples from places that are non-accessible to existing macroscopic tools. For example, the main requirement for medical devices operating inside human bodies is being less invasive, with less volume and smaller cross sectional areas for the operating tool. Area and volume both decrease favorably in microdomain, proportional to the inverse of square and cubic of the length scale respectively. The latest MEMS applications in biomedical products have confirmed the effectiveness of using MEMS in this field. Some catheter heads have been developed to gather data such as video, audio, or electrical signals from inside the human body, and to take samples from the environment. To improve functionality by using conventional technologies, the devices' cross-sections and volumes must be increased, making the devices more invasive. The possibilities of developing MEMS for these and similar applications seems very promising. Although ways of addressing these expectations are at present limited, there is no limitation for the imagination: in the *Fantastic Voyage,*written by Isaac Asimov, a submarine is shrunken to the size of a few hundred micrometers and injected into a human body for microsurgery.

1.1 Motivation

Research shows that MEMS-based applications are not being widely developed, and there is a discrepancy between expectations for these microsystems and reported achievements. Comparison of the two confirms that microelectromechanicalsystems and their applications will not effectively progress unless both more capable microfabrication technologies and enhanced performance microactuators are introduced. This section discusses the costs of not developing high performance microactuating systems, the benefits for introducing microactuator designs achievable with existing fabrication technologies, and the potential rewards for suggesting designs that can be used in a system or in a product for an application.

What is the cost of not developing high performance microactuating systems? Rate gyros, for example, are one of the recently developed applications of MEMS that have been commercialized on a large scale. By comparison, conventional gyroscopes are massive, expensive, and too big for most applications. Furthermore, many growing needs in biomedical, aerospace, defense, and even consumer markets require solutions that are not provided by conventional methods: less invasive instruments for biomedical applications; small size, light weight, and low power

consumption solutions for aerospace; highly reliable, small size components (sensing and actuating elements) for defense applications; low cost and mass producible items for the consumer market. Lack of development in high performance microactuating systems means not having solutions to satisfy these needs.

Developing microactuator designs is significantly affected by mandatory design rules and constraints that are the requirements of current fabrication technologies. However, introducing microactuator designs achievable with existing fabrication technologies is beneficial to many parties. The direct benefit is to MEMS itself. New applications and markets for MEMS can advance the involved industries, motivating researchers to work on fabrication technologies that have more capabilities. The more flexible fabrication technologies become, the greater the potential for further MEMS applications. In addition, new designs for high performance microactuating systems will create more options for researchers to address existing needs. Upon developing MEMS products, even by using current fabrication technologies, researchers can receive feedback from end users on the strengths and weaknesses of the microsystems. Market response to a newly developed product facilitates the improvement of future products. Such benefits are rarely received if a product is developed and evaluated only in a research environment.

Finally, a design introduced in MEMS will be more attractive if its utility is demonstrated in an application. Even from the very beginning, incorporating a developed technique in a system to show its utility will facilitate its further developments. Therefore, in this thesis research, not only has METMA, a capable microactuating technique, been proposed, but also various designs to demonstrate potential applications, which can motivate interested parties to support future research: linear in-plane, linear in-plane and out-of-plane microactuators, and multi-turn, bi-directional micromotors.

1.2 Research Objectives

- *Deriving scaling laws*
  Derivation of scaling laws is part of this research to provide a tool for predicting a microactuating system's behavior. Scaling laws will also enable one to identify the optimized conditions for creating and employing a microactuation technique, and therefore has also application in adjusting the design parameters.

- *Proposing a high performance microactuating technique, METMA, for MEMS*
  As mentioned earlier, MEMS development depends on both more capable

fabricating technologies and high performance microactuating systems. Developing high performance microactuating systems with a large stroke-force and high degree of controllability is the objective in this research.

- *Modeling a microbridge actuated by METMA*
  The modeling of the actuating element, a microbridge, which is driven by METMA, is intended to formulate the effects of the physical *dimensions* involved in creating force and motion: heat transfer and temperature distribution, thermoelastic behavior of the structural material, magnetic force created by the interaction of a magnetic field and the current in the conducting microstructure, and the combined effects of thermomagnetic forces. The result is an integrated model to represent the microactuating element and its functionality when it is actuated by METMA.

- *Introducing new designs of microactuators by using METMA*
  The proposed microactuating technique, METMA, is applied to develop various designs of microactuating systems, which is also a demonstration of the utility and potential of METMA for MEMS applications.

1.3 Contributions

The research in this thesis generally contributes to the field of microactuating mechanisms and systems in order to advance science and technology of MEMS. However, the most significant specific contributions are listed below, with the emphasis on incorporating novelty, uniqueness, and utility.

- Proposes a technique, METMA, to use out-of-plane buckling or displacement of a single-layer fixed-fixed microbeam as the actuating element being driven electrothermomagnetically

- Initiates and introduces a new series of highly controllable and large stroke-force microactuators by using METMA as the microactuating technique and microbridges as the actuating element: in-plane and out-of-plane single-degree-of-freedom linear microactuator; two-degree-of-freedom linear microactuator, in-plane and out-of-plane; bidirectional, multi-turn, and high torque micromotors

- Introduces a design of a two-layer fixed-fixed microbeam as an actuating element to produce larger stroke-force in comparison to a single-layer fixed-fixed microbeam

- Introduces a unique electrical driving method for generating large force or torque peaks in magnetic and thermomagnetic microactuation by applying powerful current pulses
- Electrothermally, thermoelastically, electromagnetically, and electrothermomagnetically analyses and models a microbridge actuated by METMA
- Simulates in ANSYS the introduced technique actuated electrothermally, electromagnetically, and electrothermomagnetically
- Effectively applies dimensional analysis in deriving scaling laws, illuminating the aspects of the physical effects involved
- Highlights potentials of magnetic microactuation by displaying favorable scaled features
  Developing and applying scaling laws on magnetic microactuation show proper conditions for optimized application of magnetic techniques. This work suggests ways for researchers to take advantage of magnetic microactuation, including low voltage driving and higher output forces in comparison with electrostatic methods
- Recognizes unclear aspects of analysis and modeling in a few prior works and suggests corrections (Sections 4.3 and 9.2)

1.4 Outline

Chapter 2, **Literature Review**, surveys prior achievements to recognize the background and related works, to highlight relevant prior contributions, to avoid repetition, and to base new contributions on previous works. Some publications are referred to that are not specifically about MEMS; however, they are included to provide a solid foundation for his work in the fields of science and engineering related to this research: advanced mathematics, elasticity, heat transfer principles and thermodynamics, electromagnetic, and static. In fact, research on this multidisciplinary topic, MEMS, requires extensive investigations that are relevant to the above-mentioned fields. However, this literature review may not include some other valuable resources that have inevitably been omitted because they did not fit within the context or could not be found at all because of the limitations of the investigation method, research tools, or time available.

In Chapter 3, **Scaling Laws and Microactuation**, the focus is on dimensional analysis and scaled physical phenomena. One of the important applications of

dimensional analysis is to investigate how physical phenomena are related in two *similar* systems. Predicting the behavior of a *non-accessible or not yet existing* system is usually investigated by measuring the involved physical *quantities* on a model of the actual system, which is called a prototype or just simply an actual system. Scaling laws are the relationships between different physical phenomena in a prototype and its model representing two similar systems. Because each physical *dimension* in these two similar systems has its own unique relationship, scaling laws are crucially important for identifying these unique relationships that reflect the effectiveness of each *dimension* in a scaled system. The risks of not knowing scaling laws, important terms in scaling laws, methods in deriving scaling laws, and the utility of scaling laws in design and research on MEMS are discussed in this chapter. Furthermore, the specific related physical *quantities* involved in the proposed microactuating technique, METMA, are investigated for deriving scaling laws. These *quantities* include heat transfer and thermal actuation, elasticity and strength of material, and magnetic actuation.

In Chapters 4, **Heat Generation and Transfer in a Microbeam**, heat transfer principles and the electrothermal response of a fixed-fixed microbeam are investigated. In modeling heat transfer, there are requirements for making some assumptions, identifying the dominant terms in heat loss, for example. Recognition of these dominant terms facilitates finding negligible terms in heat transfer, which simplifies modeling. However, challenges in making such assumptions and the consequences on derived results must be studied. These studies are needed to develop a model, a relationship between input electrical current and the temperature distribution over the microbeam. Obtaining knowledge about temperature distribution in the microbeam enables the researcher to predict thermoelastic behavior of the microbridge, which is the topic of the next chapter.

In Chapter 5, **Thermoelastic Actuation**, the induced stress is computed by applying the temperature distribution derived for a fixed-fixed microbeam from the previous chapter. However, a complete analysis of this multi-physical domain problem requires some independent analyses included in this chapter. The mechanical properties of the structural material, i.e., polysilicon, for example, are reviewed. Linear and non-linear equations for microbridge deflection are derived, which are fundamental discussions in elasticity for small and large deflections. The thermal effects on the microbeam must be taken into account where microbridge buckling is investigated. The complete beam's curve equation is derived by applying boundary conditions under steady-state operation.

Chapter 6, **Magnetoelastic Actuation**, implements an analysis on pure electromagnetic microactuation. Formulating the interaction of an external magnetic

field with a current carrying microbeam, the electromagnetic force is computed. Depicted in figure 6.1, for a constant magnetic field perpendicular to the microbeam, given that the current in the microbridge is constant, the relationship for magnetic pressure on the microbridge is derived. It is shown that the acting magnetic force under given conditions is similar to a constant lateral pressure without any axial component. The general equation for a fixed-fixed microbeam deflection under a lateral magnetic pressure is discussed and formulated based on the assumption that the current in the microbeam does not create significant thermal stress. Applying the boundary conditions results in the complete relationship for microbridge deflection. Furthermore, a technique for generating powerful peak forces and torques using electromagnetic actuation is proposed. Deriving an equation representing a relationship between input electrical current and output force-displacement is the ultimate goal in modeling a pure electromagnetic actuation.

Chapter 7, **Electrothermomagnetic Microactuation**, investigates the conditions in which an electrical current in the microbeam is large enough to produce stress as discussed in Chapter 5. However, unlike in Chapter 5, an external magnetic field is also present and interacting with the electrical current as discussed in Chapter 6. Therefore, the analysis in this Chapter is an integration of the discussions in Chapters 5 and 6. It is further shown that the induced thermal stress, which is acting on the microbeam axially, and the magnetic pressure, which is operating on the microbeam laterally, do not produce their effects independently. For example, the lateral force by an external magnetic field dramatically changes the buckling conditions in comparison with the conditions in which thermally induced stress is the only cause of buckling. Therefore, electrothermomagnetic actuation provides a more controllable large-force-stroke actuating technique. Applying the proposed technique, METMA, various designs of microactuating systems are developed and introduced.

Chapter 8, **Results and Evaluation**, reports analytical solutions and simulation results. Tables and graphs show the results and demonstrate a comparison of computed values from the mathematical models and results obtained in simulations. The designed microactuators are evaluated for their functionalities and compared with a conventional design, a bimorph type, for example. The results are discussed and evaluated. The discrepancy between the computed data and simulation results is explained, and the need for further experiments in future work is emphasized.

Chapter 9, **Conclusions and Future Works**, provides a summary and the concluding points of the chapters of this thesis. The contributions are highlighted, and the limitations of the method and analysis and simulations are discussed. Finally, future plans are outlined.

1.5 Summary

This research is an investigation of a proposed microactuating technique, METMA, which is applicable in the design of microactuators and development of MEMS applications. Highlighting the necessity and motivation for this research, this chapter outlines the costs of not developing MEMS applications. The need to advance MEMS research and to develop high-performance microactuating techniques and more capable fabrication technologies is explained. Research objectives are described, which include deriving and applying scaling laws, modeling microactuators, and developing various microactuator designs by employing METMA. The contributions are listed to give a preview of achievements in this research. Finally, the contents of the chapters are outlined in section 1.4.

Chapter 2

Literature Review

2.1 Introduction

This literature review illuminates the background of this research on the proposed microactuating technique, METMA, focusing on two almost independent areas: the first area includes achievements on thermal, magnetic, and thermomagnetic microactuations; the second area covers prior works on a microbridge, which is used as an actuating element for thermomagnetic microactuation in this work. In the latter area, previous achievements in identifying, analyzing, and modeling of physical effects involved in METMA are introduced. A review of scaling laws is given in Section 2.2. The extent of prior works in thermal, magnetic, and thermomagnetic microactuation, and in multi-disciplinary fields related to buckling or out-of-plane displacement of a microbridge are introduced in Sections 2.3 and 2.4.

In Section 2.3, relevant works prior to METMA, which include achievements in thermal, magnetic, and thermomagnetic microactuators, are highlighted. This information is provided to facilitate recognition of the unique features and contributions in this present work. In comparison, thermal microactuators have been of rather more interest to researchers than magnetic microactuators, and integrated thermomagnetic microactuators have been the topic of research in relatively few of previous works. The samples of past achievements relevant to METMA provided in this literature review do not necessarily show the most important ones; however, the objective here is to demonstrate the area and the range of options that have drawn attention.

Microbridges have been the topic of research in a variety of different applications such as the microheaters for bubble creation used in ink jet printers, micro-

lamps, and Radio frequency (Rf) micro-switches. Requirements in such different applications motivated researchers to investigate microbridges. For example, heat transfer and temperature distribution in microbridges, and analysis of fixed-fixed microbeam deflections. The publications are significant in number and variety; their extent ranges from PhD and Master theses, which are specifically focused on microbridges, to papers and books, parts or chapters of which are devoted to microbridge analysis. Section 2.4 reviews prior works on the physical effects involved in the application of a microbridge as the actuating element in METMA such as electrothermal behavior and thermoelastic effects.

Thermal effects in a microbridge have been investigated in a number of previous works for various applications. For example, a fixed-fixed microbeam is a sensing element in the sensitive flow meters that are used in medical devices and environments. This sensitive application requires a very reliable functioning component. The study of thermal effects is a requirement for formulating the behavior of the microbeam in such an application. A significant number of publications also report studies on various other topics, the results of which are applicable in the thermal analysis of a microbridge. One example is the study of the properties of structural materials that are used in the fabrication of a fixed-fixed microbeam. Formulated electrothermal behavior of the material is the essential part in the modeling of a microbridge. Elastic deformation of a microbridge as a MEMS component has also been studied for various applications such as Rf micro-switches. Elastic deformation of a microbridge by heat effects or the microbridge's thermoelastic behavior is included in the analyses in this research and is supported by a large number of publications. In Section 2.4, previous works on modeling and analysis of physical phenomena relevant to METMA are reviewed.

2.2 Scaling Laws and Dimensional Analysis

It is well known that Trimmer, in his paper, "Microrobots and Micromechanical Systems," published in 1989, was the person who developed the idea of using scaling laws to evaluate how physical phenomena are scaled when the dimension of a system is scaled down [10]. In his work, Trimmer introduces a column or a single-column matrix to display the scaling laws. Trimmer's work has been used and referenced by a number of researchers including Madou in *Fundamentals of Microfabrication* [11], [12], Cugat et al. in "Magnetic Micro-Actuators and Systems MAGMAS" [13], [14], Sarkar [15], in his Master thesis, and Hsu in *Mechanics of Microelectromechanical Systems* [16]. There are also published works that use the same concepts mentioned by Trimmer without referencing Trimmer's work, for example, Elwenspoek and

Wiegerink in *Mechanical Microsensors* [17], Liu and Bar-Cohen [18], in "Scaling Laws of Microactuators and Potential Applications of Electroactive Polymers in MEMS," Beeby et al. in *MEMS Mechanical Sensors* [19]. However, although Trimmer's work has provided a straightforward reference for researchers who have used it, Trimmer's scaling laws are basically the same concept that has been developed and used by many mathematicians and researcher under the same and different names [20], [21], [22], [23], [24].

Scaling laws are one of the direct consequences of dimensional analysis and non-dimensionalization. Further to dimensional analysis and non-dimensionalization techniques, other analytical methods have also been developed and applied to derive scaling laws. For example, a physical quantity and the equation representing its relationship with other physical quantities are considered. Then a scale factor for each of the quantities in the relationship is inserted. The simplified equation results in a scaling law for that interested quantity. These methods are discussed further in Chapter 3. Lin and Segel, in their book, *Mathematics Applied to Deterministic Problems in the Natural Sciences*, employ examples to convey the concept [20]. Numerous books contribute to the application of this concept of using dimensional analysis techniques to derive and apply scaling laws [21], [22], [23], [24].

2.3 Thermal, Magnetic, and Thermomagnetic Microactuation

Favorably scaled thermal properties of matter in a microdomain have made thermal actuation a very attractive method in microactuation. Therefore, numerous publications report investigations on thermal microactuators. Magnetic microactuating techniques have not received the same attention as thermal microactuation; however, there are still a significant number of papers published about magnetic microactuation. A few published works on thermomagnetic effects are also available. This literature review includes selected relevant works on thermal, magnetic, and thermomagnetic microactuation.

Deladi et al. have proposed a couple of out-of-plane buckling microbridges that operate in coordination with each other [25]. The midpoints of two buckling microbeams, which are actuated electrothermally, are joined by a third microbeam, the tip of which can have an out–of–plane motion depending on the status of the two buckling microbeams. Szyszkowski et al. have reported research on modeling and simulation of an electro-thermally driven cascaded microactuator made of Nickel, with a peak force output of about $1420 \mu N$ [26]. In general, three types

of thermal microactuators are well known: cascaded fixed-fixed microbeams with in-plane displacements, V-shaped, and Bimorph. Each of these thermal microactuators has been investigated and used by a number of researchers. Lott et al. have worked on modeling the thermal behavior of an array of cascaded–in–plane fixed-fixed straight microbeams [27]. This group of beams buckles in plane when heated. The V-shaped microactuators are interesting for their larger output force. These microactuators have usually been developed in an array of cascaded-in-plane moving microbridges [28]. The difference between the V-shape and previous straight type is that V-shapes do not require that the phenomenon of buckling occurs in order for the microactuator to create displacement, but straight-types do require it. The Bimorph microactuators have been developed in various configurations [29], [30], [31], [32], [1], [33]. Simple operating principles, low force output, and the curved-path of the moving tip are the common specifications of the Bimorph microactuators. There are also other types of thermal microactuators using features of both Bimorph and in-plane buckling microbeams [34]. Hill et al. have proposed a design for a cascaded thermal microactuator [35]. Michal et al. have studied an initially buckled bi-layer microbridge [36]. The initial buckling is induced by residual stress in fabrication. The interesting point mentioned in the paper is that the clamped-clamped microbridge does not snap at all. The reason given is that a clamped-clamped microbeam has infinite rotational stiffness at both its ends, while the rotational stiffness of a pinned-pinned beam is zero, but for a microbeam to snap, there must be a minimum of rotational stiffness.

A study of the publications introducing microactuation techniques shows that magnetic microactuation has received less attention than electrostatic methods. This fact implies that electrostatic microactuation has been considered a more advantageous technique. However, there are people who believe that magnetic microactuation is not less effective, and that it is even more capable than electrostatic techniques. Some investigators have recognized the confusion and conducted research to find the truth. Busch-Vishniac in his paper, "The case for magnetically driven micro-actuators," has compared electromagnetic microactuation to electrostatic techniques [37]. He has shown that not only is electrostatic microactuation not more advantageous than electromagnetic microactuation, but that the opposite in some conditions is true. In Chapter 3 of this present paper, the analysis of scaling laws shows the advantages and more favorable potentials of electromagnetic microactuation techniques. Holzer et al. have proposed various out-of-plane microbeams to be used as magnetic actuating elements [38]. Their work includes suggestions on using fixed-fixed microbeams and U-shaped-fixed-ends as well. Ko et al. [39], and Han et al. [40], have reported design and optimization of a laterally-driven electromagnetic microactuator respectively. The papers report a large deflection

that is continually increasing to a value of about 15 microns, but which suddenly snaps to a maximum of 60 microns. The magnetic field is supplied by an external permanent magnet placed beneath the substrate. However, no measurement has been reported for output force. Nami et al. have analyzed magnetic actuation in microscale and proposed an energy-based criterion for optimizing magnetic force in microscale [41]. Miller et al. have reported their work on applying an external magnetic field on a permalloy layer deposited on the substrate of a scanner mirror [42]. The work also notes the effect of an external magnetic field on a 30-turn copper wire. Yi and Liu [43], Miller et al. [42], and Judy et al. [44], [45], have detailed the effects of applying an external magnetic field on a permalloy deposited layer for microactuation. Their experiment results show that the magnetization in the magnetic material is proportional to the volume of the deposited material. Nemirovsky et al. have proposed a methodology and an analysis for the Pull-In parameters of magnetostatic microactuators, which are similar to the Pull-In effect found in using electrostatic techniques [46].

Guckel et al., in their work “Thermo-Magnetic Metal Flexure Actuators,” have proposed a thermomagnetic technique for RF switches and other microactuating applications [47]. The proposed technique was developed in deep x-ray lithography and high aspect ratio fabrication technology. Due to the design’s similarity to the design of Bimorph thermal microactuators, the proposed technique produces force as low as bimorph thermal microactuators. However, regarding the time, 1992, at which the actuating technique was proposed, the work has been an effective contribution to the developing field of microactuation. Cao et al. have outlined the result of their work on a bi-directional microactuator driven by a combination of electrothermal and electromagnetic methods [48]. Their analysis is limited to the application of a lorentz force to control the direction in which buckling occurs. Bahreyni and Shafai have used the interaction between an external magnetic field and an electrical current in a fixed-ends beam to develop a very sensitive magnetic sensor [49]. In their work, they consider both pure magnetic and thermomagnetic effects.

A literature review on thermal, magnetic, and thermomagnetic microactuators shows a significant growth in the number of relevant publications within recent years. As mentioned above, thermal microactuators are the topic in most of these publications. Nevertheless, works on magnetic microactuation are also appreciable in number and variety. A few works on thermomagnetic microactuation show that researchers have also paid attention to this technique in some prior works. However, using a buckling microbridge as the actuating element to be actuated electrothermally, electromagnetically, and/or electrothermomagnetically is the spe-

cific features of this present paper's research.

2.4 Modeling

Modeling of a buckling microbridge in the proposed microactuation technique, METMA, is an integration of the models of various physical effects. Each of these effects involved has been the topic of independent investigations. Selected works in this broad range of investigations are introduced to illuminate the background. Previous works on heat transfer, temperature distribution, and modeling thermal behavior of microbridges show a variety of approaches, techniques of analysis, and results. The rich literature on these topics includes specific works on modeling microbridges for different applications. However, the reference books and publications in relevant disciplines, i.e., heat transfer, elasticity, thermoelasticity, and magnetism, are still the main resources on modeling. Accordingly, the specific requirements in this research have encouraged the researcher to refer to those original resources. For example, large deflection analysis of the buckling microbeam under simultaneous thermal and magnetic effects is the specific analysis requirement in this problem. Therefore, the background of the research on microbridge modeling is found under different topics: heat transfer analysis and temperature distribution; elasticity; small- and large-beam-deflection; buckling microbeams; thermoelastic behavior of a fixed-fixed microbeam; electromagnetic force creation and application on a current-conducting microbeam.

Heat transfer analysis and temperature distribution in a microbridge have been investigated by a number of researchers for different applications. In his PhD thesis [50], "Thermal Applications of Microbridges," and in his papers with others on similar research topics [51], [52], [53], Mastrangelo analyses electrothermal and heat transfer in a microbridge. In his analysis, heat transfer by conduction has been considered the dominant mode of heat loss, while other terms of heat loss, including heat loss by convection and radiation, have been ignored. In order to show that radiation and free convection are negligible, Mastrangelo and Muller first assumed that two terms are negligible and then confirmed their assumption by comparing computed values [54]. These assumptions are further discussed in Sections 4.4 and 4.3. However, Dhananjaya in his thesis has explained his approach in taking into account all three terms of heat loss in developing a heat transfer model for a fixed-fixed microbeam [4]. This work is among a few examples of research in modeling heat transfer in a microbridge that take into account the effects of heat loss by convection and radiation in the heat equation. Yuxing Zhang et al. have compared

analytically computed values of heat loss due to different terms showing that a radiant term in the range of $300°C$ to $800°C$ is negligible [55]. Vapor bubble formation in a microheater, which has its application in ink jet printers, for example, has been the topic of research in a number of publications. In the analysis of microheaters, researchers need to investigate electrothermal driving, heat transfer, and temperature distribution in the fixed-fixed microbeam-microheater. Wang [56], and Lin et al. [57], [58], [59], have carried out such an electrothermal analysis in a microbridge. Geisberger et al. have investigated the electrothermal behavior of heavily doped polysilicon, which has a potential application in the fabrication of a heating fixed-fixed microbeam [1]. Mastrangelo's works have been referenced in closely relevant topics by Lin et al. [59], [58], [57]. In most of their works, Lin et al. have disregarded the heat loss due to terms other than conduction. Lin has analytically compared the terms for an average temperature of $300°C$ to show that those two terms are negligible [58]. Some other researchers (Wang [56], Motamedi [60], Amarendra Atre [61]), have also published works on similar topics and referenced Masterangelo or Lin. These works include modeling of heat transfer and electrothermal behavior of microbridges. However, there are some differences and even some contradictions between the reported results, perhaps because of the different assumptions and applied reference values. For example, Atre has extensively paid attention to the effects of electrothermal properties of the structural material in his modeling [61]. However, in his analysis of a polysilicon microactuator, he uses thermal and electrical properties that have been taken from the work by Okada and Tokumaru [5]. The data in Okada and Tokumaru's work is for crystalline Silicone [5]. Some of the electrothermal properties of Silicon, the heat conductive coefficient, for example, are dramatically different from polysilicon. The research by Geisberger et al. on electrothermal properties of polysilicon is also very interesting and provides very useful results in modeling electrothermal effects [1].

Investigations on mechanical analysis of a fixed-fixed microbeam, its small and large–nonlinear–deflection, and its buckling conditions have been inseparable parts of research on MEMS design. It is a most straightforward approach to refer to original books in this field for these analyses. Timoshenko's books are among the most important resources [62], [63], [64]. *Applied Elasticity* by Wang gives a very useful analysis on buckling fixed-ends beams [65]. *Mechanics of Materials* by Gere [66], *Mechanics of Materials* by Beer et al. [67], *Roark's Formulas for Stress and Strain* [68], [69], and *Engineering Analysis in Applied Mechanics* [70], [71] by Brewer are useful for further study. For a beam's large deflections and Elastica problem, *Advanced Mathematics for Engineers* by Reddick and Miller is an excellent resource that elaborates on the application of eliptical integrals for solving the Elastica problem [72]. *Theory of Elastic Stability* by Timoshenko [63], *Applied Elasticity* by Wang [65]and *Theory*

of Beam-Column by Chen and Wai-Fa [73] also provide readers with a detailed analysis of large deflections. Senturia [74], in his book, *Microsystem Design*, discusses mechanical deformation of microbridges, small and large deflections, and buckling conditions; Lobontiu and Garcia devote their book specifically to the mechanics of MEMS, discussing elasticity, deformation, and analysis of MEMS components [75]; Pelesko and Bernstein in their book on *Modeling MEMS and NEMS*, have worked on MEMS modeling, including small and large deflection of microbeams [6]. Analysis on buckling microbeams has also been of interest to some researchers who use it for other actuating systems in which the buckling microbeam is not an actuating element but an actuated one. Ichiki et al. have achieved such an application in their proposed microactuating technique [76]. An external independent mechanical actuator actuates the buckling microbeam. The "cold" buckling feature has been used to actuate, latch, and release a mechanism for in-vivo magnetic resonance imaging. Chiao has researched a fixed-fixed microbeam and proposed that it can be used for microactuation [77], [78]. He has modeled the thermoelastic behavior of the fixed-fixed microbeam and derived deflection equations by applying the temperature distribution in the microbeam. The relationship for temperature distribution is referenced from his previous research with Lin on thermal behavior of a fixed-fixed microbeam [57]. However, their electrothermal modeling is very similar to the work by Mastrangelo [50]. Gianchandani and Najafi in "Bent-Beam Strain Sensors," have analyzed small and large deflections in microbeams [79].

Thermoelastic behavior of a structural material is largely dependent on both its thermal and mechanical properties. Thermally induced stress results in buckling in a clamped-clamped microbeam. This topic has been investigated and addressed in various publications. *Theory of Thermal Stresses* by Boley et al. provides readers with a detailed thermoelastic analysis [80]. *Foundations of Solid Mechanics* by Fung has a discussion on thermoelasticity [81]. *Mechanics of Microelectromechanical Systems* by Lobontiu and Garcia analyses the thermoelastic behavior of a buckling microbridge [75]. Timoshenko's book, *Theory of Elasticity*, which is a very good resource on elasticity and beam deflection, provides little on thermal stresses [82], [83]. However, papers published on the analysis of a heated microbridge and its buckling provide more specific details on relevant aspects. Chiao and Lin have published papers addressing the thermoelastic behavior of a buckling microbridge [78], [57], [77]. The majority of publications on thermal actuators include discussions on thermoelasticity. Examples are the papers by Atre [61], Sinclair et al. [84], Enikov et al. [28], and Johnstone and Parameswaran [33].

Discussions of magnetic microactuators in the literature include information on modeling electromagnetic force, creation, and application [44], [85], [41]. However, nu-

merous books on magnetism provide the fundamentals required for electromagnetic analysis and modeling in this research: *Electricity and Magnetism* by Nayfeh and Brussel [86], *Elements of Electromagnetics* by Sadiku [87], *Electromagnetic Devices* by Roters [88], and *Permanent Magnets in Theory and Practice* by McCaig and Clegg are the resources used in this present research [89].

2.5 Summary

Thermal, magnetic, and thermomagnetic techniques for microactuation have been the topics of research in a significant number of publications. Microelectrothermomagneticactuation, the microactuation technique proposed in this paper, is based on both thermal and magnetic microactuations. Work on deriving scaling laws, which are the tools used to evaluate the proposed microactuating technique, is included in this literature review. However, the background of the present work in this thesis can be recognized in two areas: the method of microactuation, METMA; the microactuating element, a microbridge. Literature review on microactuators introduces some selected works on thermal, magnetic, and thermomagnetic microactuation to show the extent of previous works. Prior work in modeling the actuating element, a microbridge, falls within a broader range of research: electrothermal, elastic deformation and buckling, thermoelastic, and electromagnetic effects in a microbridge. Using out-of-plane buckling of a fixed-fixed microbeam for microactuation has been suggested in some prior works [78], [57], [77], and reported in some limited applications [48], [47]. However, few direct applications, or a method for practical use of an out-of-plane buckling microbridge as an actuating element to be actuated electrothermomagnetically have been observed. In brief, the research on the background shows that the proposed multi-mode operational technique of electrothermal, electromagnetic, and/or electrothermomagnetic actuation using out-of-plane buckling of a fixed-fixed microbeam in this present research has features of novelty and uniqueness, and outstanding potential applications.

Chapter 3

Microactuation and Scaling Laws

3.1 Introduction

It might naturally be expected that if a length, regardless of its direction, in a system decreased or increased by a given scale, any physical property involved in that system would also change by the same scale. However, the physical *dimensions* of a system can be variably scaled with respect to the corresponding *dimensions* in its model, for a given length scale. Consequently, the functionality of an isomorphically scaled system can differ dramatically, although the primary system and the scaled one are still similar. Dimensional analysis is a powerful tool to uncover the hidden potentials of a scaled physical quantity. Identified favorable scaled *dimensions* can be used for developing more effective actuating techniques. This chapter discusses the risks of not knowing scaling laws, important terms and methods of deriving these laws, and the need for designers or researchers of MEMS to understand scaling.

What is the risk of not knowing scaling laws? Predictions about full-scale behavior of very large or very small size systems are usually based on observations made in the laboratory on models of those systems. A suitable model of the full-scale system is investigated to estimate the behavior of the actual system. Avoiding disastrous mistakes and obtaining considerable economies have been the consequences of working on models instead of actual prototypes. The kind of relationship by which models represent the actual systems is called a similarity. This similarity results from the model, which is a geometrically scaled representation of the actual system. As mentioned in the above paragraph, for an isomorphically scaled system,

although the ratio of homologous[1] lengths is constant, the physical properties involved may change with very different ratios. Consequently, any physical property measured in the model has its own unique relationship with the same physical property in the actual system. Not knowing how a physical property is scaled carries the same risks as not being able to predict the behavior of the actual system from the measurement made on its model. Understanding the applicable terms defined in the following paragraph will facilitate deriving the relationship between a model and its actual system.

Important terms in scaling laws are *quantity, variable, dimension, unit of measurement, similarity, and scale factor*. The terms *quantity*, *variable*, and *dimension* are largely interchangeable, representing concepts that are measurable by some well-defined process. Hence, *dimensions* are the measurable properties of a system or a body which are describing its physical state. However, a unit of measurement is generally a requirement for measuring a quantity. Two systems are technically similar if each quantity in one system can be represented by an equivalent quantity in the second system and if the quantities in one system are related to one another in the same way as the corresponding quantities in the other [21], [22]. The ratio of the magnitude of *dimension* x at a point in a model to the magnitude of the same *dimension* at the homologous point in the actual system it is representing is the scale factor of that dimension x. Represented by S, the scale factor for a given *dimension* x is defined in equation 3.1. The following paragraph clarifies the concepts involved in the above-defined terms by introducing methods to derive scaling laws.

$$S_x = \frac{x_m}{x_A} \quad (m \text{ and } A \text{ represent the model and actual system, respectively}) \tag{3.1}$$

Dimensional analysis and known scale factors are applied in deriving the unknown relationship between corresponding physical quantities in a model and its actual system. The dimensional analysis of any problem can produce an equation in the form of $f(q_1, q_2, q_3, ..., q_n) = 0$, in which $q_1, q_2, q_3,$ and q_n are dimensionless parameters. By deriving an explicit relationship for q_1, $q_1 = \psi(q_2, q_3, ..., q_n)$, and assigning certain values to $q_2, q_3, ..., q_n$, a value for q_1 is determined. Then, for the physical similarity between two systems, if the relationships are arranged so that the dimensionless quantities q_1, q_2, q_3, and q_n between a model and its actual system remain constant, the resulted equations, $(q_i)_m = (q_i)_A$ for $i = 2, 3, ..., n$,

[1]A model and its actual prototype are homologous provided that each point and time of the model (x_m, y_m, z_m, t_m) can be associated with a unique point and time of the prototype, and also there is a biunique and continuous correspondence between the points [23].

produce information about the unknown *quantities* in the actual system, from the measurement on the model. In fact, if it is assumed that an actual system and its model represent two similar systems, by knowing the scale factors of some *quantities*, any other scale factors are derived by using known dimensional relationships. As an alternative approach, the known scale factors can also be inserted in the basic equations related to the situation to derive the unknown scale factors. For example, if for a given actual system and its model, S_l and S_t represent the scale factors for length and time which are assumed to be known, the scale factor for acceleration can be computed, $S_a = \frac{S_l}{S_t^2}$. These techniques are further illustrated in the following sections.

Scaling laws are employed in design and research on MEMS to serve two objectives: predicting the effects of physical *quantities* in microstructures is the first objective. The required physical *quantities* are measured in the macroscale model. Then, applying scaling laws on the model's measured *quantities* results in a prediction of the corresponding values in an actual system, the microstructure. The second objective is to identify the most favorable scaled physical properties. By using the identified favorable properties, highly efficient microactuator designs can be developed. Hence, people who do research in microsystems either for microactuator design or other applications need to recognize and develop a thorough understanding of scaling laws. Lacking enough knowledge of how physical phenomena are scaled in a microdomain, whether their effectiveness decreases, increases, or does not change, is the same as not having any estimation of the functionality of a developed design.

The above discussions on the risks of not knowing scaling laws, important terms in scaling laws, methods of deriving scaling laws, and the utility of scaling laws in design and research on MEMS stress their necessity, application, and benefits. In the following sections, scaling laws are derived for the physical phenomena that are effective in the functionality of the proposed microactuating techniques, METMA. The physical properties involved in METMA are electrothermal and heat transfer for thermal microactuation and magnetic effects for electromagnetic microactuation. However, a discussion on the scaled strength of the structural material is also included.

3.2 Scaling Laws in Heat Transfer and Thermal Microactuation

The modes of heat transfer in a thermal microactuator depend on the temperature profile, the design configuration, the application environment, and the thermal capacity of the microactuator. These conditions, which determine if one or more modes of heat loss are significant, are discussed in Chapter 4. However, regardless of whether or not some terms of heat loss in a developed thermal microactuating technique are negligible, scaling laws are investigated in equations representing different modes of heat transfer. Scaling laws for heat loss and heat generation are investigated to give a measure of how the effectiveness of each term is scaled.

A simplified form of Fourier equation represents heat conduction under steady-state conditions:

$$Q_{cond} = -\frac{kA(T_1 - T_2)}{d}, \quad Q_{cond} = -k\nabla T \;\Rightarrow\; H_{(flux)} = \frac{Q}{A} = -\frac{k(T_1 - T_2)}{d} \quad (3.2)$$

in which, Q_{cond} is the total amount of conducted heat, k is the bulk heat conductivity, A is the conducting surface area, T_1 and T_2 are temperatures of the two parallel plates making the end surfaces of the conducting medium, H is heat flux–the heat flow per unit area and time–and d is the length of the conducting medium between two surfaces. Assuming that k is constant and the temperature gradient is the same for the actual system and its model, the scale factor for total heat flow is derived from equation 3.2.

$$S_l = \frac{l_m}{l_A};\; k_m = k_A;\; (T_1 - T_2)_m = (T_1 - T_2)_A \Rightarrow (\frac{Qd}{A})_m = (\frac{Qd}{A})_A \quad (3.3)$$

$$\frac{Q_m l_A S_l}{l_A^2 S_l^2} = \frac{Q_A l_A}{l_A^2} \;\Rightarrow\; \frac{Q_M}{Q_A} = S_l \text{ (Scale factor for heat flow by conduction)} \quad (3.4)$$

Equation 3.4 shows that the heat flow in a microstructure is proportional to the length scale factor, the ratio of a length in the macroscale model to the corresponding length in an actual system. For example, if a length in a thermal microactuator is ten times less than the corresponding one in its macroscale model, the heat flow in the microactuator is ten times less than that of its macroscale model. Accordingly, the scale factor for heat flux–heat flow per unit area and time–is derived from the last part of equation 3.2.

$$(H_{(flux-cond)}d)_m = (H_{(flux-cond)}d)_A \;\Rightarrow$$

$$\frac{(H_{(flux-cond)})_m}{(H_{(flux-cond)})_A} = (\frac{l_A}{l_A S_l}) = S_l^{\ -1} \text{ (Scale factor for heat flux by conduction)} \quad (3.5)$$

Equation 3.5 shows that the heat flux in a microstructure is proportional to the inverse of the scale factor for length. For example, if the length of a thermal microactuator is ten times less than its macroscale model, the heat flux in the microactuator is ten times more than that of its macroscale model. A more general non-steady-state condition form of Fourier equation, including the heat generation term, is given in 3.6.

$$\nabla^2 T(r,t) + \frac{P_g}{k} = \frac{1}{\alpha}\frac{\partial T(r,t)}{\partial t} \quad (3.6)$$

The relationship for thermal diffusivity, α, is given in 3.7.

$$\alpha = \frac{k}{\rho c} \quad (3.7)$$

Specific thermal capacity at constant pressure and specific mass are denoted by c and ρ respectively. Thermal diffusivity is a criterion of how fast heat is conducted. Equation 3.7 is used in this Section to derive a thermal time constant, a demonstration of scaling law, and consequent effects in microscale. Heat loss by convection is represented by Newton's Cooling equation:

$$Q_{conv} = hA(T_1 - T_2) \ \Rightarrow \ H_{(flux-conv)} = h(T_1 - T_2) \quad (3.8)$$

As shown in table 4.3, h depends on the fluid velocity, $h \propto v \rightarrow \frac{l}{t}$. The scaling law is derived[2] as follows:

$$(T_1 - T_2)_m = (T_1 - T_2)_A = (\frac{Q_{conv}}{hA})_m = (\frac{Q_{conv}}{hA})_A \ \Rightarrow$$

$$\frac{(Q_{conv})_m}{(Q_{conv})_A} \Rightarrow (\frac{l_A^3 S_l^3}{l_A^3}) = S_l^3 \text{ (Scale factor for heat flow by convection)} \quad (3.9)$$

$$\frac{(\frac{Q_{(Conv)}}{A})_m}{(\frac{Q_{(Conv)}}{A})_A} = \frac{(H_{(Conv)})_m}{(H_{(Conv)})_A} = S_l^1 \text{ (Scale factor for heat flux by convection)} \quad (3.10)$$

equation 3.10 shows the same scaling law for heat flux by convection as the one by conduction derived in 3.5.

[2]The assumption for h proportional to l is a suggestion by Madou [11]. However, it seems that this assumption is not valid if a thorough dimensional analysis on h is carried out. The convective coefficient h is determined experimentally and is highly dependent on Nusselt's dimensionless parameter, $Nu = \frac{hL}{k}$. Nusselt's parameter is also a function of Reynold's number, Re, Prandtl number, Pr, and Grashoff number, Gr.

Heat loss by radiation is displayed by the Stefan-Boltzman relationship.

$$Q_{rad} = \epsilon\sigma AT^4 \;\Rightarrow\; H_{(flux-rad)} = \frac{\epsilon\sigma AT^4}{A} = \epsilon\sigma T^4 \tag{3.11}$$

Assuming that the macroscale model and its microscale actual system are in the same absolute temperature, provided that both systems are in the same radiation conditions, i.e., the same emitting-absorbing angle for a given wavelength, the emissivity is independent of scale. Therefore, the heat flow is proportional to the surface, and the heat flux is constant, independent of scale. From equation 3.11, the scaling law for heat flow and heat flux by radiation are derived.

$$(\epsilon\sigma T^4)_m = (\epsilon\sigma T^4)_A = (\frac{Q_{rad}}{A})_m = (\frac{Q_{rad}}{A})_A \;\Rightarrow$$

$$\frac{(Q_{rad})_m}{(Q_{rad})_A} = \frac{S_l^2 l_A^2}{l_A^2} = S_l^2 \text{ (Scale factor for heat flow by radiation)} \tag{3.12}$$

$$\frac{(\frac{Q_{rad}}{A})_m}{(\frac{Q_{rad}}{A})_A} = S_l^0 \text{ (Scale factor for heat flux by radiation)} \tag{3.13}$$

The term for heat generation by Joule effect or resistive heating

$$P_g = \rho_e \frac{l}{A} J^2 A^2 = \rho_e l J^2 A \Longrightarrow \frac{Pg_m}{Pg_A} = \frac{l_m J_m^2 l_m^2}{l_A J_A^2 l_A^2} = S_l^3 \frac{J_m^2}{J_A^2} \tag{3.14}$$

The heat generation in the unit volume of the microstructure is given in relationship 3.15.

$$\frac{P_g}{V} = \frac{\rho_e \frac{l}{A} J^2 A^2}{lA} = \frac{\rho_e l J^2 A}{lA} \Longrightarrow \frac{Pg_m/V_m}{Pg_A/V_A} = \frac{\frac{l_m J_m^2 l_m^2}{l_m l_m^2}}{\frac{l_A J_A^2 l_A^2}{l_A l_A^2}} = S_l^0 \frac{J_m^2}{J_A^2} \tag{3.15}$$

The heat generation term is denoted by P_g. Electrical resistivity, ρ_e, is not constant and depends on temperature, but for a given temperature, it has the same value in both the prototype and its model. A variety of operating conditions can be kept constant between the actual system, microstructure, and its macroscale model. The scaling laws will be different depending on either of these operating conditions. For example, if the current density has the same value in both the actual system and its macroscale model, a different scaling law will be derived in comparison with the status in which the same value of the current is applied in the two systems. Thus, the scaling law for power generation is derived, assuming the current density is constant, which is one selected option among various scenarios. From equation 3.14

$$(\rho_e J^2)_m = (\rho_e J^2)_A \;\Rightarrow$$

$$\frac{Pg_m}{Pg_p} = \frac{S_l^3 l_A^3}{l_A^3} = S_l^3 \text{ (Scale factor for power generation, cosntant } J) \tag{3.16}$$

From equation 3.15

$$\frac{(P_g/V)_m}{(P_g/V)_A} = S_l^0 \text{ (Scale factor for power generation per unit volume)} \tag{3.17}$$

The internal energy of structural material with a volume V is equal to

$$Q_{total} = \rho c V \frac{dT}{dt} \tag{3.18}$$

Assuming c, specific thermal capacity, dT, temperature difference, and ρ, mass density are constant, the scaling law for internal energy is derived in 3.19.

$$\frac{(Q_{total})_m}{(Q_{total})_A} = \frac{V_m}{V_A} = \frac{S_l^3 l_A^3}{l_A^3} = S_l^3 \tag{3.19}$$

As the final part in investigating scaling laws in heat transfer, the thermal time constant is derived. Applying the Newton Cooling equation, and from relationships 3.8 and 3.18

$$\rho c V \frac{dT}{dt} - hA(T - T_\infty) = 0 \Rightarrow \frac{T - T_\infty}{T_0 - T_\infty} = e^-(\frac{hA}{\rho c V})t \tag{3.20}$$

equation 3.20 shows that the temperature decreases exponentially with time, and its time-constant is equal to

$$t_{\text{(thermal time constant)}} = \frac{\rho c V}{hA} \tag{3.21}$$

For given experimental values, the scaling law for thermal time constant is investigated in Chapter 8.

The above results for scaling laws are summarized in tables 3.1 and 3.2.

Table 3.1: Scaling Factors for Heat Dissipation

Conduction		**Convection**		**Radiation**	
Heat flow	**Heat flux**	**Heat flow**	**Heat flux**	**Heat flow**	**Heat flux**
S_l^1	S_l^{-1}	S_l^3	S_l^1	S_l^2	S_l^0

Table 3.2: Scaling Factors for Heat Generation and Thermal Capacity

Heat Generation	**Power per Unit Volume**	**Thermal capacity**
S_l^3	S_l^0	S_l^3

3.3 Scaling Laws in Elasticity and Strength of Material

The relative efficiency, e, of a structure is sometimes measured by its *strength-to-weight ratio*, which is differently defined depending on whether the component is under torsion, tension, or compression. The relative efficiency, e, is also defined as the load-carrying capacity of a structural material divided by its weight [66]. For a beam in compression or tension, *strength-to-weight ratio* is defined as

$$e_{(\sigma/W)} = \frac{\sigma}{W} \tag{3.22}$$

in which σ is normal stress, and W is the weight density of the structure. Scaling law is applied to the relative efficiency of structures, a macroscale model, and its actual system, microscale structure, assuming $S_l = \frac{l_m}{l_A}$ is the length scale.

$$e_{(\sigma/W)_m} = \frac{\sigma_m}{W_m} = (\frac{\frac{F}{l^2}}{\frac{mg}{l^3}})_m \;\rightarrow\; e_{(\sigma/W)_m} = (\frac{F}{mg})_m l_m = (\frac{F}{mg})_m l_A S_l \tag{3.23}$$

From equation 3.23, the relative efficiency of the structures is derived for the same value of $(\frac{F}{mg})$.

$$\frac{e_{(\sigma/W)_m}}{e_{(\sigma/W)_A}} = \frac{(\frac{F}{mg})_m l_A S_l}{(\frac{F}{mg})_A l_A},\; (\frac{F}{mg})_A = (\frac{F}{mg})_m \Rightarrow \frac{e_{(\sigma/W)_m}}{e_{(\sigma/W)_A}} = S_l^{-1} \tag{3.24}$$

equation 3.24 shows the favorable increased strength of the structural material proportional to the length scale S_l. This result means that if, for example, the length-size in a microstructure is 10 times less than the corresponding length-size in its macroscale model, the microstructure is 10 times stronger than its macroscale model.

3.4 Scaling Laws in Magnetic Microactuation

Predicting the potential of electromagnetic actuating techniques in microscale has been a contested issue. The utility of dimensional analysis to identify hidden favor-

able features of a scaled physical quantity is more evident in this issue. Deriving and applying scaling laws in electromagnetic actuation provide the researcher with the tools to clearly identify if these techniques are favorable and under which conditions these techniques can be employed to produce the most efficient results. In this section, in order to derive scaling laws, three ways of producing magnetic force and the equations governing them are briefly reviewed, but more detailed discussions are given in Chapter 6. Three ways of producing magnetic force are current-current interaction, current-magnet interaction, and magnet-magnet interaction. For comparison, the scaling law for electrostatic force is also derived.

1. The magnetic force produced by current-current interaction can be represented by equation 3.25.

$$F_B = \frac{\mu_0}{2\pi} I_1 I_2 \frac{l}{d} \tag{3.25}$$

in which, I_1 and I_2 are the currents in two interacting conductors, d is the distance between them, and l the effective length of one conductor subjected to the other one. The relationship between electrical current densities in two similar systems is derived. Given that $I_1 = I_2$, and $A_1 = A_2 = A$,

$$F_B = \frac{\mu_0}{2\pi} J^2 A^2 \frac{l}{d} \Longrightarrow \frac{F_m}{F_A} = \frac{(J_m^2 l_m^4 \frac{l_m}{l_m})}{(J_A^2 l_A^4 \frac{l_A}{l_A})} = \frac{J_m^2 l_A^4 S_l^4}{J_A^2 l_A^4}, \ \frac{F_m}{F_A} = S_l^4 \frac{J_m^2}{J_A^2} \tag{3.26}$$

equation 3.26 shows the conditions under which the produced magnetic force by current-current interaction can be favorably scaled. Three different examples of operating conditions are considered. Under each of these assumed physical conditions, the magnetic microactuator, actual system, is evaluated against its macroscale model, and the scaling laws are derived.

- Assuming that the current density J in both two similar systems, magnetic microactuator (actual system), and its macroscale model is constant, equation 3.25 results in the scaling law.

$$J_m = J_A \Longrightarrow (\frac{\mu_0}{2\pi} J^2)_m = (\frac{\mu_0}{2\pi} J^2)_A \tag{3.27}$$

$$S_l = \frac{l_m}{l_A}; \ (\frac{Fd}{A^2 l})_m = (\frac{Fd}{A^2 l})_A \Longrightarrow \frac{F_m l_A S_l}{l_A^4 S_l^4 l_A S_l} = \frac{F_A l_A}{l_A^4 l_A}, \ \frac{F_m}{F_A} = S_l^4 \tag{3.28}$$

Equation 3.28 shows how the output force of a magnetic actuator is scaled in two similar systems under constant current density, i.e., the current density has the same value in two similar systems. For example, if a length-size in a magnetic microactuator, actual system, which

is functioning based on current-current interaction, is 10 times less than its corresponding macroscale model's length-size, the force output in the magnetic microactuator, actual system, is $10,000$ times less than its macroscale counterpart. Obviously, this dramatic decrease of magnetic force in microscale does not make current-current interaction under constant current density conditions attractive at all, if it is to be used for microactuation.

- Assumed that the current density, J, in two similar systems, magnetic microactuator (actual system), and its macroscale model are related by $\frac{J_m}{J_A} = S_l^{-\frac{1}{2}}$. Equation 3.26 shows that the force in microdomain will be scaled to S_l^3. To make this happen, the heat flux through the surface of the wire–conductor should be constant. Heat flux is the heat flow divided by the surface area. Joule effect generates the heat proportional to the currents in two interacting conductors; it is also assumed that the heat is mainly dissipated through the conductors' surfaces. Constant heat flux means that the rate of heat dissipation with respect to the surfaces of the conductors has the same value in the microstructure, actual system, and its macroscale model. Under steady-state conditions, the rate of generated heat is equal to the rate of dissipated heat.

$$(\frac{Q}{A_S})_m = (\frac{Q}{A_S})_A \Longrightarrow (\frac{RI^2}{A_S})_m = (\frac{RI^2}{A_S})_A \tag{3.29}$$

$$(\frac{\rho \frac{l}{A_S} J^2 A_C^2}{A_S})_m = (\frac{\rho \frac{l}{A_S} J^2 A_C^2}{A_S})_A, \quad \frac{\rho l_m J_m^2 l_m^4}{l_m^4} = \frac{\rho l_A J_A^2 l_A^4}{l_A^4}, \quad \frac{J_m}{J_A} = S_l^{-\frac{1}{2}} \tag{3.30}$$

From equation 3.25

$$F_m = \frac{\mu_0}{2\pi}(J_m^2 l_m^4 \frac{l_m}{l_m}), \ F_A = \frac{\mu_0}{2\pi}(J_A^2 l_A^4 \frac{l_A}{l_A}) \Longrightarrow \frac{F_m}{F_A} = S_l^3 \tag{3.31}$$

equation 3.31 shows the output force of a magnetic actuator is scaled in two similar systems under constant heat flux. If a length-size in a magnetic microactuator, actual system, that is functioning based on current-current interaction is 10 times less than in its macroscale model, the force output in the magnetic microactuator will be 1000 times less than that of its macroscale model's. However, although the constant heat flux conditions make magnetic microactuation more efficient than the previous option in which the current density is kept constant, a scale factor of S^3 for force is still not very desirable for microactuation.

- Assumed that the current density J in two similar systems, magnetic microactuator (actual system), and its macroscale model are related by $\frac{J_m}{J_A} = S_l^{-1}$. From equation 3.26

$$\frac{J_m}{J_A} = S_l^{-1} \Rightarrow \frac{F_m}{F_A} = S_l^4 \frac{J_m^2}{J_A^2} = S_l^2 \tag{3.32}$$

  The relationship for current densities $\frac{J_m}{J_A} = S_l^{-1}$ is interpreted by an example: if a length-size in a magnetic microactuator, actual system, is 10 times less than its macroscale model's, the current density in the microactuator must be 10 times more than in its macroscale model. From equation 3.15, this higher current density produces 100 times more heat per unit volume of the microstructure that must be removed. If this higher relative current density is supposed to apply, $\frac{J_m}{J_A} = S_l^{-1}$, there is a requirement to remove heat from the microstructure in order that the temperature gradient, ∇T, of the wire-environment remains constant [3]. A comparison of the scaled force of S_l^2 with a scaled electrostatic force, which is analyzed at the end of this section, shows the favorably scaled magnetic force in the microdomain.

2. The magnetic force produced by current-magnet interaction can be represented by equation 3.33.

$$F_B = Il \times B \tag{3.33}$$

   in which, the magnetic flux produced by a magnet depends on its magnetic polarization $j = B_i$. The magnetic polarization j is a material property and independent of scale. Therefore, from equation 3.33, the scaling law for magnet-current interaction is derived.

$$F_B = IlB \Longrightarrow \frac{\frac{F_m}{J_m l_m^3}}{\frac{F_A}{J_A l_A^3}}, \; \frac{F_m}{F_A} = \frac{l_m^3 J_m}{l_A^3 J_A} = S_l^3 \frac{J_m}{J_A} \tag{3.34}$$

   From equation 3.34, for each of the above assumptions, $J_m = J_A$, $J_m = S_l^{-\frac{1}{2}} J_A$, and $J_m = S_l^{-1} J_A$, the magnetic force is scaled.

[3]It has been assumed that the microactuator in a steady-state condition has reached its maximum allowed temperature, but no further temperature increase happens because the amount of generated heat is equal to the dissipated one. However, although the computed result of assuming a constant temperature gradient, ∇T, makes sense, the researcher must accurately take into account all effective terms of heat loss rather than conduction only [10]

- For constant current density, $J_m = J_A$,

$$J_m = J_A \implies \frac{F_m}{F_A} = S_l^3 \tag{3.35}$$

In comparison with the constant current density in current-current interaction in which magnetic force in microstructure is scaled to S_l^4, equation 3.35 shows that the force by current-magnet interaction is scaled to S_l^3.

- For constant heat flux, $J_m = S_l^{-\frac{1}{2}} J_A$, equations 3.30 and 3.34 result in

$$\frac{J_m}{J_A} = S_l^{-\frac{1}{2}} \implies \frac{F_m}{F_A} = S_l^3 \frac{J_m}{J_A} = S_l^{\frac{5}{2}} \tag{3.36}$$

In comparison with the constant heat flux in a current-current interaction in which the magnetic force in a microstructure is scaled to S_l^3, equation 3.36 shows that the force by current-magnet interaction is scaled to $S_l^{\frac{5}{2}}$.

- For constant temperature gradient ∇T, or $J_m = S_l^{-1} J_A$, from equation 3.34 and equation 3.32,

$$\frac{J_m}{J_A} = S_l^{-1} \Rightarrow \frac{F_m}{F_A} = S_l^3 \frac{J_m}{J_A} = S_l^2 \tag{3.37}$$

3. The magnetic force produced by a magnet-magnet interaction is independent of scale. This phenomenon is also valid when the interaction is between a magnet and a magnetic material. As mentioned earlier, in the current-magnet interaction's case, the magnetic flux produced by a magnet depends on the intrinsic property of the magnet, which is its magnetic polarization j. However, the problem can be viewed from another perspective, which is an analysis that is using a scalar magnetic potential concept. The effect of a magnet with a volume v at a point q located at a distance r can be represented by a scalar potential $\psi(q)$ [86], [13],.

$$\psi(q) = \frac{v}{4\pi\mu_0} \frac{\vec{j} \bullet \vec{r}}{r^3} \tag{3.38}$$

in which, j is the magnetic polarization. The magnetic field $\vec{H}$ is defined as the local gradient of the scalar potential $\psi(q)$.

$$\vec{H} = \overrightarrow{grad}\, \psi \tag{3.39}$$

Scaling laws for the scalar potential, 3.38, and the magnetic field, 3.39, are derived:

$$(\frac{j}{4\pi\mu_0})_m = (\frac{j}{4\pi\mu_0})_A,\ (\frac{r^3\psi}{vr})_m = (\frac{r^3\psi}{vr})_A \Rightarrow \frac{(\psi)_m}{(\psi)_A} = S_l \tag{3.40}$$

By comparing equation 3.38 with equation 3.39, the scaling law for equation 3.39 is derived from the result in equation 3.40.

$$\frac{(\vec{H})_m}{(\vec{H})_A} = S_l^0 \tag{3.41}$$

equation 3.41 shows that the magnetic force from a magnet-magnet interaction is independent of scale[4].

For comparison, the scaling law for electrostatic force is derived. A capacitor represents an electrostatic microactuator.

$$E_{(e-energy)} = -\frac{1}{2}CV^2 = -\frac{\epsilon wv(E_{(e-field)}d)^2}{2d} \tag{3.42}$$

Assuming that $\frac{\epsilon E^2_{(e-field)}}{2}$ is constant, having the same value in a microactuator, actual system, and its macroscale model, the scaling law for electrostatic energy is derived.

$$(\frac{\epsilon E^2_{(e-field)}}{2})_m = (\frac{\epsilon E^2_{(e-field)}}{2})_A \ \Rightarrow \ (\frac{E_{(e-energy)}d}{wvd^2})_m = (\frac{E_{(e-energy)}d}{wvd^2})_A$$

$$\frac{(E_{(e-energy)})_m}{(E_{(e-energy)})_A} = \frac{(l_AS_l)(l_AS_l)(l_AS_l)^2l_A}{l_Al_Al_A^2(l_AS_l)} = S_l^3 \text{ (Scale for electrostatic energy)} \tag{3.43}$$

From equation 3.43, assuming that the movement direction of one capacitor's plate is perpendicular to the plates' surfaces, $z-$axis, the relationship for electrostatic force results.

$$F_e = -\frac{\partial E_{(e-energy)}}{\partial z} = -\frac{1}{2}V^2\frac{\partial C}{\partial z} = -\frac{\epsilon vwV^2}{2x^2} \tag{3.44}$$

[4]However, in a magnet-magnet interaction, two applicable conditions can be considered: the condition in which the distance between the magnets is scaled; another status can also occur in which the distance between magnets is not scaled. These conditions will be investigated in future work.

Table 3.3: Comparison of Scaled Magnetic and Electrostatic Forces

	Current–Current	**Current–Magnet**
Current Density ($\frac{J_m}{J_A} = 1$)	S_l^4	S_l^3
Current Density ($\frac{J_m}{J_A} = S_l^{-\frac{1}{2}}$)	S_l^3	$S_l^{\frac{5}{2}}$
Current Density ($\frac{J_m}{J_A} = S_l^{-1}$)	S_l^2	S_l^2
	Magnet–Magnet	**Electrostatic**
	S_l^0	S_l^2

With the same assumptions applied for deriving scaling law of electrostatic energy, the scaling law for electrostatic force is derived as follows:

$$(\frac{\epsilon E^2_{(e-field)}}{2})_m = (\frac{\epsilon E^2_{(e-field)}}{2})_A \Rightarrow (\frac{F_e x^2}{wvx^2})_m = (\frac{F_e x^2}{wvx^2})_A$$

$$\frac{(F_e)_m}{(F_e)_A} = \frac{(l_A S_l)(l_A S_l)(l_A S_l)^2 l_A^2}{l_A l_A l_A^2 (l_A S_l)^2} = S_l^2 \text{ (Scale for electrostatic force)} \qquad (3.45)$$

Scaling laws derived for electrostatic and electromagnetic forces are shown in table 3.3. The table shows a comparison between scaled electromagnetic forces under different conditions and electrostatic force.

3.5 Summary

A macroscale model is denoted by m and is considered to represent a microactuator. The microactuator, which is the actual system and is denoted by A, is an isomorphically scaled down system that is represented by the macroscale model. The model facilitates the estimation of a microstructure's behavior by using relationships between *quantities* in the model and in the microstructure the model is representing. Scaling laws demonstrating these relationships serve design and research on microsystems in two ways:

1. Predicting the behavior of the microactuator from the measurements achievable on a macroscale model of the microactuator; recognition of the effective physical quantities and the unique relationships between physical quantities in two similar systems, the microactuator and its macroscale model

2. Identifying more favorable scaled physical quantities to be used for microactuator design; identifying optimized conditions in which a physical effect can be used in research or design in microscale

The scaling laws derived for heat transfer under different conditions, which are displayed in tables 3.1 and 3.2, give an evaluation of the favorable features of electrothermal microactuation. The scaling law for strength of material, S_l^{-1}, shows that the scaled-down systems are stronger than their macroscale model with respect to the scale. The scaling laws in magnetic actuation under different conditions produce dramatically different results, displayed in table 3.3. However, it is important to ensure that the derived scaling laws are valid within the assumptions and under the roughly defined conditions. The discussion will be more sophisticated and interesting when each specific case is analyzed under more accurately defined conditions. For example, many parameters are assumed to be constant when going from a macroscale model to its actual system, microactuator, but in some circumstances, they may not be constant and can be affected by the scaled *dimensions*.

Chapter 4

Heat Generation and Transfer in a Microbridge

4.1 Introduction

A thermal microactuator is a transducer converting electrical energy into mechanical displacement and force. In the process of energy conversion, electrical to thermal, heat is generated and dissipated. The major objective of the analysis of heat generation and loss in a microbridge is to determine the temperature distribution. The temperature distribution applies in the computations of thermally induced stress, expansion, and deflection of a microbridge, which are discussed in the next chapter. Once the temperature variation is known, for example, the conductive heat flux at any point in the medium or on its surface can be computed from Fourier's law. The heat transfer analysis is a process to formulate a microbridge's design parameters. These design parameters are the electrothermal properties of the structural material, heat transfer conditions, and temperature distribution.

Electrothermal properties of a structural material include its electrical specifications, thermal conductivity, and thermal expansion coefficient. These properties are usually nonlinear functions of temperature. However, the variations of electrothermal properties over temperature are more important than their absolute values in the analysis of microactuators. In a thermal microactuator, force and displacement result from resistive heating or Joule effect. Thus, a resistivity variation of a conductor or semiconductor over temperature usually has a direct effect on the output force and displacement. Similarly, the specific heat and thermal conductivity of a structural material and their changes with temperature are effective in

the operation of a microactuator. Finally, for specific application in thermal and thermomagnetic microactuators, the thermal expansion coefficient of the structural material is also a determining factor. Therefore, predicting a microactuator's functionality largely depends on estimating these parameters and their variations over temperature. In microscale, this prediction is more dependent on electrothermal behavior of the structural material because of two reasons:

1. Faster operation cycle in microscale
2. Broader temperature range in thermal microactuators

Heat transfer, including heat generation and loss in a system, depends on a number of variables. In an electrothermally heated microstructure, there are generally three modes of heat loss and one mode of heat generation. The balance of energy equation includes five terms: three terms for heat loss, one term for heat generation and one term for the initial energy or thermal capacity of the actuating element. These five terms are mostly nonlinear relationships and functions of temperature–dependent coefficients. The relationships for electrical resistivity and thermal conductivity of a structural material are introduced in Section 4.2. These relationships apply in the formulation of the terms representing heat generation and loss. However, in deriving relationships for heat loss by conduction, the conducting coefficient is assumed to be constant. There are two reasons for this assumption, the first being that deriving the equation for heat loss by conduction will be significantly simplified, and the second reason, that the variation of thermal conductivity over the average temperature change is not significant. Heat transfer analysis in Section 4.3 provides more detail on these concepts by modeling and analyzing each term. The results are used in Section 4.4 to derive an equation for temperature distribution over a microbridge.

Deriving temperature distribution in microbridges requires solving heat transfer equations. If every temperature–dependent coefficient and term of heat loss is supposed to be included in the equation, analytical solution of this problem will be very complicated if not impossible. However, not all of the terms representing different modes of heat loss are important in every problem. Depending on the problem conditions, some of these terms can be negligible in comparison with other ones. Therefore, the problem conditions are carefully examined to exclude the negligible terms in advance. Furthermore, for simplifying a solution, some applicable assumptions are usually made. Small nonlinearities in the variations of temperature-dependent coefficients are neglected. This neglect is applicable when the consequent inaccuracy in the results is acceptable. For example, in a heavily

doped polysilicon, the variations of the electrothermal parameters over temperature are assumed to be linear. The assumptions will significantly simplify the solution. However, although temperature distribution over a microbridge depends on heat transfer, both the heat transfer and the temperature distribution are shaped by initial and boundary conditions. In steady-state conditions, the contacting areas and temperatures at the boundaries impose temperature gradients over the microbridge and toward its surrounding environment. Knowledge of temperature distribution is key in understanding the interface between thermal environment and mechanical field, an essential requirement in the analysis of thermoelastic behavior of the microbridge, the topic in the next chapter.

The above paragraphs introduce the content of this chapter and clarify the necessity of each topic. However, in the following sections, the discussions are more specifically continued. First, the electrothermal properties of polysilicon, the structural material used here as an example, are described. Then, the heat transfer in an electrothermally–heated microbridge is analyzed. Finally, a relationship for temperature distribution in the microbridge is derived. In fact, the discussion in the following sections aims at developing a model for the microbridge behavior in which electrical current applies as the input and temperature distribution is derived as the output.

4.2 Polysilicon Electrothermal Properties

Polysilicon is not the only structural material used in fabrication of MEMS, neither is it the most suitable one for design and fabrication of the proposed microactuating technique, METMA. The small thermal expansion coefficient of polysilicon is the main limitation of using this structural material for thermal microactuation and METMAS as well. In comparison with most metals, polysilicon's thermal expansion, $[2 - 2.9\ (\times 10^{-6}/\,^{\circ}K)]$, is about five times less than that of nickel's, $[13.4\ (\times 10^{-6}/\,^{\circ}K)]$, for example. Nevertheless, the electrothermal properties of polysilicon are reviewed in this study for two reasons. First, polysilicon is a very well known structural material for MEMS. Second, it is used in PolyMUMPs, which is the fabrication technology supported by the Government of Canada, Canadian Microelectronics Corporation (CMC), for research in Canadian universities. Furthermore, for any chosen structural material, a similar process of discussion on the role of physical properties is applicable. In this section, the electrical properties, specific heat, thermal conductivity, and thermal expansion coefficient of polysilicon are reviewed.

Polysilicon's electrical conductivity is significantly dependent on doping concentrations and grain structure. The process of doping can change not only the base values of the properties but also their variation with temperature, in a significant way. Among the electrical properties of polysilicon, its electrical resistivity is more important in its application for thermal microactuators and METMA. Low to moderately doped polysilicon ($\leq 10^{18}.cm^{-3}$) shows a negative temperature coefficient of resistance (TCR) because pure or slightly doped polysilicon has few charge carriers to conduct electricity. Temperature increase facilitates release of charge carriers. More charge carriers contribute to conduction, which results in a decreased resistivity (Johnstone and Parameswaran [33], Geisberger [1], Gad-el-Hak [90], Borovic et al. [29]). The significant temperature dependency of the resistivity makes a low to moderately doped polysilicon unsuitable for electrothermal microactuation. A comparison between resistivities of a low to moderately doped polysilicon in different temperatures shows the extent of this instability [91], equation 4.1.

$$\rho_{(300\,^\circ K)} = 10^{13}\,(\Omega.m);\ \rho_{(600K)} = 7 \times 10^{4}\,(\Omega.m);\ \rho_{(1300\,^\circ K)} = 0.04\,(\Omega.m) \tag{4.1}$$

However, heavily doped polysilicon shows more stable electrothermal properties. It displays an increasing resistivity over temperature increase, similar to most metals and other conductors. The suggested relationship for the resistivity is given in equation 4.2 [61].

$$\rho_{e(T)} = (2 \times 10^{-3})[1 + (1.25 \times 10^{-3})(T - 300)]\ (\Omega.cm) \tag{4.2}$$

The resistivity of polysilicon may be formulated in another way (Geisberger et al. [1], and Tuck et al. [2]).

$$\rho_{e(T)} = n_1 + n_2 T^{\,n_3} \tag{4.3}$$

The values for n_1, n_2, and n_3 were experimentally derived for PolyMUMPs polysilicon, shown in table 4.1 [2]. The simplified relationship 4.4 is also valid for heavily doped polysilicon to some extent[1].

Table 4.1: Parameters in Equation 4.3 for Resistivity of Polysilicon [1], [2]

Parameters	**Experimentally Determined Values [2], [1]**
n_1	2.6×10^{-3}
n_2	8.16×10^{-9}
n_3	1.946

$$\rho_{e(T)} = (2 \times 10^{-3})[1 + \xi(T - T_0)] \tag{4.4}$$

[1]The symbol e is used to distinguish electrical resistivity ρ_e from mass density ρ_m.

The temperature coefficient of resistivity, $\xi = 0.0012(\frac{1}{°K})$, has been determined experimentally [50]. Equation 4.4, with the given value for ξ, is valid at least until $900\,°K$. However, at very high temperatures ($\approx 1200\,°K$), polysilicon experiences a sudden change in its electrical behavior, which causes a sharp decrease in the resistivity. The reason for this phenomenon is that in lower temperatures, (below $1200\,°K$), the limitation in carrier mobility is the cause for gradual resistivity increase. However, when the thermal generation of electrical carriers is dramatically high, its effect overweighs the limitation of carrier mobility. The values for resistivity of heavily doped polysilicon layers and the only metal layer used in PolyMUMPs are displayed in table 4.3. Sheet resistance, $R_S(\frac{\Omega}{sq})$, is used to show the resistivity of thin films. It is defined

$$R = \rho_e \frac{l}{A} = \frac{\rho_e}{z}\frac{l}{w} = R_S \frac{l}{w} \Rightarrow R_S = \frac{R_{(Resistance)} w_{(width)}}{l_{(length)}} \tag{4.5}$$

Specific heat, c, in polysilicon is also a function of temperature. The variations of specific heat are defined in two temperature ranges (Geisberger et al. [1], Atre [61]): For $292\,°K \leq T \leq 700\,°K$

$$c(T) = (1.976362 \times 10^{-6})T^3 - (3.766786 \times 10^{-3})T^2 + (2.622954)T + 214.9586 \tag{4.6}$$

For $701\,°K \leq T \leq 1685\,°K$

$$c(T) = -(3.377784 \times 10^{-5})T^2 + (2.388945 \times 10^{-1})T + 7.324063 \times 10^2 \tag{4.7}$$

However, Manginell has suggested a different relationship for a temperature range between $20\,°K$ and $2000\,°K$ [3].

$$c(T) = (9.4 \times 10^{-9})T^3 - (1.8 \times 10^{-5})T^2 + (0.0011)T - 0.36 \;\; (Jcm^{-3}.°K^{-1}) \tag{4.8}$$

Figure 4.1 shows variations of specific heat in silicon/polysilicon versus temperature.

The thermal conductivity of polysilicon is also a strong function of the grain structure of the film, lower values for fine grain and higher values for large grain, and the highest value is for single-crystal silicon [90].

$$k_{cb}(T) = [(-2.2 \times 10^{-11})T^3 + (9 \times 10^{-8})T^2 - (10^{-5})T + 0.014]^{-1} \; (\frac{W}{m.°K}) \text{ [90]} \tag{4.9}$$

Figure 4.2 shows variations of electrical resistivity and thermal conductivity of the heavily doped polysilicon, which is used in PolyMUMPs, investigated by Geisberger et al. [1]. For the thermal conductivity of polysilicon, a suggested average value

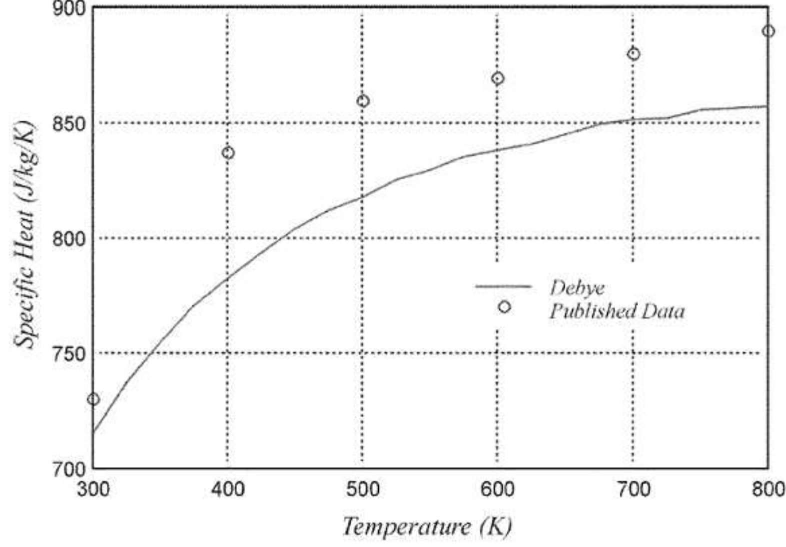

Figure 4.1: Silicon-Polysilicon Specific Heat Variations over Temperature [1]

is $k_{cb} = 0.32$ $(W/cm.^{\circ}K)$. The summarized results for electrothermal properties of polysilicon are given in table 4.3. The relationship for temperature dependent conductivity k may also be obtained if the temperature dependent specific heat, c, is known.

$$k_{cb} = a_d c$$

Okada and Tokumaru in their paper, "*Precise determination of lattice parameter and thermal expansion coefficient of silicon between 300 and 1500K thermal*," have reported their research on deriving the thermal expansion coefficient of silicon [5]. Assuming that doping does not affect the thermal expansion coefficient [1], and the relationship for thermal expansion of silicon is also applicable for polysilicon, the suggested formulation by Okada and Tokumaru is given [5].

$$a(T) = (3.725[1 - \exp^{(-5.88\times10^{-3}(T-124))}] + 5.548 \times 10^{-4}T) \times 10^{-6} \ (^{\circ}K^{-1}) \quad (4.10)$$

Figure 4.3 depicts variations of the silicon thermal expansion coefficient over temperature [4], [5]. Computed values for the thermal expansion coefficient of a single crystal silicon in various temperatures are given in table 4.2 [1], which are assumed to be valid for polysilicon as well.

Table 4.3 shows values for electrical resistivity, the coefficient of temperature dependent resistivity, thermal conductivity, specific heat, and thermal expansion coefficient of heavily doped polysilicon at given temperatures.

Table 4.2: Single Crystal Silicon Thermal Expansion over Temperature [1]

Temperature ($^\circ K$)	**a(T)**($\frac{10^{-6}}{^\circ K}$) [1]
300	2.5
400	3.1
500	3.5
600	3.8
700	4.1
800	4.3

Table 4.3: Electrothermal Specifications of Heavily-Doped Polysilicon

	Heavily-doped polysilicon
Electrical Resistivity ($\frac{\Omega}{sq}$) [92]	$30 - P_0, 10 - P_1, 20 - P_2, .06 - M$
Temp. Resistivity Coefficient ($\frac{1}{^\circ K}$)	$\xi = 0.0012$ [50], [90]
Thermal Conductivity ($\frac{W}{cm \cdot ^\circ K}$)	$0.29 \rightarrow 0.34$ [51]
Thermal Expansion ($\frac{10^{-6}}{^\circ K}$)	$(2.59 \pm 0.05) At 298.2\,^\circ K$ [5]
Specific Heat ($\frac{J}{^\circ K \cdot g}$)	0.77 (At 300 $^\circ K$) [3]

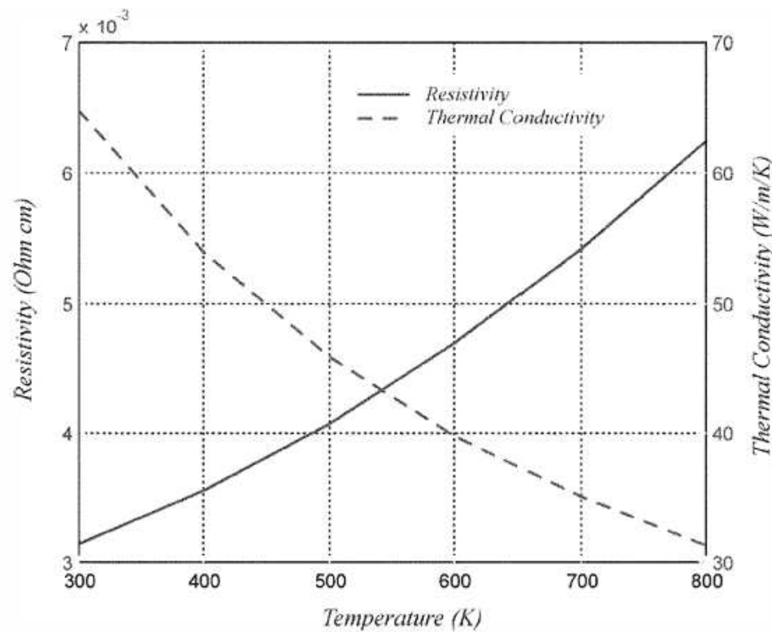

Figure 4.2: Resistivity and Thermal Conductivity in MUMPS polysilicon [1], [3]

In the above paragraphs, the polysilicon electrothermal properties are reviewed. In this review, electrical resistivity, thermal conductivity, and the thermal expansion coefficient of this structural material are discussed. The emphasis is on temperature dependency of these parameters because the variations of these parameters over temperature are even more important than their absolute values. In the following Section, heat transfer analysis in a microbridge is investigated to formulate the terms of heat transfer, which are required for modeling temperature distribution in the microbridge.

4.3 Steady-state Heat Transfer in a Microbridge

Conduction, convection, and radiation are modes of heat transfer. All of these modes of heat transfer can occur simultaneously in the *Steady-State Conditions* model. The steady-state conditions dictate that the heated microbridge has reached a state of equilibrium in which the generated heat is equal to the dissipated heat.

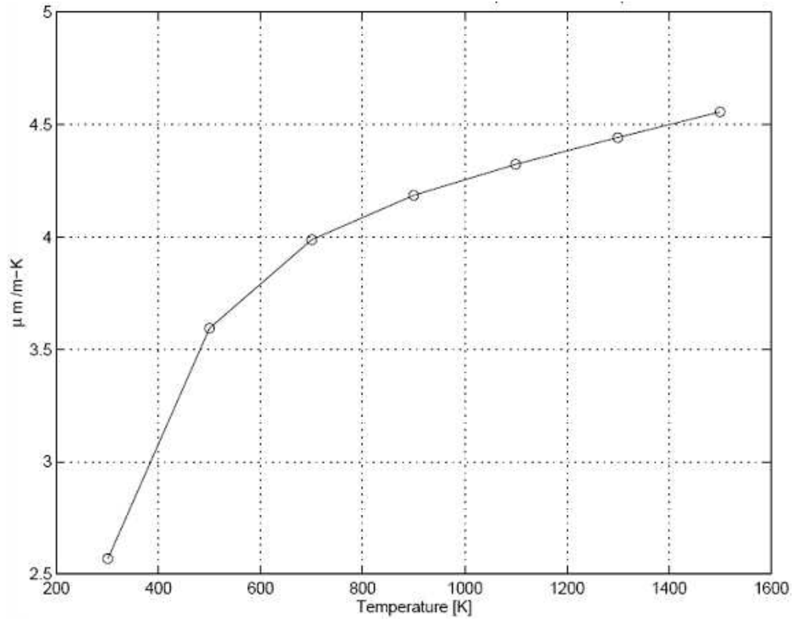

Figure 4.3: Silicon Thermal Expansion Coefficient over Temperature [4], [5]

A one–dimensional model[2] for heat transfer applies in a microbridge. However, the model must be extended in order to include the convective and radiative loss, *heat transfer from extended surface* [93]. In this section, formulation of a heat equation, electrothermal heat generation, conduction, convection, and radiation are discussed.

Principles of heat transfer and the first thermodynamic law apply to formulate the heat equation in a microbridge. Equation 4.11 shows such a formulation.

$$\frac{dQ_T}{dt} = \frac{dQ_g}{dt} + \sum_{i}^{N} \frac{dQ_i}{dt} \tag{4.11}$$

Figure 4.4 displays a fixed-fixed microbeam and a microbeam element as an arbitrary control volume along the length of the microbeam. This figure also shows the potential modes of heat dissipation as well as electrothermal heat generation in the microbridge. At a certain point in time, the beam element, $\Delta V = wz\Delta x$ in figure 4.4, has thermal energy per unit volume equal to $\rho_m cT$, thus the change of energy

[2]By choosing a one-dimensional model for heat transfer, an assumption can also be made that conduction is the dominant heat transfer mode, which means that other terms are negligible. However, heat transfer can occur in other directions perpendicular to the length of the microbridge in the form of convection or radiation.

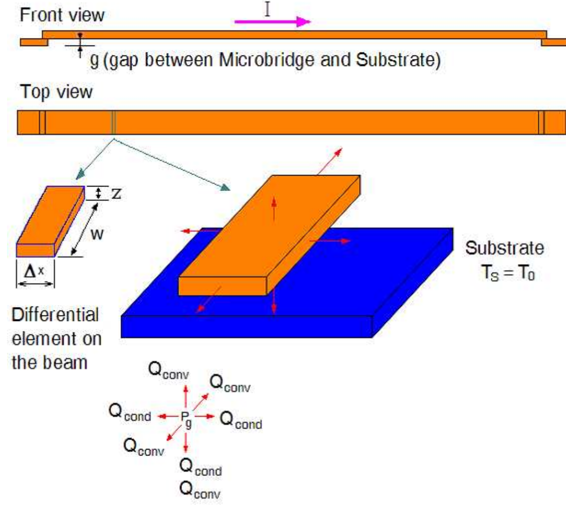

Figure 4.4: Microbridge, Joule Effect Heating, and Heat Transfer Modes

is equal to

$$\frac{dQ_{Total}}{dt} = \frac{d}{dt}\int_V \rho_m cT dV, \tag{4.12}$$

in which ρ_m, c, and T are density of the material, specific heat at constant pressure, and its temperature, respectively. From equation 4.12, the relationship for heat transfer which is even valid for an anisotropic inhomogeneous medium is derived so:

$$\rho_m c\frac{\partial T}{\partial t} = \nabla .k\nabla T \tag{4.13}$$

An anisotropic material may be modeled by treating its thermal conductivity, k, as a tensor. The tensor nature of the thermal conductivity reflects the fact that heat flux may vary with the direction in the material. As explained in the above section, k also changes over temperature for most substances. The parameters ρ_m, c, and k in an inhomogeneous material depend on position. However, polysilicon is treated as both homogeneous and isotropic. Hence, equation 4.13 is simplified, which results in equation 4.14.

$$\frac{\partial T}{\partial t} = \frac{k}{\rho_m c}\nabla^2 T = \alpha_d \nabla^2 T \tag{4.14}$$

α_d is the thermal diffusivity, which is a function of microbridge dimensions and its thermal properties. α_d is a very important parameter in evaluating and predicting

heat transfer in a medium. Equation 4.15 shows the energy balance relationship for the element of the beam displayed in figure 4.4.

$$\frac{dQ_T}{dt} = \frac{dQ_g}{dt} + \frac{dQ_{cond}}{dt} + \frac{dQ_{conv}}{dt} + \frac{dQ_{rad}}{dt} \tag{4.15}$$

The electrothermal heat generation in a microbridge is represented by $\frac{dQ_g}{dt}$, and the modes of heat transfer are denoted by $\frac{dQ_{cond}}{dt}$, $\frac{dQ_{conv}}{dt}$, $\frac{dQ_{rad}}{dt}$, respectively.

Problem conditions allow some assumptions and simplifications to be applicable to equation 4.15. The first assumption is based on the system being analyzed in *steady-state conditions*. Thus, the temperature distribution at each point of the microbridge is independent of time. The second assumption is that only one coordinate is needed to describe the spatial variations of the dependent variables. In such a *one-dimensional* system, it is assumed that temperature gradients exist along only the single coordinate direction–the length of the microbridge. Heat transfer also occurs exclusively in this direction. However, the transferred energy from a given point on the microbridge to the environment by convection depends on the rate that energy reaches the point through conduction. The energy that reaches the point by conduction is in directions other than (x)'. However, due to low thickness of the microbridge, the temperature gradients in the longitudinal direction are practically much larger than in other directions. Thus, the assumption of the one-dimensional model in the x-direction is justified, and more generally, these conditions justify treating the microbridge as an operating microstructure under *one-dimensional steady-state conditions*[3].

The electrothermal heat generation by Joule effect or resistive heating is a function of applied current and the microbridge's electrical resistance:

$$P_g = \frac{dQ_g}{dt} = IV = RI^2 \tag{4.16}$$

The polysilicon's temperature–dependent resistivity is represented in equation 4.4. The resistance of the microbridge is also a function of its physical dimensions.

$$R = \rho_e \frac{L}{A} \ (A_{(\text{beam cross-Section})} = wz) \tag{4.17}$$

$$P_g = \rho_{e(T)} \frac{\Delta x}{wz} (J(wz))^2 = \rho_{e(T)} (J^2 wz \Delta x) \tag{4.18}$$

[3]A one dimensional, steady-state heat transfer model is useful in various engineering applications. Although such a model may not match exactly in some applications, appropriate assumptions can often be made to obtain reasonably accurate results [93].

$\rho_{e(T)}$ is the electrical resistivity of the medium in temperature T. The term $\frac{dQ_g}{dt}$ in equation 4.15 shows electrothermal heat generation, the equation for which is given in 4.18.

In order to clarify the terms used in the analysis and the distinction between three modes of heat transfer, I borrow a definition for heat transfer modes from Mikheyev, narrated in "Thermal conductivity of gases and liquids" [94]. The differences between forced convection and free convection, or between conduction in gases and convection by gases are examples, which necessitate such definitions:

> The phenomenon of heat conduction exists in the exchange of energy by direct contact between particles of the body. In liquids and solids–dielectrics–the transfer of energy occurs by means of elastic waves, in gases by means of diffusion of atoms or molecules, and in metals by diffusion of electrons. Convection occurs only in liquids and gases, and occurs in the transfer of energy by displacement of particles. Both the state and the type of motion of the fluid are important. Convection is always accompanied by conduction. Thermal radiation is a process of propagation of energy in the form of electromagnetic waves. This phenomenon is different from both conduction and convection and is accompanied by a double conversion of energy, that is, heat energy is converted into radiation energy and the latter is converted back into heat energy [94].

In general, all three modes of heat transfer (conduction, convection, and radiation) can occur simultaneously. Thus, the heat equation includes three terms for heat loss and one term for electrothermal heat generation[4]. However, the effectiveness of each of these three terms for heat loss dramatically changes over temperature and operating conditions. For example, a microstructure operating in a vacuum has no effective convective heat loss, and a device operating in a relatively low temperature will not transfer considerable heat by radiation. Identifying the dominant modes of heat transfer is necessary for further simplifications and modeling, which is discussed in Section 4.4.

Conduction has two terms, one term refers to conduction inside the microbridge and another one to conduction from the lower surface of the microbridge through the air gap underneath the microbridge and toward the substrate. Fourier's law of heat conduction in solids, equation 4.14, is simplified by assuming that k is

[4]It is assumed that the initial energy of the system is canceled from the computations because the focus is on the changes of energy in the system.

constant and the heat transfer is under *one-dimensional steady-state conditions*. These assumptions result in equation 4.19.

$$Q_{cond} = -Ak\frac{dT}{dx} \tag{4.19}$$

Two terms for heat loss by conduction are given in 4.20.

$$\Delta Q_{cond} = -k_{cb}wz([\frac{dT}{dx}]_x - [\frac{dT}{dx}]_{x+\Delta x})\Delta x - k_{air}\eta w \Delta x \frac{T - T_s}{g} \tag{4.20}$$

In equation 4.20, the parameters denote the physical quantities, respectively: the microbridge's thermal conductivity by k_{cb}, the air's thermal conductivity by k_{air}, the beam's width by w, the beam's thickness by z, the substrate's temperature by T_s, the reference temperature by T_0, the excess-flow coefficient by η [50], and the air gap between the substrate and the suspended microbridge by g. The reference temperature T_0 is assumed to be equal to T_s. The excess-flow coefficient or shap factor, η, takes account of the fringing heat flux of each differential element. A computed value for k_{air} is equal to 2.60 $(\frac{W}{cm. ^\circ K})$ [27]. The relationship for the temperature–dependent conductivity of air is given $(9.97 \times 10^{-3} + 5.89 \times 10^{-5})T$ $(\frac{W}{cm. ^\circ K})$.

The first conduction term refers to conduction inside the microbridge. The microbridge has been anchored to the substrate at both its ends. The substrate has a temperature of $T_s = T_0$, which is assumed to be constant for the large thermal capacity of the substrate versus the microbridge. Therefore, the electrothermally generated heat in the microbridge has its maximum temperature at about the midpoint of the microbridge because of the microbridge's symmetry and geometry. As a result, there are two equal temperature gradients in the microbridge in opposite directions, from about the midpoint toward the two ends. The heat loss due to conduction is also along these two directions. Hence, the conducting area must be considered double that of the microbridge cross-section. In heat equations in a microbridge formulated by most previous researchers, the conducting area has been considered equal to the beam's cross section[5].

[5] In formulating heat conduction, many researchers have taken the heat conducting area to be equal to the cross section of the microbridge [50]. However, the heat-conducting area in the microbridge must be taken to be double that of the beam cross-section because the maximum temperature at the mid point of the microbridge would result in heat conduction from the midpoint toward the two ends. Therefore, the integrals' limits must be between the minimum and the maximum temperature and over half of the length of the microbridge that experiences these two temperature extremes'. In heat transfer by conduction modeling in the PhD thesis of Masterangelo, the beam's

The second term of heat loss by conduction is a heat exchange between the surfaces of the microbridge underneath and the substrate through the air gap. The very small thickness of the air gap conducts heat loss through the "trapped air" to the substrate. As the air gap is changing above the buckling temperature, the conductive heat loss through the "trapped air" changes as well. The heat exchange is mostly radiative when the air gap separating the faces is quite wide, which occurs when the beam has buckled. The heat exchange is a combination of conduction and convection when the two surfaces are more closely spaced. To examine the significance of the effect of a varying air gap, two analyses are considered [61]. In one, the gap is assumed to be constant, and the maximum deflection of the microbridge is computed. In the second, the result of the first analysis, the maximum buckling amplitude is applied to calculate an average air gap 4.21. This calculated average air gap is used to derive a new maximum buckling amplitude. The air gap is maximum at the microbridge's midpoint and almost linearly decreases, for example, to a minimum of 2 microns at the microbridge's ends, in a fabricated microbridge by PolyMUMPs. Therefore, an average air gap is computed so:

$$g_{ave} = g_{min} + \frac{g_{max}}{2} \tag{4.21}$$

The heat loss by **convection** is derived from Newton's Cooling Law, equation 4.22.

$$Q_{conv} = -hA(T - T_0) \;\Rightarrow\; \Delta Q_{conv} = 2h(w + z)\Delta x(T - T_{air}) \tag{4.22}$$

The convective heat transfer coefficient is $h(u, P)$, the unit of which is $\frac{Watt}{m^2.K}$. It is a function of u and P, the velocity and absolute pressure of air flow, respectively. The value of h is derived experimentally from Nusselt's parameter, Nu [60]. The Nusselt's parameter also depends on R_e, Reynold's number, P_r, Prandtl's number, and G_r, Grashoff's number. Reynold number, R_e, has the most effective role in the value of h. Nevertheless, the value of h has been derived experimentally; typical ranges are shown in table 4.4 [95]. However, an important point is that the heat

---

cross-section has been taken as the heat conducting area [50]. Masterangelo's work has been referenced by many other researchers following the same assumption that the heat conducting area is equal to the beam's cross section (Lin et al. [59], [58], [57], Wang [56], Motamedi [60], Amarendra Atre [61]). Assuming the heat conducting area is equal to the beam cross section, the computed value for heat conduction from this assumption can still give a correct result because the integral is over the whole length of the microbridge rather than half of its length. Although the analytical calculation over the range of integration produces a correct result, the assumed heat conducting area in the microbridge equal to the cross section of the microbridge does not seem to be correct.

Table 4.4: Typical Values of Convective Heat Transfer Coefficient h

Type of Flow	**Heat Transfer Coefficient** h $(\frac{W}{m^2.\,^{\circ}C})$
Free convection	$6 - 28$
Turbulent forced convection inside pipes	
Air	$6 - 570$
Water	$284 - 17,000$

transfer in the solid-air is by conduction, and the energy is then transferred away by convection through moving air. For a thin beam, an assumption of an equal temperature on the beam's surface along the width of the microbridge is applicable. Computing the convective coefficient h shows whether the conduction or convection by air is dominant. In order to estimate the value of h from the problem conditions in a microbridge, the procedure advised in heat transfer analysis is followed [93]. Using the relationship for the Grashoff's number, and assuming that the range of temperature is between $300\,^{\circ}C \rightarrow 800\,^{\circ}C$, the convective coefficients computed for an infinite flat plate at different temperatures are given in table 4.5 [1],

$$G_{r_L} = \frac{g_m \beta (T_b - T_\infty)}{\nu^2} \tag{4.23}$$

in which, g_m is gravitational acceleration, β is the volumetric expansion coefficient, L is the characteristic length, ν is the viscosity, T_b and T_∞ are the temperatures at the surface of the microbridge and ambient, respectively. It is assumed that $T_\infty = T_0$, and T_0, which is the reference temperature, are constant. Equation 4.23 represents a ratio and a measure of buoyancy to viscous forces acting on a fluid. This number establishes a criterion of whether conduction or convection by air is dominant. For example, if the force due to gravitation is negligible versus viscous forces, the air layer in the air gap conducts heat, rather than transferring heat by convection because viscous forces are strong enough to prevent air motion in the gap [1]. The computed values for h in table 4.5 are assumed to be valid for a buckling microbridge operating at the same range of temperature.

The main difference between a **radiant mode** of heat transfer and the two previously mentioned modes is that radiation is proportional to the fourth power of the absolute temperature; however, conduction and convection are linearly proportional to temperature differences. Radiant energy transfer occurs regardless of whether the medium is a fluid or vacuum. For the microbridge in figure 4.4, the heat loss by radiation can be from the side and top surfaces to the surrounding air

Table 4.5: Convective Coefficients h for an Infinite Flat Plate at Different Temperatures

Temperature (K)	**Convective Coefficient h ($\frac{W}{m.^\circ K}$)[1], [93]**
300	1101.7
400	1214.3
500	1381.0
600	1520.7
700	1660.3
800	1799.9

and from the lower surface to the substrate. Equation 4.24 gives the term of heat transfer by radiation.

$$Q_{radiation} = \sigma_b(w + 2z)\Delta x(T^4 - T_{air}^4) + \sigma_b w \Delta x(T^4 - T_S^4) \tag{4.24}$$

The Stefan-Boltzmann constant is $\sigma = 5.6697 \times 10^{-8}(\frac{W}{m^2.^\circ K^4})$. The constant is independent of medium, surface, and even temperature. A *black body* which is an *ideal emitter*, radiates according to equation $E_r = \sigma A T^4$. The radiation by all other surfaces, which are not a black body, is less than that obtained from the Stefan-Boltzman equation. This fact requires a modified Stefan-Boltzamnn constant to be used in equation 4.15: $\sigma_b = \epsilon\sigma$. The emissivity of a surface, ϵ, is specific to that surface and has a value between zero and one. In equation 4.24, T_{air} and T_S are the temperatures of the surrounding air and the temperature of the substrate, respectively. Given that the substrate has considerably larger thermal capacity in comparison with the microbridge, the ambient temperature and the substrate temperature are assumed to be equal and equal to the reference temperature: $T_s = T_0 = T_{air}$

4.4 Temperature Distribution in a Microbridge

As outlined in the above introduction, identifying the terms in heat transfer equations that are negligible facilitates problem solving. Some assumptions are made based on the problem conditions for an average temperature. Then various terms in heat loss are computed and compared. This practice is continued in an iterative manner. At high temperatures, the convective and radiative loss can be more

effective in heat dissipation. If these two terms, losses due to convection and radiation, are not included in modeling, the functionality predicted by the model of the device may have significant discrepancy with the actual performance [4]. Furthermore, it is expected that surface-dependent heat transfer phenomena such as radiation and convection become more appreciable in microscale. This possibility is a consequence of the increase of the surface to volume ratio when the dimension is scaled down as discussed in Chapter 3.

However, in most prior investigations on an electrothermally heated microbridge, conduction has been considered as the dominant mode of heat loss. Comparing computed values from equations 4.19, 4.22, and 4.24 also shows that conduction has the dominant role in heat loss [58], [55], [60]. Mastrangelo and Muller in their analysis of the microbridge's electrothermal behavior first assumed that two terms, free convection and radiation, are negligible and then confirmed their assumption by computation [54]. However, the range of temperature, $150\,^{\circ}C \rightarrow 300\,^{\circ}C$, they considered in their work is far less than the operating temperature of the microactuating techniques in this research ($300\,^{\circ}C$ versus $750\,^{\circ}C$). Their assumptions for the terms to be negligible were also correct because the microbridge in their work was covered with heat insulating layers, silicon Nitride, and the average operating temperature was relatively low. Conduction is the dominant mode of heat loss if the given temperature is not too high. Assuming that in actuation applications the average temperature usually does not exceed $600\,^{\circ}C$, the heat loss by infrared radiation is negligible [60].

The above discussions suggest an iterative investigation. By neglecting infrared radiation, a model for heat transfer is considered including both convective and conductive terms along with a term for electrothermal heat generation. The derived temperature distribution can be later applied in equation 4.24 to compute the radiation term, whether or not the assumed neglect was accurate. Axial conduction along the microbridge, conduction between substrate and the down surface of the microbridge, and convection from the perimeter are assumed as heat loss modes. From the above assumptions and the equations 4.18, 4.19, 4.20 and 4.22,

$$Q_x = Q_{cond} + \Delta Q_{air-cond} + \Delta Q_{conv} + P_g \tag{4.25}$$

$$\Delta Q_{air-cond} = k_{air}\eta w \Delta x \frac{T - T_s}{g} \tag{4.26}$$

$$\Delta Q_{conv} = 2h(w + z)\Delta x(T - T_{air}) \tag{4.27}$$

$$Q_{x+\Delta x} = [k_{cb} w z \frac{dT}{dx}]_{x+\Delta x} \tag{4.28}$$

$$Q_x = [k_{cb} w z \frac{dT}{dx}]_x \tag{4.29}$$

$$\lim_{\Delta x \to 0} \frac{Q_{x+\Delta x} - Q_x}{\Delta x} = \frac{d}{dx}(k_{cb} w z \frac{dT}{dx}) = k_{cb} w z \frac{d^2T}{dx^2} (\text{Assumed } k_{cb} \text{ is constant}) \tag{4.30}$$

$$k_{cb} w z \frac{d^2T}{dx^2} = k_{air} \eta w \frac{T - T_s}{g} + 2h(w+z)(T - T_{air}) - \rho_{e(T)}(J^2 w z) \tag{4.31}$$

Assumption of $T_s = T_{air} = T_0$, which is also applied in equation 4.22, is justified by the fact that the substrate has a large thermal capacity versus the microbridge.

$$m^2 = -\frac{\rho_0 \xi . J^2}{k_{cb}} + \eta \frac{k_{air}}{k_{cb} z g} + \frac{2h(w+z)}{k_{cb} w z} \Rightarrow m = \sqrt{\eta \frac{k_{air}}{k_{cb} z g} + \frac{2h(w+z)}{k_{cb} w z} - \frac{\rho_0 \xi . J^2}{k_{cb}}}$$

$$\frac{d^2T}{dx^2} - m^2(T - T_0) = \frac{\rho_0 J^2}{k_{cb}} \tag{4.32}$$

Equation 4.32 is a linear, but non-homogeneous, second-order differential equation with constant coefficients. Equation 4.32 is modified to be in a homogenous form. By substituting a new variable, $\acute{T} = T - T_0 - \frac{\rho_0 J^2}{k_{cb} m^2}$ in 4.32, and using equation Eq420, equation 4.33 is derived as follows:

$$\frac{d^2\acute{T}}{dx^2} - m^2 \acute{T} = 0 \tag{4.33}$$

The general solution of 4.33 is given in 4.34.

$$\acute{T} = C_1 \exp^{mx} + C_2 \exp^{-mx} \tag{4.34}$$

Constants C_1 and C_2 are derived by applying the boundary conditions of the microbridge. The mid point of the beam has the maximum temperature, and both ends' temperatures are T_0. The boundary conditions as shown in figure 4.4 are

$$T(x=0) = T(x=L) = T_s = T_0 \;\; (L \text{ is the length of the microbridge}) \tag{4.35}$$

$$(x = \frac{L}{2} \Rightarrow \frac{d\acute{T}}{dx} = 0) \text{ and } (x = 0 \Rightarrow \acute{T} = \acute{T}_0) \tag{4.36}$$

$$C_1 = \frac{-\rho_0 J^2 \exp^{-\frac{mL}{2}}}{k_{cb} m^2 (\exp^{\frac{mL}{2}} + \exp^{-\frac{mL}{2}})} \Leftrightarrow C_2 = \frac{-\rho_0 J^2 \exp^{\frac{mL}{2}}}{k_{cb} m^2 (\exp^{\frac{mL}{2}} + \exp^{-\frac{mL}{2}})} \tag{4.37}$$

Therefore, from equations 4.36, 4.37 and $\acute{T} = T - T_0 - \frac{\rho_0 J^2}{k_{cb} m^2}$, the relationship for temperature is derived.

$$T - T_0 = (\frac{\rho_0 J^2}{k_{cb} m^2})(1 - \frac{\cosh m(\frac{L}{2} - x)}{\cosh m(\frac{L}{2})}) \tag{4.38}$$

In equation 4.38, m is

$$m = \sqrt{\eta\frac{k_{air}}{k_{cb}zg} + \frac{2h(w+z)}{k_{cb}wz} - \rho_0\xi.J^2k_{cb}} \tag{4.39}$$

Equation 4.39 shows that the maximum temperature results when $\cosh m(\frac{L}{2} - x)$ is minimum. Equation 4.39 is minimized, if $x = \frac{L}{2}$ is satisfied, which confirms the primary estimation.

$$x = \frac{L}{2} \Rightarrow T_{max} - T_0 = (\frac{\rho_0 J^2}{k_{cb}m^2})(1 - \frac{1}{\cosh m(\frac{L}{2})}) \tag{4.40}$$

The average temperature over the microbridge is derived from equation 4.31

$$T_{average} = \frac{\int_0^{\frac{L}{2}} Tdx}{\frac{L}{2}} = \frac{\rho_0 J^2}{k_{cb}m^2} - (\frac{2}{Lm})(\frac{\rho_0 J^2}{k_{cb}m^2})tanh(mL/2) + T_0 \tag{4.41}$$

The assumption for Steady-State conditions removes the initial condition requirement.

4.5 Summary

Knowledge on heat generation and distribution in a microbridge is a requirement in predicting force and displacement. This chapter formulates temperature distribution in an electrically driven microbridge by deriving governing equations on electrothermal heat generation, heat loss, and heat distribution in the microbridge. The structural material's electrothermal properties are also taken into account. The studied structural material is polysilicon; however, the process of analysis is applicable for any other structural material, including those materials that are more suitable for METMA, nickel, for example, because of their larger thermal expansion. The electrothermal properties of the structural material include the electrical resistivity, thermal conductivity, specific heat, and thermal expansion coefficient, which are mostly nonlinear functions of temperature. The significant variations of electrothermal properties of the structural material over temperature and the appreciable changes these variations may cause on predicted functionality for a microactuator are discussed.

The derived relationships for electrothermal behavior of the structural material are inserted in the heat transfer equation. In identifying negligible terms of heat loss

in the heat equation, neglect of nonlinearity in varying resistivity and assumption of a constant value for thermal conductivity are necessary simplifications. Recognition of dominant terms in heat loss is a major step prior to the problem solving. The heat transfer equation is formulated by including all significant terms of heat loss, heat generation, and thermal capacity of the system. Changing the variables converts the derived non-homogeneous equation to a homogeneous equation. Applying boundary conditions results in a complete solution with known coefficients for temperature distribution over the microbridge.

Chapter 5

Thermoelastic Actuation

5.1 Introduction

Very few MEMS products are found whose functionalities are not dependent on the elastic behavior of their structural material. In fact, elastic deformation is the operating principle in both MEMS sensors and MEMS actuators. Various physical phenomena can cause an elastic deformation in a structural material, which is converted to either a signal in sensors or a displacement in actuators. For example, a magnetostrictive material in a magnetic field experiences deformation and produces force and displacement; a piezoelectric material in an electric field generates force and displacement; an accelerometer or a rate gyro senses force by the elastic deformation of its structural material and produces signals proportionally. In thermal microactuators, thermal effects cause force and displacement. Characterizing a thermal microactuator, which uses a buckling microbridge as the actuating element, requires a thorough analysis from various aspects outlined in the following sections: thermomechanical properties of the structural material, i.e., polysilicon; a microbridge deflection analysis; thermal stress and buckling.

Studying the mechanical properties is required to identify the elements of the material's behavior: the material's ability to recover its original shape after being deformed; the limits beyond which permanent deformation or fracture may occur; the relationship governing applied stress and produced strain. These elements of a material's behavior are, in fact, the design parameters in a thermal microactuator. This study also includes the temperature dependency of these mechanical properties, which are important in formulating the thermoelastic changes in the material. Examples include the temperature dependency of the modulus of elasticity, the fracture strength, fatigue, plasticity, and creep of the material. Formulated

thermomechanical properties are applied in modeling thermoelastic deflections of the microbridge, which are discussed in Section 5.3 and Section 5.4. However, the thermomechanical properties of thin films, i.e., polysilicon, are variable over the conditions in the fabrication process. Furthermore, there is a limitation in taking a specimen from fabricated microstructures, polysilicon films, for example, in order to measure their mechanical properties. Consequently, a range of different reported values for the polysilicon's thermomechanical properties have been published.

Section 3, Microbridge Deflection Analysis, presents a brief review of deriving equations for microbridge deflections. Both conditions in which a microbridge is subjected to large and small deflections are studied. In most problems, the assumption of small deflection is accurate enough to simplify the deflection equations and their solution. However, when a microbridge experiences large deflections or when the deflections are in the non-linear region of the elastic deformation, the approximated equation and solution are not applicable. In these conditions, the problem, which is also known as the Elastica problem, is solved by advanced mathematical techniques. Elliptical integrals are used to derive the exact solution. Nevertheless, there are also some approximate methods giving accurate enough results for most applications. One of these techniques is shown in Section 5.4.

A thermal stress, an axial force, a lateral force, or a bending moment can cause buckling or deflection in a fixed-fixed microbeam. An electrothermally heated microbridge experiences a thermal stress. If the thermal stress in a microbridge exceeds a certain limit, buckling occurs. This status is similar to the conditions in which a fixed-fixed microbeam is under axial force. In Section 4, using the results from previous sections and assuming that thermal stress is the only effective force in a microbridge, the microbeam deflection equation is derived. Applying boundary conditions on the derived equations results in a relationship with known constants. Then the buckling conditions are discussed by evaluating the derived relationships. The temperature and the critical stress in the microbridge at which buckling occurs are also computed.

The above paragraphs introduce the contents of this chapter, which are outlined in the following sections. The results in each section are fed into the equations in the next section, facilitating formulations in thermoelastic analysis. These investigations produce a model for out-of-plane buckling and thermoelastic actuation of a microbridge, which is used as the actuating element in various designs.

5.2 Polysilicon Thermomechanical Properties

As discussed in Section 4.2, polysilicon is not the only structural material used in the fabrication of MEMS, neither is it the most suitable one for the design and fabrication of the proposed microactuating technique in this research, METMA. However, except for the low thermal expansion coefficient, most thermomechanical properties of polysilicon are favorable for thermal microactuators and thermomagnetic microactuators, METMA, as well. Advantages include its large modulus of elasticity, which is comparable to steel's; polysilicon is even superior to steel for withstanding fatigue failure. However, the thermomechanical properties of polysilicon's films largely depend on the fabrication process. There is also a limitation in taking a specimen of the thin film material for testing and measurement. In fact, many difficulties exist in measuring material properties of thin films, which are not present with bulk materials. Therefore, unlike bulk materials, which usually have clear and exact physical properties, there is a range of reported values for the mechanical properties of a thin film, i.e., polysilicon (table 5.2). In this section, some selected features of polysilicon applicable in thermoelastic actuation are discussed: stress–strain in polysilicon, temperature–dependent elastic properties, and residual stress.

Almost no plastic or creep region in polysilicon stress–strain's curve below a certain temperature is observed. Consequently, polysilicon microstructures can withstand fatigue failure when subjected to high cyclic load. However, polysilicon is a brittle material that will yield when a stress beyond its yield limit, i.e., fracture strength, is applied. The slope of the stress-strain curve in its linear region is the modulus of elasticity and denoted by E. Polysilicon is assumed to be both homogeneous and isotropic, which is reasonable for its polycrystalline structure, which is annealed at high temperature. By definition, a material is isotropic if the elasticity constant, E, is independent of the direction; a material is homogeneous if the elasticity constant does not depend on the location in the material. The assumption of a homogeneous and isotropic material simplifies the problem by reducing the constitutive property tensors, modulus of elasticity E, to a scalar quantity. The reported results for polysilicon strength in literature ranges from 1 to 4 GPa (LaVan and Buchheit [96]). The variations between reported values by different authors have been explained in terms of micro-structural differences due to deposition conditions, sample size effects, and release processing. In polycrystalline materials, the fracture strength is dependent upon two factors, the grain size, d, and the fracture surface energy, γ_S. Griffith's equation shows the fracture strength,

σ_f, of a material.

$$\sigma_f = \sqrt{\frac{4E\gamma_S}{\pi d}} \tag{5.1}$$

For small-grained polycrystals, the energy needed to fracture a grain surface is smaller, but this energy increases with grain size. For example, the annealing process, which decreases dislocations and increases the grain size, will cause the fracture strength to be higher. As a result, larger grains will be stronger due to the increased energy needed to produce a crack across the material. In several studies, the mean fracture strength of polysilicon has been found to be between 2 to 3 GPa, which is clearly less than that of a single crystal silicon [97]. Sharpe et al. have conducted research reporting the results of 48 tests on five different sets of PolyMUMPs specimens [98]. The derived material properties are as follows: Young's modulus $\rightarrow 169 \pm 6.15$ GPa, Poison's ratio $\rightarrow 0.22 \pm 0.011$, and tensile strength $\rightarrow 1.20 \pm 0.15$ GPa. Sharpe and Bagdahn have also experimentally determined values for polysilicon's mechanical properties in another set of tests [99]. The results are slightly different from their own previous tests on the same polysilicon. Bin Yuan in his PhD thesis, "Mechanical Testing of Microsamples from Weldments and MEMS," has investigated the mechanical properties of some structural materials including polysilicon [100]. His studies demonstrate the following mechanical values, for polysilicon: Young's modulus of 169 ± 6 Gpa, tensile strength 1.2 ± 0.15 Gpa, and Poisson ratio 0.22 ± 0.01. However, some different values are also suggested in other works. Lavan and Buchheit worked on polysilicon fabricated in Sandia's Microelectronic Development laboratories [96]. They derived an average value of 2.24 Gpa, with a standard deviation of 0.35 Gpa among the number of measurements on different samples.

However, the mechanical strength of a designed microstructure does not depend only on Yield strength; the geometry is also an effective parameter. For example, there is a requirement for inserting etch holes in large area polysilicon components. Etch holes are required to facilitate release of the microcomponents after fabrication. The requirement has become a mandatory design rule for microfabrication technologies. However, implementing these etch holes modifies mechanical properties of the structural material, i.e., polysilicon, significantly. Sharpe et al. have investigated the effect of etch holes on the mechanical properties of polysilicon [101]. In their work, they have shown the appreciable effect of etch holes on reducing the strength of the polysilicon in comparison to the same solid components without etch holes. This fact requires a designer to take into account the effect of inserting etch holes if they are required on the designed microbridge.

Temperature–dependent elastic properties of polysilicon have been investigated

by a number of researchers, who report results with slight differences. Polysilicon at temperatures above 925 $°C$ begins to exhibit plastic deformation [33]. This temperature is called the ductile-brittle transition (DBT) temperature. Above the DBT temperature, plastic deformation will occur. Research by Sharp et al. shows that polysilicon thin films deform inelastically at temperatures above 750 $°C$ [102]. However, Rybicki and Pirouz have reported that polysilicon continues to behave in a linear brittle manner at 540 $°C$ with increasing stress but begins to deform nonlinearly at 770 $°C$ (61.973 % TM)[1] with increasing stress [103], [2]. The Young's modulus decreases with increasing temperature [104], and a small temperature dependence for a modulus of elasticity is predicted [33].

$$E = E_0(1 + \iota\Delta T) \quad (290\,°K \rightarrow 550\,°K) \tag{5.2}$$

The value of ι, which is the temperature coefficient of a normalized modulus, is equal to -3.7×10^{-5} ($°K^{-1}$) and is given for boron-doped Silicon. For phosphorous-doped polysilicon in PolyMUMPs, this value might be different. However, the given value can be considered as a rough estimation in this application. Research on MEMS components operating at high temperatures also shows that the reliability is greatly affected: the MEMS components operating at high temperatures are vulnerable to creep-deformation upon actuation. Nevertheless, fatigue is not the leading factor in the failure of moving MEMS components made of polysilicon (Allameh) [104].

Residual stress is among the properties that are largely dependent on the fabrication process. In thin films, residual stress is mostly compressive, but it can be controlled by pressure and temperature at the deposition, or by annealing the films at high temperature, for example. This possibility is important because in micromechanical structures made of polysilicon, the residual stress in the films can considerably affect the performance of the microstructure. However, for the same deposition conditions, thick polysilicon films have lower residual stress than thin ones.

The values for mechanical specifications of polysilicon reported from experiments by some selected resources are summarized and compared in table 5.2. The polysilicon in these experiments is either the same polysilicon used in PolyMUMPs or a similar heavily doped polysilicon.

The discussion in this section reviews the dominant elastic properties of the structural material, i.e., polysilicon, and their variations over temperature that are determining factors in a microactuator design. The linear region of changes in the stress-strain curve of polysilicon is of the most interest of a microactuator designer.

[1]TM stands for Melting Temperature of polysilicon.

Table 5.1: Selected Typical Polysilicon Mechanical Properties

	MEMSCAP-PolyMUMPs [92]	Sharpe etal [99]
Young's Modulus (GPa)	158 ± 10	
Fracture Strength (GPa)	$(1.21 \pm 0.8) \rightarrow (1.65 \pm 0.28)$	1.10 ± 0.01
Poisson's Ratio	0.22 ± 0.01	
Residual Stress (MPa)	$P_1(-10), P_2(-10), M(50)$	
	Gad-el-Hak [90]	Sharpe et al. [105]
Young's Modulus (GPa)	160	170 ± 6.7
Fracture Strength (GPa)	$1.2 - -3.0$	1.21 ± 0.16
Poisson's Ratio	0.22	
	Yuan [100]	Sharpe et al. [98]
Young's Modulus (GPa)	169 ± 6	169 ± 6.15
Fracture Strength (GPa)	1.2 ± 0.15	1.20 ± 0.15
Poisson's Ratio	0.22 ± 0.01	0.22 ± 0.011
Residual Stress (MPa)		

In fact, the temperature dependency of these thermomechanical properties must be taken into account because of the significant changes of these properties with temperature.

5.3 Microbridge Deflection Analysis

Microbeams are the most used components in MEMS. Thus, beam deflection analysis is a requirement in most MEMS designs. The deflection analysis of a microbridge is not different from a deflection analysis of a microbeam in general. Applying the boundary conditions of a fixed-fixed microbeam on the general equation of a microbeam deflection results in a relationship for a microbridge's deflection curve. The fixed ends conditions make the problem of a microbridge statically indeterminate, which means that static equations are not enough to solve the problem. In other words, the number of unknowns is more than the number of equations definable by applying static laws. For example, for the microbridge shown in figure 5.1, two reactions and two reactive moments at the fixed ends make four unknowns. If the pressure on the microbeam is known, four successive integrations are required to find the curve equation. These four successive operations add four more unknown constants of integration. Therefore, further to relationships derived from known

boundary conditions, equations of a beam's elastic deformations are also applied in finding additional unknowns. This section reviews large and small microbridge deflections and derives the general form of a microbeam deflection. In deriving the

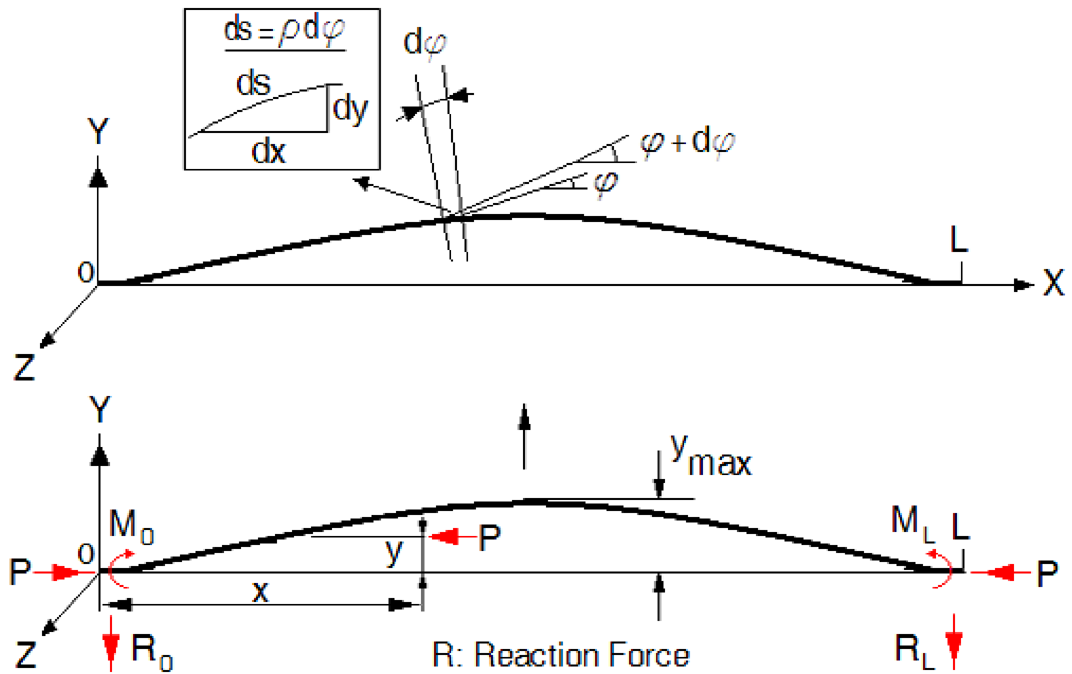

Figure 5.1: Buckling Microbridge Experiences, P, Thermally-induced Axial Force.

curve equation of a microbeam, the conventional approach suggests the following three steps:

- First, the effective forces and moments are recognized and displayed on a diagram.
- Second, using Hook's law, the general form of the beam's elastic deformation is derived.
- Third, applying boundary conditions, the unknown coefficients are identified.

Figure 5.1 depicts a buckling fixed–fixed microbeam experiencing an axial force. A thermally–induced stress in a microbridge similarly produces an axial force, which will be discussed in Section 5.4. The figure also shows the effective forces and moments on the microbridge. In this figure, the axial force, which is denoted by P,

is causing moment, $M(x)$, on the microbridge[2]. In the following, a review of deriving relationships between deflections and moments affecting the beam is outlined.

$$ds = \sqrt{dv^2 + dx^2} = dx\sqrt{1 + (\frac{dv}{dx})^2} = \rho d\varphi \;\Rightarrow \frac{1}{\rho} = \frac{d\varphi}{ds} = \frac{d\varphi}{dx}\frac{dx}{ds} \tag{5.3}$$

$$\tan\varphi = \frac{dv}{dx} \;\Rightarrow\; \varphi = \arctan\frac{dv}{dx} \;\Rightarrow\; \frac{d\varphi}{dx} = \frac{\frac{d^2v}{dx^2}}{(1 + (\frac{dv}{dx})^2)} \tag{5.4}$$

The above–derived equations are valid when the microbridge's deflection, $v(x)$, is in the xy plane. In beam equations, y and dy are usually replaced by v and dv respectively. This is according to convention; it is also to emphasize the beam deflection versus its coordinates. Some applicable terms in deriving beam equations are introduced: the moment of inertia of a beam's cross-section about an axis parallel to z-axis passing in the cross-section, and the Modulus of elasticity of the beam are denoted by I and E. In a homogenous beam with a constant cross-section, EI or flexural rigidity is constant. The assumptions that polysilicon is a homogenous material and that the microbridge has a constant cross-section result in the flexural rigidity, EI, to be constant. Equations 5.3 and 5.4, and the relationship for bending moment, $\frac{1}{\rho} = -\frac{M}{EI}$, are used to formulate exact and approximate deflections, equations 5.5 and 5.6 respectively. This formulation is used in the modeling of a microbridge, in the next section and the next two chapters.

$$\frac{1}{\rho} = \frac{\frac{d^2v}{dx^2}}{(1 + (\frac{dv}{dx})^2)(\frac{1}{(\sqrt{1+(\frac{dv}{dx})^2})})} \;\Rightarrow\; \frac{1}{\rho} = -\frac{M}{EI} = \frac{\frac{d^2v}{dx^2}}{(1 + (\frac{dv}{dx})^2)^{\frac{3}{2}}} \tag{5.5}$$

Equation 5.5 gives an exact value for the microbridge's deflection that is valid for large slopes and deflections. In order to derive buckling amplitude and large deflections of the beam, full nonlinear equations governing the elastic microbridge must be solved. However, a microbridge's deflections in its elastic region are usually very small, and the assumption of small deflections is applicable. The elastic region includes stresses below the proportional limit on the beam's strain-stress curve. The assumption on small deflections applies to simplify equation 5.5.

$$\frac{1}{\rho} = -\frac{M}{EI} = \frac{d^2v}{dx^2} \tag{5.6}$$

[2]Sign attributions to forces and moments depend on the microbridge's concave–shaped direction, which is caused by that force or moment. If the generated concave shape is toward the positive direction of the y-axis, the sign is considered positive; otherwise, it will be designated negative. For example, a compressive axial force is signed negative, but a tensile force is considered positive.

As shown in equation 5.6, the term $\frac{d^2v}{dx^2}$ is considered to be very much smaller than 1 and negligible. This is true when the slope in any given point of the microbridge is small resulting in $\tan\varphi \approx \varphi$. Double differentiating of equation 5.6 results in the relationship between beam curvature and experienced pressure.

$$\frac{d^2}{dx^2}(EI\frac{d^2v}{dx^2}) = -\frac{d^2M(x)}{dx^2} \tag{5.7}$$

Equation 5.7 can be written in a more general form, as shown in 5.8.

$$\frac{d^2}{dx^2}(EI\frac{d^2v}{dx^2}) + P\frac{d^2v}{dx^2} = F \tag{5.8}$$

in which, F is given

$$F = -q - \frac{d^2M(x)}{dx^2} \quad (q \text{ is the lateral pressure on the microbridge}) \tag{5.9}$$

After deriving a static equation for the microbridge, the second step is to derive relationships between forces and produced deflections. The most important stage in this part of the analysis is to derive an equation for $M(x)$, moments on the beam as a function of the position. Having derived such a relationship for $M(x)$, two successive integrations on $M(x)$ lead to a deflection equation with two integration constants. In the third step of the analysis, boundary conditions apply, which results in the microbridge's curve or deflection equation. In the next section, the thermally induced stress is considered as the only acting force in a microbridge, and the curve equation for the buckling microbridge is derived. Then, the buckling conditions, including critical temperature and buckling load, are computed.

5.4 Thermal Stress and Buckling

Non-equal temperature distribution or a temperature increase in a mechanically confined microstructure produces stress, which is called thermal stress. Thermal stress can cause elastic deformation when the stress is under the proportional limit. By exceeding above the proportional limit, the thermal stress may lead to plastic deformation or fracture as discussed in Section 5.2. An electrically heated microbridge creates compressive thermal stress, which is temperature dependent. Upon reaching a critical value, the microbridge buckles; however, depending on the stress and the microbridge conditions, the microbridge's behavior is different before, during, and after buckling. The fixed-fixed microbeam buckles in the plane in which it

has the least, EI, flexural rigidity. In the configuration shown in figure 5.1, the microbridge has a thickness much smaller than its width, so a microbridge buckles out of plane when it experiences stress equal to or greater than the buckling condition. In this section, thermoelastic behavior of a fixed-fixed microbeam is formulated to derive relationships of force and displacement for linear and nonlinear deflections. Formulating of the linear deflections under thermal stress is considered in three steps: deriving a thermoelastic equation for a microbridge by using results from the previous section; solving the derived equation by applying the boundary conditions; computing the critical values of the buckling temperature, buckling load, and maximum deflection.

- In the first step, the microbridge's thermoelastic behavior is formulated, which is a relationship for the microbridge's temperature–dependent curve. A Duhamel-Neumann equation is a modified Hook's law that includes temperature dependent terms in elastic equations. Relationship 5.10 shows the general form of the Duhamel-Neumann equation. [80].

$$\sigma_{ij} = 2\mu\epsilon_{ij} + \lambda\delta_{ij}\epsilon kk - \delta_{ij}k_{eb}(3\lambda + 2\mu)(T_{avg} - T_0) \tag{5.10}$$

The parameters represent physical quantities in the microbridge: average temperature by T_{avg}; the reference temperature[3] by T_0; stress components by σ_{ij}; Lame's constants by λ and μ; strain components by ϵ_{ij}; and the thermal expansion coefficient for the microbridge by k_{eb}. The temperature distribution obtained from Chapter 4, equation 4.41 or 4.38, is inserted in the thermoelastic equations. Forces and moments, other than the ones produced by the thermally induced stress, can also be included in equation 5.10. However, representing a microbridge in a *One-Dimensional Model* makes the stresses and strains in the two other dimensions zero and simplifies the Duhamel-Neumann equation results in the given equation 5.11.

$$\sigma = E\epsilon - k_{eb}E(T_{avg} - T_0) \tag{5.11}$$

In equation 5.11, E is a modulus of elasticity, σ is the stress along x-axis, and ϵ is the strain.

$$\sigma = \frac{P}{A} \;\Rightarrow\; P = A(E\epsilon - k_{eb}E(T_{avg} - T_0)) \tag{5.12}$$

$$\epsilon = \frac{L - L_0}{L_0} \tag{5.13}$$

[3] At the uniform reference temperature T_0, the material is assumed to be stress-free.

The thermal stress in equation 5.12 is the only force acting on a microbridge, P, which is an axial force. As no lateral pressure exists, $q = 0$, the expression for the moment term, $M(x)$, is derived from the relationship in 5.9.

$$M(x) = -Pv \;\Rightarrow\; (\frac{d^2M_z(x)}{dx^2})_T = -P\frac{d^2v}{dx^2} \tag{5.14}$$

$$\frac{M}{EI} = \frac{d^2v}{dx^2} \;\Rightarrow\; \frac{d^4v}{dx^4} + \frac{P}{EI}\frac{d^2v}{dx^2} = 0 \;\text{ (assuming small deflections)} \tag{5.15}$$

$$k'^2 = \frac{P}{EI} \;\Rightarrow\; \frac{d^4v}{dx^4} + k'^2\frac{d^2v}{dx^2} = 0 \tag{5.16}$$

The general solution for equation 5.16 is shown in 5.17, in which B_1, B_2, B_3 and B_4 are constants with their individually different physical meanings. [65].

$$v(x) = B_4 + B_3x + B_2\cos k'x + B_1\sin k'x \tag{5.17}$$

- In the second step, the boundary conditions, which are given in 5.18, are applied on the equation derived in the previous step.

$$v(0) = v(L) = 0;\; (\frac{dv}{dx})_{x=0} = (\frac{dv}{dx})_{x=L} = 0 \tag{5.18}$$

$$B_2[(\cos k'L - 1)^2 + \sin k'L(\sin k'L - k'L)] = 0 \;\Rightarrow$$

$$B_2\sin\frac{k'L}{2}(\sin\frac{k'L}{2} - \frac{k'L}{2}\cos\frac{k'L}{2}) = 0 \tag{5.19}$$

The nontrivial solution, i.e., a solution where $B_n \neq 0$, which is also called an eigenvalue problem, is given in 5.20.

$$\sin\frac{k'L}{2} = 0 \;\Rightarrow\; \frac{k'L}{2} = n\pi \;\; (n = 1, 2, ...) \;\Rightarrow\; k'^2 = \frac{P}{EI} = \frac{4n^2\pi^2}{L^2} \tag{5.20}$$

using the results from equations 5.17 to 5.22, the microbridge's curve relationship is derived, 5.21, with B_2 undetermined.

$$V(x) = B_2(1 - \cos\frac{2\pi x}{L}) \tag{5.21}$$

- In the third step, from the derived solution in 5.20, the buckling temperature, buckling load, and maximum deflection are computed.

$$P_n = \frac{4n^2\pi^2EI}{L^2} \;\; (n = 1 \text{ results in the min load}) \Rightarrow P_{cr} = \frac{4\pi^2EI}{L^2} \tag{5.22}$$

From a one-dimensional Duhamel-Neumann equation, 5.11, by setting the Poisson ratio equal to zero, a relationship for P, 5.23, is derived.

$$P = k_{eb}AE(T - T_0) \tag{5.23}$$

Inserting equation 5.22 in equation 5.23 results in a relationship for the critical temperature at which buckling occurs.

$$T_c = T_0 + \frac{4\pi^2 I}{k_{eb}AL^2} \tag{5.24}$$

Equations 5.23 and 5.24 give the critical temperature and load-pressure-at which buckling occurs [6].

It is important to know the microbridge's deflection as a function of temperature when the temperature exceeds the buckling condition that requires a post buckling analysis. However, in deriving equations 5.23 and 5.24, it is assumed that deflections are small.

$$\frac{M}{EI} = \frac{\frac{d^2v}{dx^2}}{(1 + (\frac{dv}{dx})^2)^{\frac{3}{2}}} \Rightarrow \frac{M}{EI} \approx \frac{d^2v}{dx^2} \tag{5.25}$$

In fact, the linearization made in equation 5.16, which is then used in deriving successive equations, will not result in a prediction of the buckling beam in the nonlinear region. However, an exact calculation of buckling amplitude would require formulation without linearizing. Nonlinear stability theory applies in deriving the exact and complete nonlinear equations governing elastic deformations of microbridges. Solving the non-linear equations results in a more exact value for buckling amplitude. Two methods for computing buckling amplitudes are more common: the first method is an approximate method, which satisfies the need in many applications. However, the second method, which uses elliptical integration to calculate the length of the buckling beam, is more accurate.

The approximate method uses thermoelastic and length computation of a free end beam at a given temperature, which is intended to determine the constant B_2 in equation 5.12. If the temperature in the microbridge is above the reference temperature but less than or about the buckling temperature, thermal stress is induced; however, the microbridge's length does not change. At the buckling temperature, T_{cr}, the length begins to increase. Therefore, at any given temperature above buckling, T, the length of the beam is computed from equation 5.26, when L_0 is the initial length at room temperature [6].

$$S = L_0 + L - L_{cr} \tag{5.26}$$

The length of a free end beam, which is assumed to be at the buckling temperature, is equal to 5.27.

$$L_{cr} = L_0(1 + k_{eb}(T_{cr} - T_0)) \tag{5.27}$$

The length of a free end beam assumed at a given temperature, T, is computed in 5.28.

$$L = L_0(1 + k_{eb}(T - T_0)) \tag{5.28}$$

The length of the curved beam may also be computed from equation 5.29.

$$S = \int_0^{L_0} \sqrt{1 + (\frac{dv}{dx})^2} \cong \int_0^{L_0} (1 + (\frac{1}{2})(\frac{dv}{dx})^2)dx \tag{5.29}$$

The derivative of equation 5.21 is inserted in equation 5.29, and the result is taken equal to equation 5.26. The result is a computed value for the unknown constant, B_2, in equation 5.21.

$$\frac{dv(x)}{dx} = \frac{2\pi B_2}{L} \sin \frac{2\pi x}{L} \Rightarrow S = 2\int_0^{\frac{L_0}{2}} (1 + (\frac{1}{2})(\frac{2\pi B_2}{L})^2 \sin^2(\frac{2\pi x}{L}))dx \tag{5.30}$$

$$(\int \sin^2 mx dx = \frac{x}{2} - \frac{\sin 2mx}{4m}) \Rightarrow S = L_0 + (\frac{L}{4})(\frac{4\pi^2 B_2^2}{L_0^2}) \tag{5.31}$$

Equating 5.26 with 5.31:

$$S = L_0 + L_0 k_{eb}(T - T_{cr}) = L_0 + (\frac{L}{4})(\frac{4\pi^2 B_2^2}{L_0^2} \Rightarrow B_2 = \frac{L_0}{\pi}\sqrt{k_{eb}(T - T_{cr})} \tag{5.32}$$

The buckling microbridge maximum amplitude is equal to B_2, which is computed in equation 5.32. Thus, the complete relationship for the beam's curve is

$$v(x) = B_2(1 - \cos\frac{2\pi x}{L}) = \frac{L_0}{\pi}\sqrt{k_{eb}(T - T_{cr})}(1 - \cos\frac{2\pi x}{L}) \tag{5.33}$$

In another method, the axial stress proportional to the strain,

$$\epsilon_{(stiff)} = \frac{L - L_{cr}}{L_0} = \frac{S - L_0}{L_0}; \quad \sigma_{(stiff)} = \epsilon_{(stiff)}E \tag{5.34}$$

which is called stiffening effect, is computed and inserted in the differential equation of the microbridge, 5.16, resulting in the maximum amplitude of the microbridge, B_2. In fact, when a microbridge is laterally deflected, an axial stress is produced that opposes this deflection and decreases the effect of the lateral load. Therefore, the actual amplitude is slightly less than the computed value in which this stiffening effect is disregarded. However, both of these methods give the same results: the method outlined through equations 5.26 to 5.32 and the above described technique in which the directly computed stiffening effect from equation 5.34 along with the curve equation 5.21 are applied in the differential equation, 5.16.

5.5 Summary

Under the topic of thermoelastic microactuation, the thermomechanical properties of a structural material, i.e., polysilicon, and their effects in the thermoelastic behavior of a thermal microactuator are explained. It is shown that thermoelastic analysis produces a formulation for the interface between two physical environments, heat transfer and elasticity. Microbridge deflection analysis results in beam deflection equations, which are linearized for small deflections. However, the large deflections and non-linear conditions are also investigated. The boundary conditions of the microbridge are applied, resulting in the curve equation of the microbridge. The temperature distribution formulated in the previous chapter applies in a one–dimensional Duhamel-Neumann equation to compute the stress-strain in a microbridge. These computations identify critical conditions: the buckling temperature, buckling load, and maximum microbridge deflection. The three critical values are the main design parameters of thermal microactuators. Finally, the complete solution of the microbridge deflection curve, assuming thermal stress is the only effective stress, is derived.

Chapter 6

Magnetoelastic Actuation

6.1 Introduction

The evaluation of microactuation techniques by scaling laws in Chapter 3 shows the strong potential of magnetic forces for actuation in microscale. The favorably scaled physical phenomena involved in a magnetic microactuation and the optimized ways to use these physical effects are highlighted in the analysis. For example, the discussion in Section 3.4 shows that keeping a constant rate of heat removal from current carrying components or a constant temperature gradient between the conductors and the environment makes magnetic microactuation more attractive than electrostatic microactuation. Magnetic actuation in microscale is not only attractive because of more favorably scaled features, but it is also attractive because of the advantages magnetic microactuation has over other techniques such as the capability to create both attractive and repulsive forces. Electrostatic force, however, cannot be employed in microactuation as a repulsive force. This advantage results in a more flexibility and design options. For microactuation, the focus in this study is on a magnet-current interaction among three options for creating magnetic force, current-magnet, magnet-magnet, and current-current. Interaction between a ferromagnetic material and a current-carrying conductor is considered in the same category as the interaction between a magnet and a current-carrying conductor.

Deriving a relationship for the magnetic force from a known current distribution that interacts with a static magnetic field is discussed in Section 6.2. The discussion is based on magnetostatic equations:

$$\nabla . B = 0 \tag{6.1}$$

$$\nabla \times B = \mu_0 J \Rightarrow \nabla \times H = J \tag{6.2}$$

In equation 6.2, if we take the divergence from both sides

$$\nabla.(\nabla \times B) = \mu_0 \nabla.J \Rightarrow \nabla.J = 0 \tag{6.3}$$

Relationship 6.3 displays that a constant field B, independent of J, has no physical meaning [86]. The above static's Maxwell equations are in differential form. For practical applications, the integral forms are more useful.

$$\oint_A B.dA = 0 \tag{6.4}$$

$$\int_A (\nabla \times B).dA = \mu_0 \int_A J.da \tag{6.5}$$

By stokes' theorem,

$$\int_A (\nabla \times B).dA = \oint_C B.dr \Rightarrow \oint_C B.dr = \mu_0 \int_A J.da \equiv \mu_0 I \tag{6.6}$$

The last relationship, 6.6, is Ampere's law. Depending on the problem and whether B or current distribution, I, which are creating the magnetic field, are known, different formulations for deriving force and displacement are applicable.

Elastic deformation of a microbridge experiencing a magnetic force is analyzed in Section 6.3. From Section 6.2, the relationship for a magnetic force on a microbridge is inserted in elastic equations. The result is a model for the electromagnetic microactuation. The microbridge deflection is formulated for a given magnetic force with known magnitude and direction. This formulation gives a prediction for the microbridge's maximum deflection, maximum allowable stress, and magnetoelastic behavior of the microbridge.

In Section 6.4, the method of driving microstructures with powerful current pulses in the presence of an external magnetic field is introduced. This proposed method uses the capability of the magnetic microactuation to create high peak force and torque. The method is based on generating pulses of current with small duty cycles. The width of the powerful current pulses is short, which prevents creation of excessive heat in the microbridge in spite of it being driven by large currents. The high amplitudes of these current pulses interact with the external magnetic field and produce large force and torque.

In the following sections, the above topics are discussed in more detail: magnetic force on a microbridge carrying an electrical current; magnetoelastic analysis; driving a magnetic microactuator by powerful current pulses.

6.2 Magnetic Force on a Microbridge Carrying an Electrical Current

Under steady-state conditions, the microbridge carrying a constant current experiences force when it is inserted in a magnetic field, regardless of whether the source of the magnetic field is from a current in a conductor, an electromagnet, or a permanent magnet.

$$F = qV \times B = \int (J_v dv \times B) \;\Rightarrow\; F = \int I dl \times B \tag{6.7}$$

A constant current density, J_A, in a microbridge whose cross-section is constant results in a constant current in that microbridge, I. Consequently, equation 6.7 is further simplified.

$$F = I \int dl \times B \tag{6.8}$$

The constant magnetic field along the microbridge causes the force to be proportional to an integral over the current path. Given that the magnetic field is perpendicular to the microbridge throughout its whole length, the force is computed from equation 6.9.

$$F = I(\int dl) \times B \tag{6.9}$$

The magnetic force in the above equations is, in fact, on the moving electrical charges. However, in an equilibrium situation, the force acting on the charges is transmitted to the atoms of the wire, because the charges are not able to leave the wire. Figure 6.1 shows the components of the magnetic force on a deflected fixed-ends microbeam. It is easily verified that no matter what the curve of the deflected beam is, the only effective magnetic force on the microbridge is the vertical components of this force. The horizontal components of the force conceal each other. Therefore, the net force on the beam is equal to

$$F_m = F_m y = ILB \;\Rightarrow\; q = \frac{ILB}{L} = IB \tag{6.10}$$

For the given directions of the external magnetic field and the electrical current in the microbridge as shown in figure 6.1, the resulting force is in the plane xy. However, when the force remains in the plane xy, the direction of the force at each point of the microbridge may change. The force's direction changes proportional to the microbridge's slope at each point, but it is always perpendicular to the microbridge at each point, as shown in figure 6.1. The net force on the microbridge

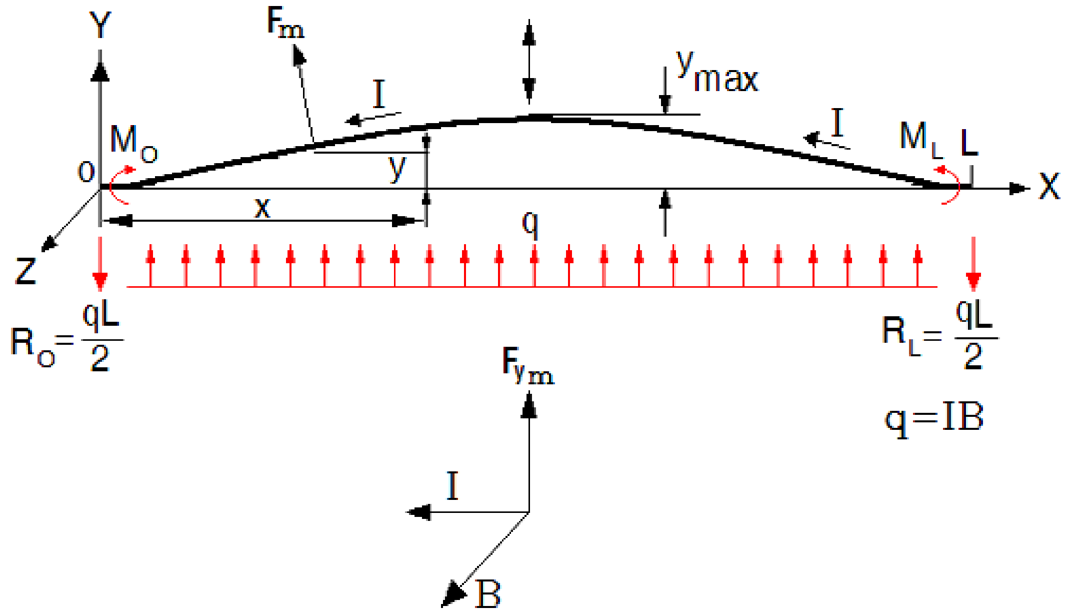

Figure 6.1: A Microbridge Experiences, $q(x)$, Lateral Magnetic Pressure.

is constant and equal to ILB, as shown in equation 6.10. However, the net force is independent of the shape of the microbridge. In the next Section, Magnetoelastic Analysis, the force computed in equation 6.10, applies to formulate the elastic behavior of the buckling microbridge.

6.3 Magnetoelastic Analysis

Pure magnetoelastic actuation is defined as the elastic actuation of the beam when magnetic force is the only acting force. In other words, the thermal stress induced by an electrical current in the microbridge is negligible. This assumption requires the current to be too small to produce significant thermal effect. Thus, there is low or no temperature increase, and the temperature at which the beam reaches steady state conditions remains close to the reference temperature.

As shown in 6.10, the microbridge carrying a constant electrical current, I, in an external magnetic field, B, experiences a constant net lateral pressure, $q(x)$, equal to IB. The sign of the force is negative because the force creates a concave shape for the microbridge toward the negative $y-$direction, as explained in Section 5.3. For the given $q(x)$, the beam's curve equation is derived by successive integration. From

equation 5.1 and because the microbridge experiences only $q(x)$, lateral pressure, the general relationship for the microbridge deflection is derived[1].

$$EI_m \frac{d^4v}{dx^4} = q = IB \Rightarrow \; v = \frac{1}{EI_m}(\frac{IB}{24}x^4 + C_1\frac{1}{6}x^3 + c_2\frac{1}{2}x^2 + C_3x + C_4) \qquad (6.11)$$

The boundary conditions are illustrated in figure 6.1.

- $x = 0 \;\Rightarrow\; [(EI\frac{d^2v}{dx^2} = M_0); (\frac{dv}{dx} = 0); (v = 0)]$
- $x = L \;\Rightarrow\; [(EI\frac{d^2v}{dx^2} = M_L); (\frac{dv}{dx} = 0); (v = 0)]$

Applying boundary conditions in 6.11 results in the complete microbridge curve equation.

$$C_4 = 0;\; C_3 = 0;\; C_2 = \frac{-IBL^2}{12};\; C_1 = \frac{IBL}{2} \;\Rightarrow \qquad (6.12)$$

$$v = \frac{IB}{24EI_m}(x^4 + 2Lx^3 - L^2x^2) \text{ and } v_{(max)} = v_{(x=\frac{L}{2})} = \frac{IBL^4}{384EI_m} \qquad (6.13)$$

6.4 Driving a Microactuator by Powerful Current Pulses

The main limitation of a conductor carrying electrical current is its ability to dissipate the generated heat before the consequent temperature increase causes deformation or melting of the conductor. This fact highlights the possibility of applying larger currents for shorter times. The higher amplitude of such powerful current pulses produces larger peaks of magnetic forces and torques. Given that the temperature increase of a microstructure can be kept below a certain limit, driving the microstructure by larger current pulses above the known allowed level for continuous current is possible. Applying larger currents is achievable either by removing excessive heat or by shortening the period of time during which the larger currents are applied. This Section analyses application of larger currents for shorter times with a focus on the technique's limitations and advantages.

[1]In this work, in order to distinguish I, electrical current, from I, the moment of inertia, the I with E which makes EI, flexural rigidity, is always moment of inertia. Otherwise, I denotes electrical current. If both moment of inertia and electrical current are present in the same equation, "I" which denotes moment of inertia receives a subscript of m.

The heat generated by Joule effect inside a microstructure causes temperature increase, which depends on the specific thermal capacity and mass of the component. In order to prevent a component failure, the temperature of a microcomponent must remain below a certain level.

$$\Delta Q_{(max)} = mc\Delta T_{(max)} = RI^2t \tag{6.14}$$

In the above equation, 6.14, I is the applied electrical current, R is the electrical resistance, and t is the duration of time in which the electrical current applies. Equation 6.14 shows that for a given $\Delta Q_{(max)}$, an electrical current with any value is theoretically applicable, given that the time duration, t, is kept short enough so that the ΔQ remains constant.

However, applying powerful current pulses to drive microstructures may face limitations in some conditions. There are reports that powerful current pulses can cause a microbridge fracture because of reasons other than excessive heat. Molokov and Allen have conducted research on this effect and shown that the fracture occurs due to some longitudinal force, the nature of which is still under investigation [104]. Equation 6.10 shows that a stronger pulsed magnetic field can produce larger peak force and torque in a microactuator.

Outstanding advantages exist in using powerful current pulses to drive microstructures. MacKay et al. have carried out experiments on microcoils to generate a magnetic field up to 50 $Tesla$ [106]. This strong-pulsed magnetic field has various applications in research and industry, i.e., for investigation of fundamental physical properties of materials. However, powerful current pulses in a buckling or deflected microbridge can be used to produce large peaks of force and torque for microactuation applications. Examples of these applications are outlined in the designs introduced in Section 7.4.

Magnetic microactuation shows a strong potential for producing large peak forces and torques by applying powerful current pulses. Powerful current pulses can produce powerful pulsed magnetic fields or can drive a microbridge. In the above paragraphs, some aspects of this potential are briefly discussed, in which limitation and advantages of using powerful current pulses in driving and actuating buckling microbridges are explained.

6.5 Summary

The interaction of a current carrying microstructure, a fixed-fixed microbeam, with an external magnetic field provides a method for microactuation. Different aspects

of this microactuation technique are introduced in the above sections. Section 6.2, Magnetic Force on a Microbridge Carrying an Electrical Current, formulates the magnetic pressure of an external magnetic field on a buckling microbridge carrying electrical current. Section 6.3, Magnetoelastic Analysis, models a microbridge deflection equation and the maximum deflection of the microbridge. In Section 6.4, Driving Microactuator by Powerful Current Pulses, a method for producing large peak force and torque in electromagnetic microactuation is proposed. The next chapter, Electrothermomagnetic Actuation, discusses the integration of the magnetic microactuation technique introduced in this chapter and the method previously introduced in Chapter 5, Thermoelastic Actuation.

Chapter 7

Electro-Thermo-Magnetic Actuation

7.1 Introduction

Analysis of thermal stress in a buckling fixed–fixed microbeam in Chapter 5 shows that thermally induced stress acts as an axial force on a microbridge. However, the discussion in Chapter 6 shows that if the microbridge carrying electrical current is inserted in an external magnetic field, it experiences lateral force, and this effect can be employed for microactuation. Thermomagnetic microactuation is a combined microactuation technique using the advantages of both thermal and magnetic microactuation and overcomes some limitations of applying either of the techniques individually.

In electrothermomagnetic microactuation, two forces operate simultaneously, thermally induced stress and magnetic pressure. The buckling condition in a microbridge is given in relationship 5.22, when an axial force is the only operating force. However, applying a lateral magnetic pressure changes the buckling condition dramatically. In Section 7.2, the simultaneous effects of thermal stress and lateral magnetic pressure on a buckling microbridge are investigated, analyzed, and modeled. The general equation for a microbridge's deflection under the influence of both forces is derived. Upon applying the boundary conditions, the exact relationship for the microbridge deflection is formulated.

In Section 7.3, a unique design for a larger stroke two-layer microbridge is proposed. Either pure electromagnetic or combined electrothermomagnetic effects can actuate the proposed configuration. The main point in this design is its larger

stroke in microactuation, almost twice as large as the maximum displacement of a simple fixed-fixed microbeam.

In Section 7.4, some of my selected designs for microactuators are introduced. These designs include single and double degree of freedom linear and rotary type microactuators. One or more than one buckling fixed-fixed microbeams are employed in each of these designs. Despite the focus of this thesis on using a buckling microbridge as the microactuating element, just for example, designs of microactuators are developed in which buckling microbridges are not the actuating element. Figure A.1 in Appendix A.2 shows one of these designs.

7.2 Thermal Stress and Magnetic Pressure on a Microbridge

Figure 7.1 depicts a microbridge that experiences both an axial force, P, (thermally-induced stress) and a magnetic pressure, $q(x) = IB$, (a lateral force by an external magnetic field). From equations 5.8 and 5.9, a relationship for the microbeam

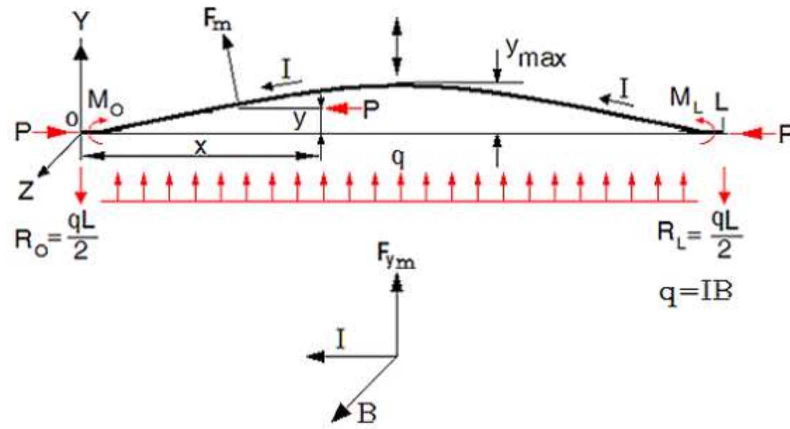

Figure 7.1: Microbridge Experiences Lateral Magnetic Pressure, $q(x)$, and Axial Thermally Induced Load, P

deflection is derived.

$$\frac{d^2}{dx^2}(EI\frac{d^2v}{dx^2}) + P\frac{d^2v}{dx^2} = EI\frac{d^4v}{dx^4} + P\frac{d^2v}{dx^2} = q(x) \tag{7.1}$$

Thermal stress produces an axial force, P, which is given in equation 5.12. The external magnetic field exerts net lateral constant pressure, $q(x) = IB$, on a microbridge under described conditions as shown in 7.1 and formulated in relationship 6.11. The general solution for equation 7.1 is given in equation 7.2.

$$v = D_1 \cos k'x + D_2 \sin k'x + D_3 x + D_4 + g(x) \tag{7.2}$$

In equation 7.2, $k' = \sqrt{\frac{P}{EI}}$, and $g(x)$ is a particular solution for the lateral load $q(x)$. The function $g(x)$ depends only on lateral loading and is equal to $\frac{q(x)}{2P}x^2$, which is verified by substituting in 7.2. Therefore, the complete solution is given in 7.3.

$$v = D_1 \cos k'x + D_2 \sin k'x + D_3 x + D_4 + \frac{q(x)}{2P}x^2 \tag{7.3}$$

Applying the boundary conditions of the fixed-fixed microbeam on 7.3, the four constants D_1, D_2, D_3, D_4 are determined.

- $(x = 0 \Rightarrow v(0) = 0,\ \frac{dv}{dx} = 0) \Rightarrow D_1 + D_4 = 0;\ D_2 k' + D_3 = 0$
- $(x = L \Rightarrow v(L) = 0,\ \frac{dv}{dx} = 0);\ (x = \frac{L}{2} \Rightarrow \frac{dv}{dx} = 0) \Rightarrow D_1 = \frac{\tan^2(\frac{k'L}{2})(\frac{qL}{k'P}) - \tan(\frac{k'L}{2})(\frac{qL^2}{2P})}{\sin k'L - k'L + 2\sin^2(\frac{k'L}{2})\tan(\frac{k'L}{2})} + \frac{1}{\sin k'L}(\frac{qL}{k'P}),\ D_2 = \frac{\tan(\frac{k'L}{2})(\frac{qL}{k'P}) - \frac{qL^2}{2P}}{\sin k'L - k'L + 2\sin^2(\frac{k'L}{2})\tan(\frac{k'L}{2})}$

7.3 Microactuation by a Two-Layer Microbridge

One of the unique advantages of using a buckling microbridge as the actuating element is its large force-stroke output. However, a design for a two-layer microbridge is proposed to further increase the stroke. Figure 7.2 depicts such a design that can be actuated by METMA similar to a simple fixed-fixed microbridge. The microbeams carry the same amount of electrical current and experience a lateral net force when a perpendicular magnetic field is established. The configuration shown in figure 7.2 facilitates out-of-plane motion of the combined microbeams leading to a larger stroke microactuation. The axial force from a thermal stress in a two-layer microbridge is considerably less than the one in a simple fixed-fixed microbeam. This decrease in the experienced thermal stress is because the two ends of the top microbeam, the longer piece, expand in opposite directions when thermally heated. The expanded ends of the two other shorter cantilever-type microbeams facilitate this movement. The freedom of motion of the top microbeam's ends decreases the axial stress in the top microbeam. However, a lateral magnetic force can actuate the microbeams in order that the midpoint of the top microbeam moves nearly twice the displacement achievable with a simple fixed-fixed microbridge.

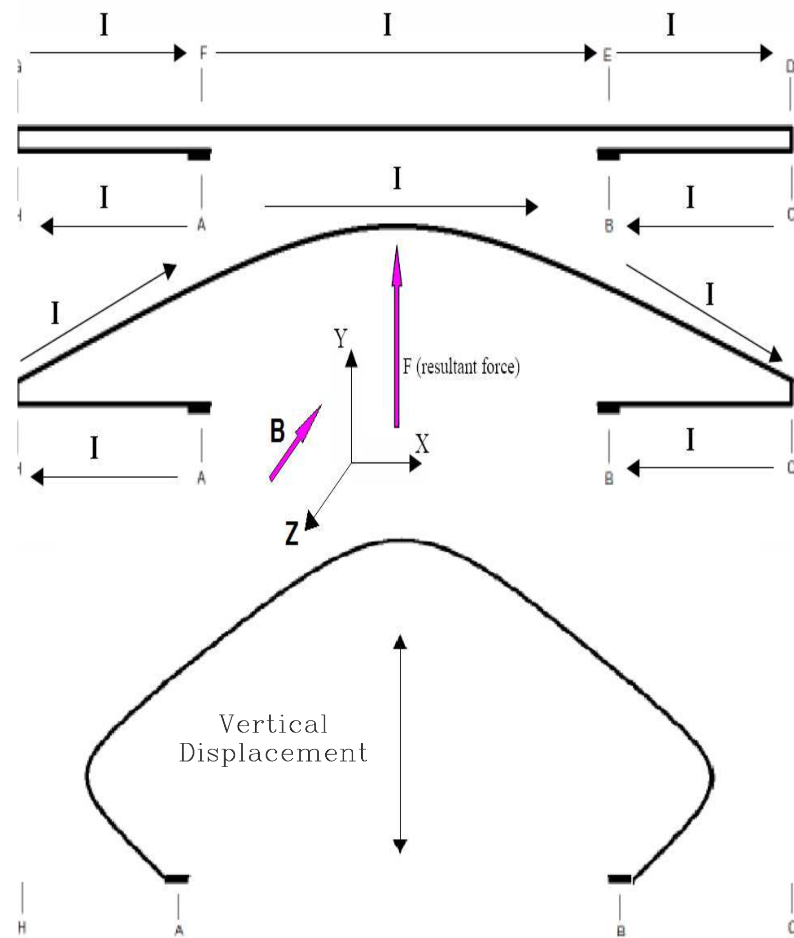

Figure 7.2: Two-Layer Out-Of-Plane Moving Clamped-Clamped Microbeam

7.4 Various Microactuator Designs

Figure 7.3 displays a design using a couple of buckling microbridges, the midpoints of which are attached to a microbeam whose one end is fixed and whose other end slides beneath a small bridge. Upon buckling, the two microbridges pull the attached microbeam out-of-plane. The pulling action forces the moving tip of the actuated microbeam to have an in-plane motion. In fact, the bridge over the microbeam confines the microbeam to slide underneath and have an in-plane motion. Figure 7.4 shows a design of a two-degrees-of-freedom linear microactuator. The

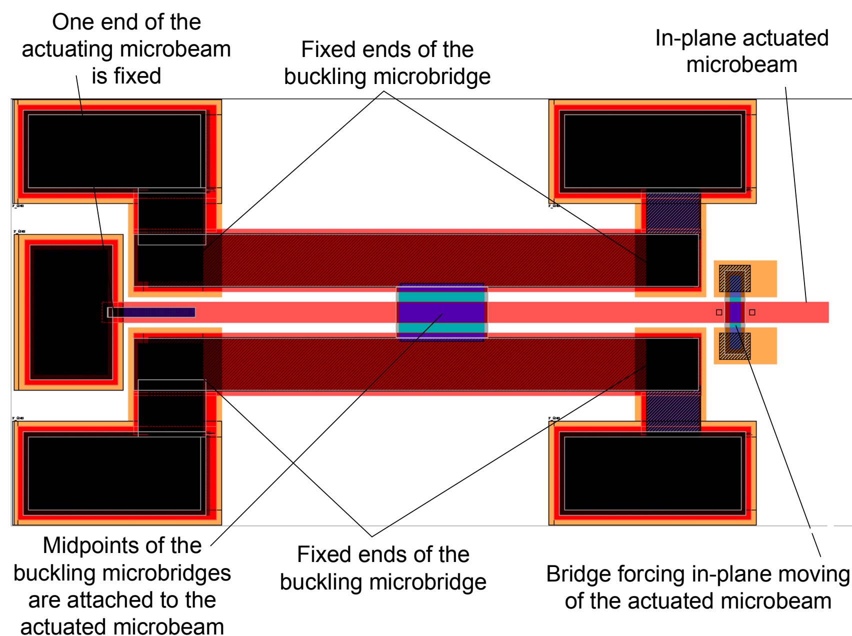

Figure 7.3: One-Degree-of-Freedom (DOF), In-plane Linear Microactuator

combination of a couple of buckling microbridges, shown in figure 7.3, and another single buckling microbridge enable a linear moving gear to have two motions, in-plane and out-of-plane. By in-plane motion, it rotates any gear engaged. With the possibility to move out-of-plane, the linear gear can engage or disengage with another gear. The two-degrees-of-freedom microactuator can also be employed in the design of a micromotor shown in figure 7.5. Figure 7.5 depicts the design of a high torque, bi-directional, and multi-turn micromotor. In this design, the previously linear microactuators have been employed to develop such a rotary microactuator. The minimum requirement for in-plane displacement of the linear microactuator is

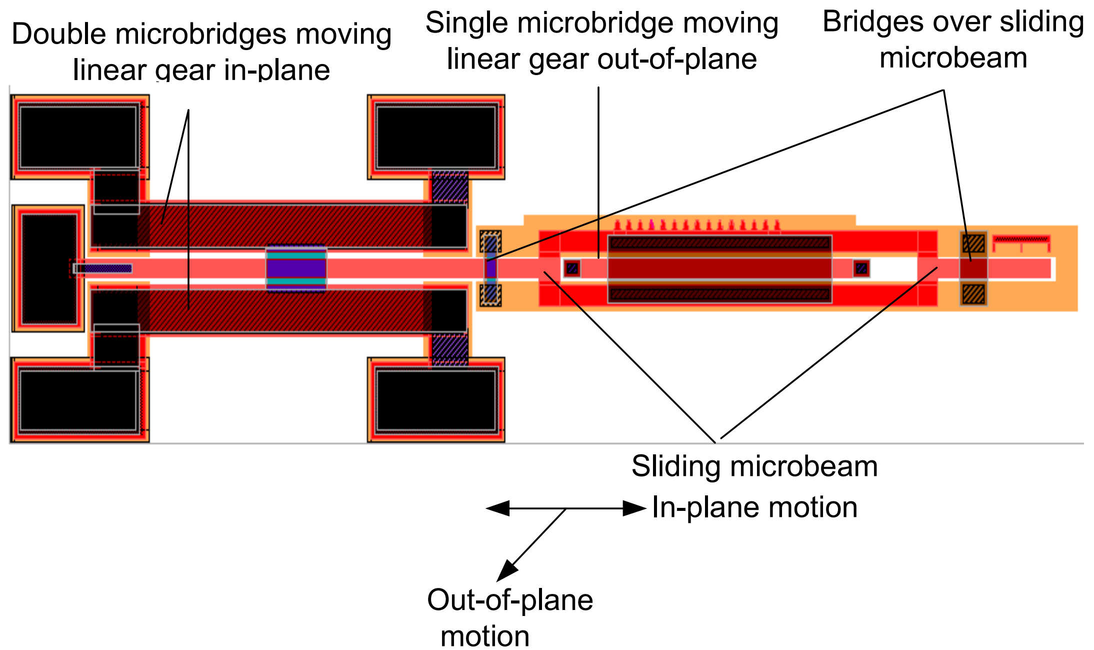

Figure 7.4: Two-DOF, In-plane and Out-Of-Plane, Linear Microactuator

about ten to twelve microns. This displacement is less than (eight microns) the distance between two successive teeth of the gear. To provide such a displacement, either the buckling microbridges must be long enough, or the microbridge must be made of a structural material, which has a thermal expansion coefficient sufficient to produce this displacement within the operating temperature range. For example, in the configuration shown in figure 7.5, the coupled microbridges are about 800 μm long and made of Poly1 of PolyMUMPS polysilicon, which has a 2 μm thickness. Such microbridges can produce a maximum allowable buckling amplitude of 32.5 μm with a safety factor of 1.7, as discussed in Section 8.2. This maximum amplitude is more than enough to create an in-plane displacement of two to three times the distance between two successive gears. The driving signals to actuate the designed micromotor are shown in table 7.1. A number of microactuators are designed without using a buckling microbridge as the actuating element. These designs are introduced in Appendix A.2.

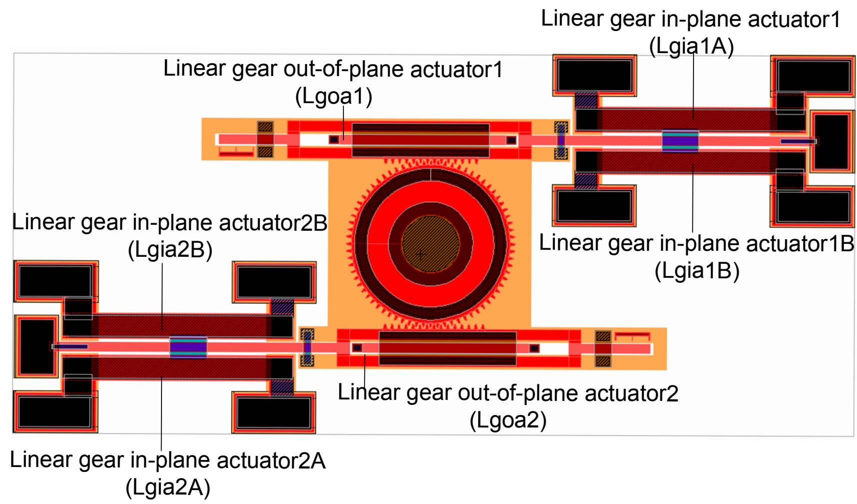

Figure 7.5: High Torque Bi-directional Multi-turn Micromotor

Table 7.1: Driving Signals for the Micromotor Shown in Figure 7.5

Stage	**Lgoa1**	**Lgia1**	**Lgoa2**	**Lgia2**
1	on	off	off	off
2	on	off	off	on
3	off	off	off	on
4	off	off	on	on
5	off	on	on	off
6	off	on	off	off
7	on	on	off	off
8	on	off	off	off

7.5 Summary

Thermomagnetic microactuation is proposed to enhance the capabilities and integrate the advantages of both thermal and magnetic microactuation. A buckling microbridge, which is actuated electrothermomagnetically, is employed as the actuating element in various developed microactuators' designs. Taking into account the effects of thermal stress as the axial force and magnetic pressure as the lateral force on a microbridge, a mathematical model representing microbridge deflection is developed, and its coefficients are determined by applying the known boundary conditions. To further increase the out-of-plane displacement of a microbridge for larger stroke microactuation, a unique design of a two-layer microbridge is proposed. Finally, by using a buckling microbridge as the actuating element, various microactuator designs are introduced. The microactuators are both linear and rotary types. Either of these microactuators can be actuated electrothermally, electromagnetically, or electrothermomagnetically.

Chapter 8

Results and Discussion

8.1 Introduction

In the previous chapters, out-of-plane buckling and deflection of a fixed-fixed microbeam are modeled and used as the actuating elements in the proposed microactuation technique, METMA. In this chapter, the numerical computations' and simulations' results are outlined and discussed. The critical and threshold values for the actuated microbridge, including maximum allowable thermal stress, load, temperature, and displacement for various modes of operations, are computed. The actuated microbridge is also simulated in the various modes of operation: electrothermal, electromagnetic, electrothermomagnetic. These investigations provide a quantitative evaluation of the models discussed.

As a standard sample, a microbridge made of polysilicon with given geometrical dimensions is assumed, and some of its technical parameters such as the allowable stress in the microbeam are computed. Knowledge about the allowable stress is required in order to keep the designed microstructures from permanent deformation or fracture. For an electrothermally actuated microbridge, the buckling load, buckling temperature, maximum deflection, and maximum load in different temperatures are calculated. The computations also include maximum amplitude of the microbridge under electromagnetic actuation.

The same standard microbridge that is considered in the numerical computations is simulated in ANSYS under various conditions. Simulations include driving the microbridge electrothermally, electromagnetically, and electrothermomagnetically. Section 4 discusses the numerical solutions and simulations' results.

8.2 Numerical Computations

A standard sample of a microbridge is defined and applied in numerical computations: length 800 μm, thickness 2 μm, and width 40 μm. The critical values for thermoelastic and electromagnetic actuation are numerically computed: allowable stress and load; maximum allowable temperature; buckling load, buckling temperature; maximum deflection and maximum load in given temperatures; maximum microbridge deflection under electromagnetic actuation.

Allowable normal stress for a material is computed from the relationship for the yield stress divided by a safety factor. For example, steel as the structural material is commonly given a safety factor of 1.67 [66], for which the safety factor is applied on yield strength. However, polysilicon has a brittle nature, and there is no definite value for yield stress in polysilicon. Therefore, a higher value for the safety factor, 1.7, applies on the ultimate stress (in tension or compression) in polysilicon. Then the allowable normal stresses are computed from equation 8.1 by taking the fracture strength for PolyMUMPs polysilicon equal to a minimum value of 1.2 GPa from table 5.2. With a safety factor of 1.7, the allowable normal stress and load for the given polysilicon microbridge are calculated in equations 8.1 and 8.2.

$$\text{Allowable stress} = \frac{\text{Ultimate strength}}{\text{Safety factor}} \Longrightarrow \frac{\sigma_U}{n_{\text{safety factor}}} = \frac{1.2}{1.7} \approx 705.88\ MPa \quad (8.1)$$

$$\text{Allowable load} = 705.88 \times 10^6 \times (40 \times 2 \times 10^{-12}) = 5.647 \times 10^{-2}\ Newton \quad (8.2)$$

The allowable maximum temperature is set, and the allowable maximum bending stress in the microbridge are calculated. Extensive research has been conducted to determine the thresholds at which plastic deformation of polysilicon begins. However, there are slight differences in the reported thresholds. In the calculations in this thesis, the suggested value by Sharp et al., 750 $^\circ C$ ($\approx$ 1050 $^\circ K$), is taken into account [102]. Protecting a microbridge from fracture in an electromagnetic actuation requires that the bending stress remains below an allowed value. Such a maximum allowed value is, in fact, a maximum allowable bending stress by the lateral magnetic pressure, which is the only operating load. For the microbridge experiencing a lateral magnetic pressure, $IB = q(x)$, shown in figure 6.1, the maximum bending moment is computed in equation 8.3,

$$M(x) = -\frac{qx^2}{2} + \frac{qLx}{2} - \frac{qL^2}{12} \Rightarrow M_{(max)} = -\frac{qL^2}{24} = -\frac{IBL^2}{24} \quad (8.3)$$

and the maximum bending stress is computed in equation 8.4,

$$\sigma_{x_{(max)}} = -\frac{M_{(max)}y}{I} = 10^9 IB \quad (8.4)$$

in which $y = 1$ (μm) is the distance of the neutral surface in the microbridge to the microbridge surface that is half of the microbridge thickness. By taking the allowable stress computed in equation 8.1, 705.88 MPa, the maximum allowed IB is calculated.

$$\sigma_{x(max)} \leq 705.88\ MPa \Longrightarrow IB \leq 0.706 \quad (8.5)$$

As far as an applied magnetic pressure, the product of IB, is below the certain computed amount given in equation 8.5, actuating a microbridge with any theoretical values of I or B is allowed. However, the current carrying capacity of a microbeam and the requirement for keeping the temperature in the microbeam below a certain limit are additional limitations for applying an electrical current. If the microbridge with the above mentioned standard dimensions is actuated electromagnetically with the configuration shown in figure 6.1, the maximum deflection of the microbridge is computed from equation 8.6 that is taken from relationship 6.13. For a given IB, the electrical current passing the microbridge times the magnetic field's magnitude, $L = 8 \times 10^-4$, $E = 160\ GPa$, and $I_m = 26.67 \times 10^-24$,

$$v_{(max)} = \frac{IBL^4}{384EI_m} \approx IB(2.5 \times 10^{-4}) \quad (8.6)$$

Assuming a value of 160 GPa for Young's module, E, taken from table 5.2, and the second moment of inertia of the microbridge equal to $I = \frac{th^3}{12} = \frac{40 \times 8 \times 10^{-24}}{12}$, from equation 5.22,

$$P_{cr} = \frac{4\pi^2 EI}{L^2} = \frac{4\pi^2(160 \times 10^9)(26.67 \times 10^{-24})}{(800 \times 10^{-6})^2} = 2.632 \times 10^{-4}\ Newton \quad (8.7)$$

The critical temperature at which buckling occurs is formulated in equation 5.24 and is computed in equation 8.8, in which, the cross section of the microbridge is denoted by A. By taking k_{eb}, the polysilicon thermal expansion coefficient, equal to 2.9×10^{-6}, and assuming the T_0 equal 300 $^\circ K$, the critical temperature at which buckling in the microbridge occurs is calculated in equation 8.8.

$$T_c = T_0 + \frac{4\pi^2 I}{k_{eb} A L^2}$$

$$T_c = 300 + \frac{4\pi^2(26.67 \times 10^{-24})}{(2.9 \times 10^{-6})(80 \times 10^{-12})((800 \times 10^{-6})^2)} = 307.1\ ^\circ K \quad (8.8)$$

The maximum amplitude of the buckling microbridge at a given temperature, T, is formulated in relationship 8.9, by using equation 5.32 and taking the value of T_c from equation 8.8.

$$V_{(max)} = \frac{L_0}{\pi}\sqrt{k_{eb}(T - T_{cr})} = \frac{8 \times 10^{-4}}{\pi}\sqrt{(2.9 \times 10^{-6})(T - 307.1)}\ (T \geq T_{cr}) \quad (8.9)$$

The maximum load in the buckling microbridge at a given temperature, T, is modeled in equation 8.10 by using equation 5.23.

$$P = k_{eb}AE(T - T_0) = 37.12 \times 10^{-6}(T - T_0) \quad \text{(Newton)} \tag{8.10}$$

From equation 8.9 and equation 8.10, maximum amplitudes and the corresponding loads in a microbridge with the given dimensions are computed in various temperatures; the results are displayed in table 8.1. These results are valid if the average temperature in the microbridge reaches the designated temperatures, which is possible for some lower average temperatures in table 8.1; however, for the higher average temperatures in table 8.1, both ends of a microbridge must experience higher enough temperatures than the reference temperature in order that the average temperatures be the larger values shown in the table. Because the maximum temperature in the microbridge can not exceed the allowable temperature, $750\ ^\circ C$ ($\approx 1050\ ^\circ K$).

Table 8.1: Amplitudes and Loads in the Microbridge in Assumed Average Temperatures Computed from equations 8.9 and 8.10

Average Temp ($^\circ K$)	**Max Deflection** (μm)	**Max Load** (μ**Newton**)
307.1	0	263.2
350	2.84	1856
400	4.18	3712
450	5.18	5568
500	6.02	7424
550	6.76	9280
600	7.42	11136
650	8.03	12992
700	8.60	14848
750	9.12	16704
800	9.63	18296
850	10.10	20152
900	10.56	22008
950	11.00	23864
1000	11.41	25720
1050	11.82	27576

8.3 Simulations

Using ANSYS, the same standard microbridge considered in analytical computations in the above section is employed and simulated under various conditions. The conditions are the ones that are modeled and discussed in Chapters 4, 5, 6, and 7. The simulation in ANSYS is based on Finite Element Analysis (FEA), which is introduced in numerous text books, for example, "Finite Element Analysis" by Moaveni, [107]. The simulations include electrothermal, electromagnetic, and electrothermomagnetic actuating of a microbridge. The "avi" files of animated simulations are listed in Appendix B and attached to this thesis. A number of the calculated critical values are required to set the thresholds in simulations. For example, the maximum allowable temperature, which is discussed in Section 8.2, is set in a simulation of an electrothermal actuation of a microbridge to prevent a microbridge from overheating.

Figures 8.1 and 8.2 depict captures of the simulations of a given microbridge that

is actuated electrothermally displaying displacements and temperature distribution over the microbridge, respectively.

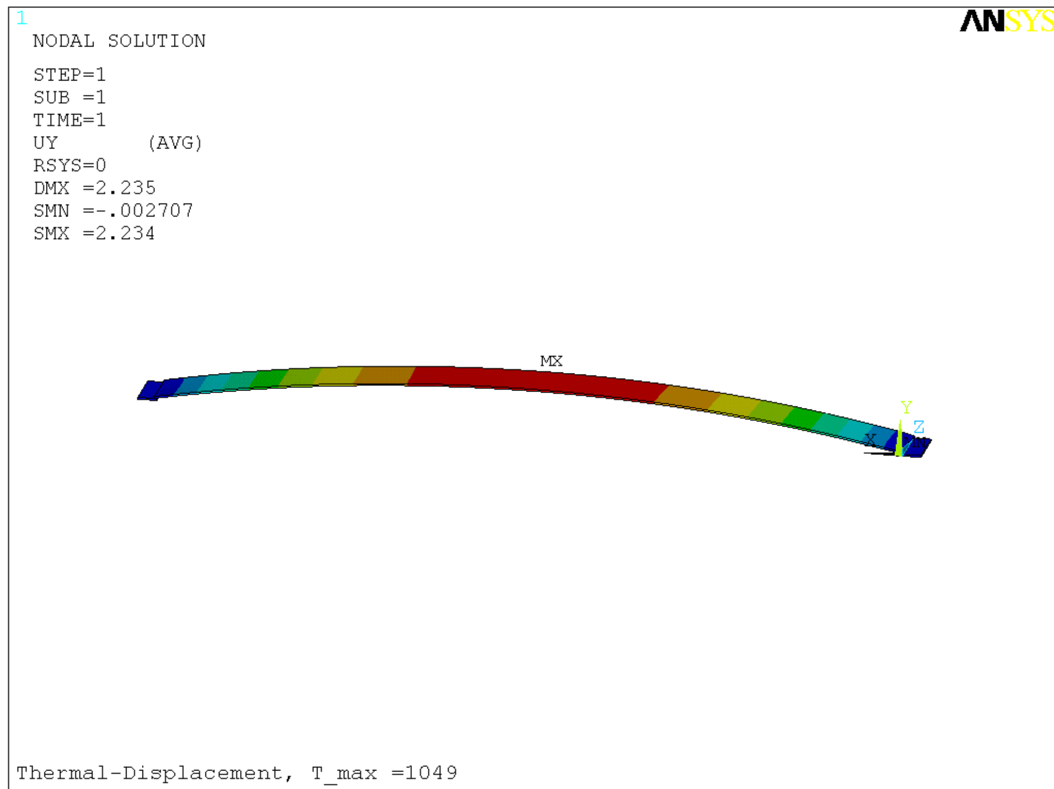

Figure 8.1: Displacement of an Electrothermally Actuated Microbridge

Table 8.2 shows the simulation results for the microbridge actuated electrothermally in which the linear method is used for simulation. Figures 8.3 and 8.4 shows images of the microbridge simulation in ANSYS, actuated electromagnetically. The applied pressures are $IB = -0.0353\ \frac{\mu N}{\mu m}$ and $IB = -0.137\ \frac{\mu N}{\mu m}$, and the maximum displacements are $D = 8.355\ \mu m$ and $D = 32.426\ \mu m$, respectively. In electrothermomagnetic actuation of a microbridge, a thermal stress as an axial load and a magnetic pressure as a lateral load are both present. Figure 8.5 displays a capture of the simulation of the given microbridge in ANSYS, actuated electrothermomagnetically. By applying a magnetic pressure equal to $0.001\ \frac{\mu N}{\mu m}$ and an electrical potential of $V = 2.0\ Volts$ across the microbridge's ends, a maximum deflection of $D = 10.23\ \mu m$ and a temperature increase of $T = 445\ ^{\circ}K$ results. For comparison, figure 8.6 shows a microbridge, which is under the exact same

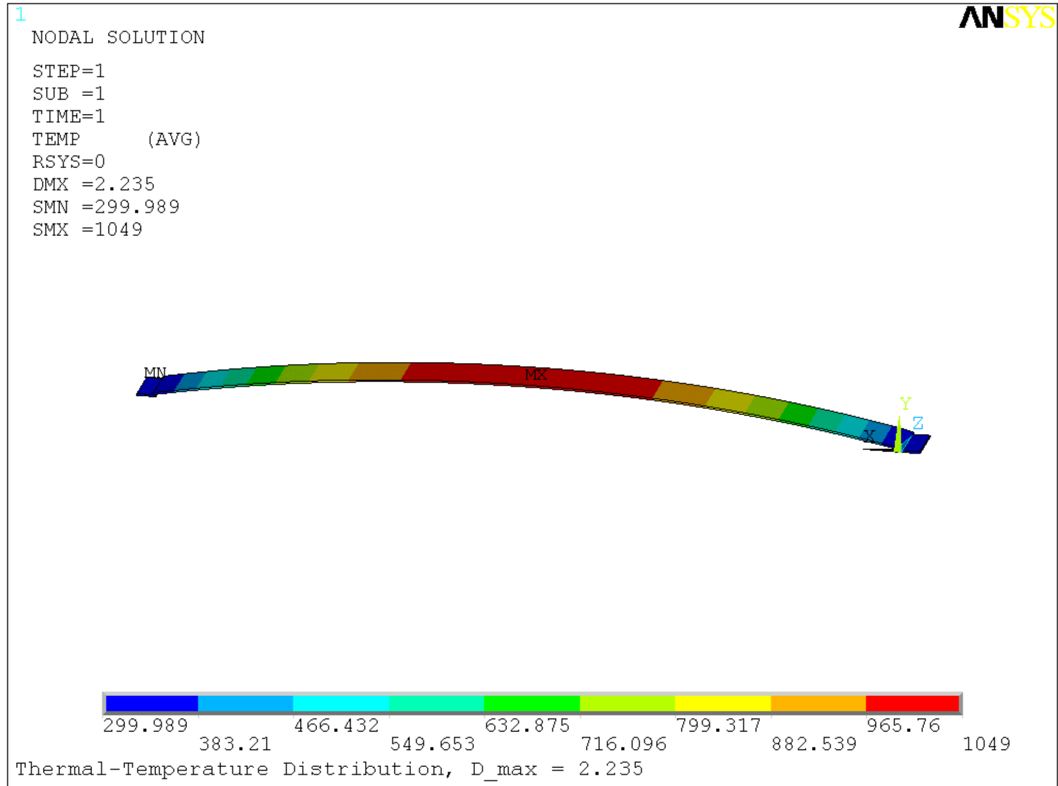

Figure 8.2: Temperature over an Electrothermally Actuated Microbridge

Table 8.2: Maximum Temperature, Displacement, and Force in a Simulated Buckling Microbridge, Actuated Electrothermally

Volt (V)	**Max Temp** ($^{\circ}K$)	**Max Deflection** (μm)	**Max Load** (μN)
2.1	1049	2.234	$29,678$
1.8	850	1.877	$24,571$
1.5	682	1.574	$20,250$
1.2	517	1.328	$16,715$
0.9	438	1.135	$13,965$

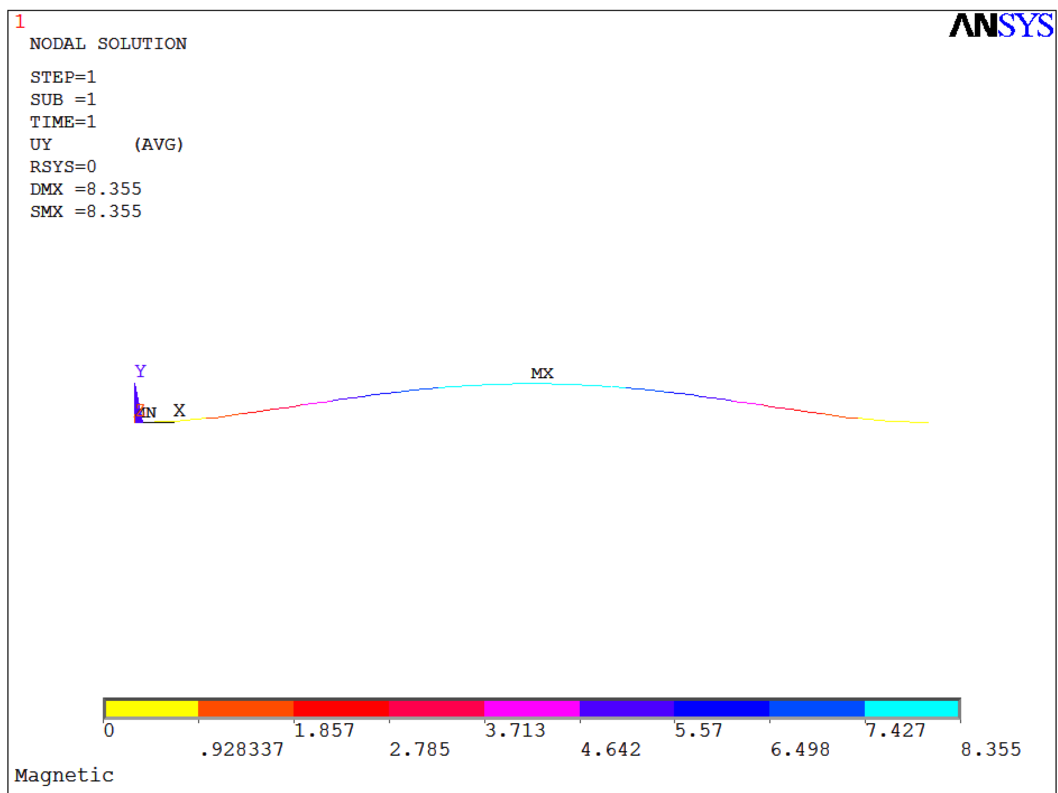

Figure 8.3: Microbridge Actuated by an Electromagnet Pressure, $IB = -0.0353\ \frac{\mu N}{\mu m}$

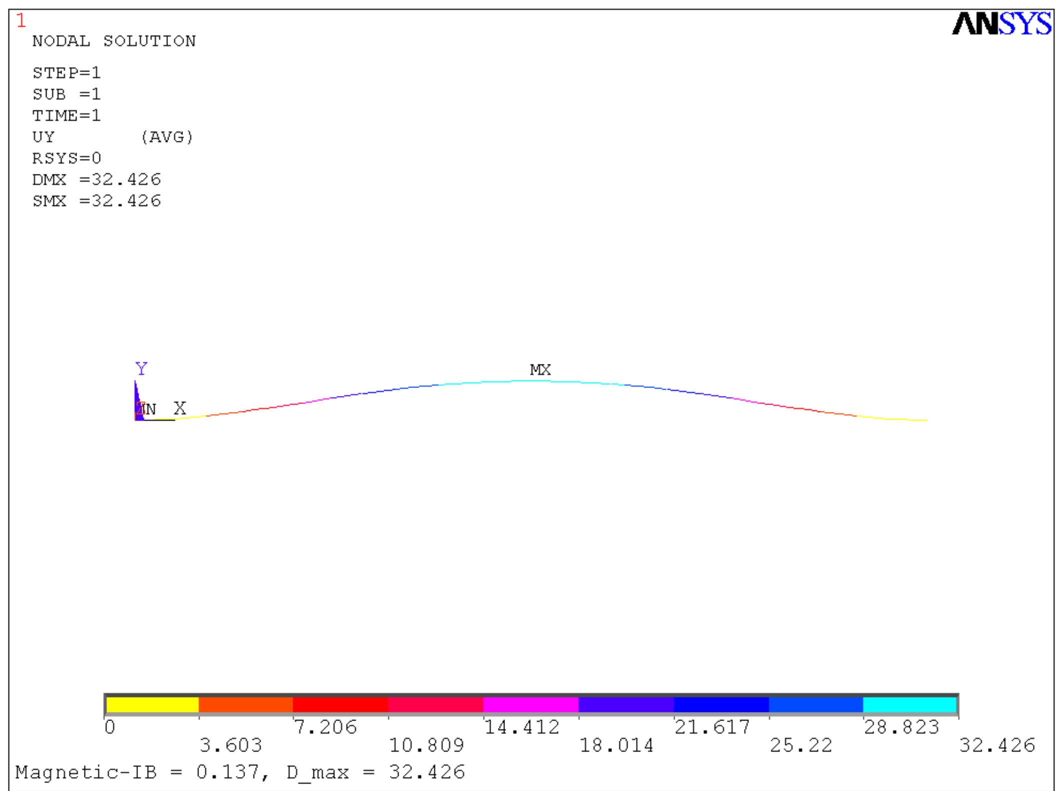

Figure 8.4: Microbridge Actuated by an Electromagnet Pressure, $IB = -0.137\ \frac{\mu N}{\mu m}$

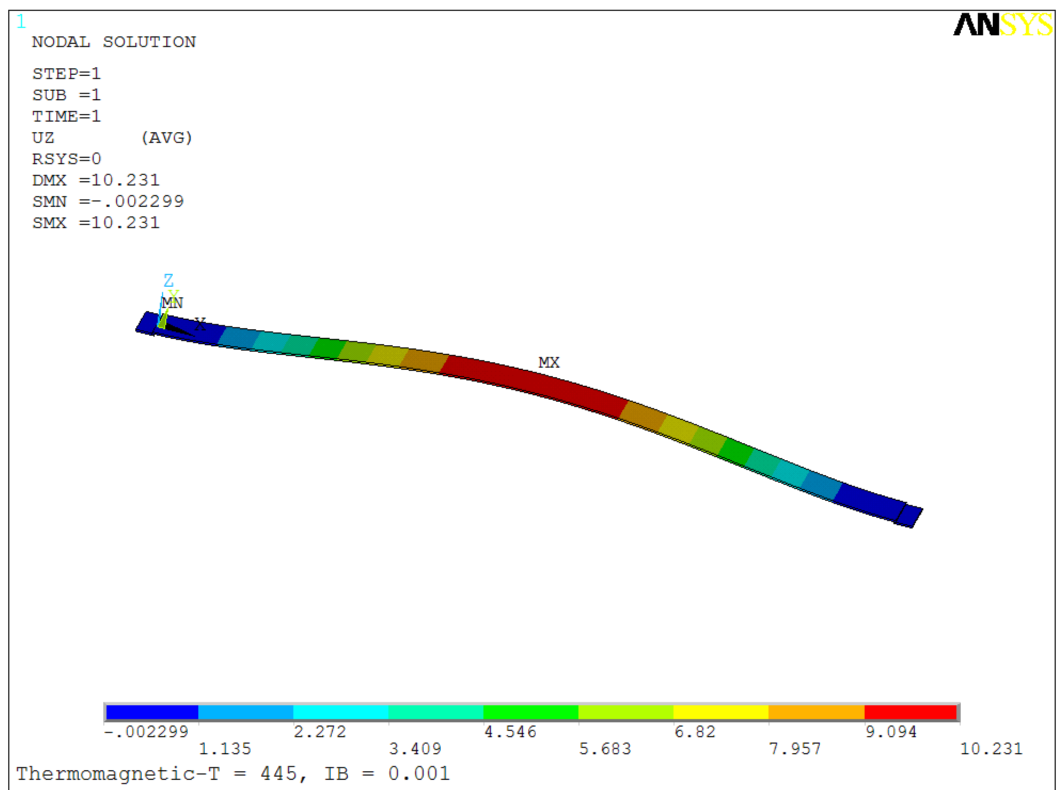

Figure 8.5: Thermomagnetical Actuation at $T_{max} = 445\ ^{\circ}K$ and $IB = 0.001\ \frac{\mu N}{\mu m}$

conditions as the ones shown in figure 8.5. However, the effect of lateral magnetic pressure on the microbridge in figure 8.6 is removed. The maximum displacement is $D = 0.734\ \mu m$, the applied voltage is $V = 2.0\ Volts$, and the temperature is $T = 445\ ^{\circ}K$.

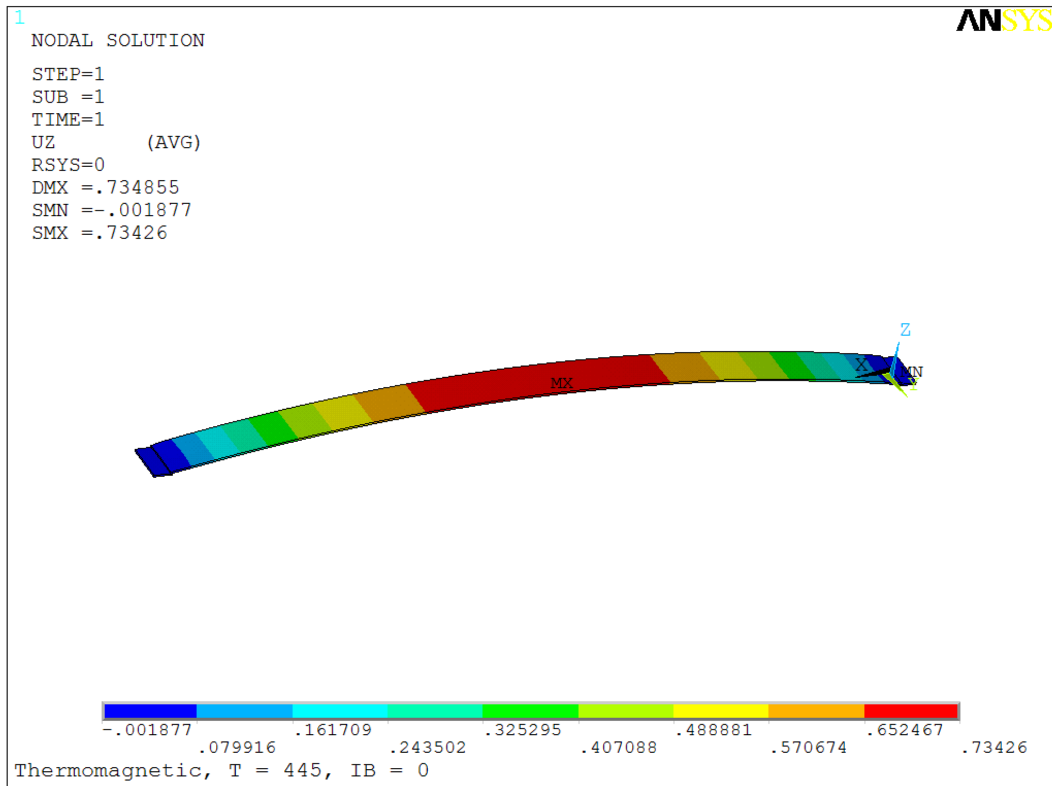

Figure 8.6: Electrothermally Actuated Microbridge at ($T_{max} = 445\ ^{\circ}K$)

8.4 Discussion

The computed critical load in equation 8.7 is significantly smaller than the allowable load calculated in equation 8.2. Therefore, this dramatic difference allows the microbridge to buckle without any concern that the induced stress may cause permanent deformation or fracture, as far as the induced stress remains below the allowable stress. Furthermore, table 8.1 displays that even at the the maximum allowable temperature of $750\ ^{\circ}C$ ($\approx 1050\ ^{\circ}K$), the maximum load is $16704\ \mu Newton$, which

is still appreciably smaller than the maximum allowable load of 56470 $\mu Newton$ computed in equation 8.2. This result confirms the acceptable operation for the microbridge as an actuating element even when it is used at the highest allowed temperature beyond which plasticity and permanent deformation of the microbridge may occur.

For a rough evaluation, the performance-related parameters of a typical bimorph microactuator shown in figure 8.7, which is a very well known microactuator in MEMS applications, are compared with the above outlined results for the proposed technique, METMA, which uses a microbridge as the actuating element. Such a typical bimorph thermal microactuator is presented and simulated by ANSYS in "ANSYS Tutorial," which has the following specifications: force output, 36 $\mu Newton$ at 936 $°C$ ($\approx$ 1236 $°K$); 3.073 μm, displacement; volume $(275 \times 80 \times 2)$[1], $44,000.\ \mu m^3$; work/volume, 0.0025 $\frac{pJ}{\mu m^3}$. However, the simulations' results of the microbridge actuated by METMA proposed in this research have the following specifications:

- Electrothermal actuation
  Force output, 16,704. $\mu Newton$ at 750 $°C$ ($\approx$ 1050 $°K$); displacement, 2.234 μm; volume $(800 \times 40 \times 2)$, $64,000\ \mu m^3$.

- Electromagnetic actuation
  Force output, 110. $\mu Newton$; displacement, 32.5 μm; volume $(800 \times 40 \times 2)$, $64,000\ \mu m^3$; work/volume, 0.056 $\frac{pJ}{\mu m^3}$.

The significant capability of the proposed technique is partially reflected in the above comparison. Larger stroke-force, higher controllability, and several options for the system driving and operation for the same design and configuration are outstanding advantages of the proposed technique in this research. For example, comparing work/volume, which is a performance criterion, of the above-described bimorph microactuator with the electromagnetic actuated microbridge shows a 22 times higher performance for the electromagnetic actuated microbridge.

Equation 8.6 shows that, for example, a magnetic field of one Tesla on a ten milliamp electrical current in the microbeam creates a 2.5 *microns* displacement. This result shows that by applying an appreciable value of electrical current, the microactuator can produce its largest possible amplitude even in the presence of a relatively small magnetic field. This sensitivity to low magnetic field is an important

[1]The volume is computed by taking largest widths and length of the design and a same height of two microns for every microactuator, assuming the fabrication technology is PolyMUMPs and Poly1, 2. μm thickness, is used

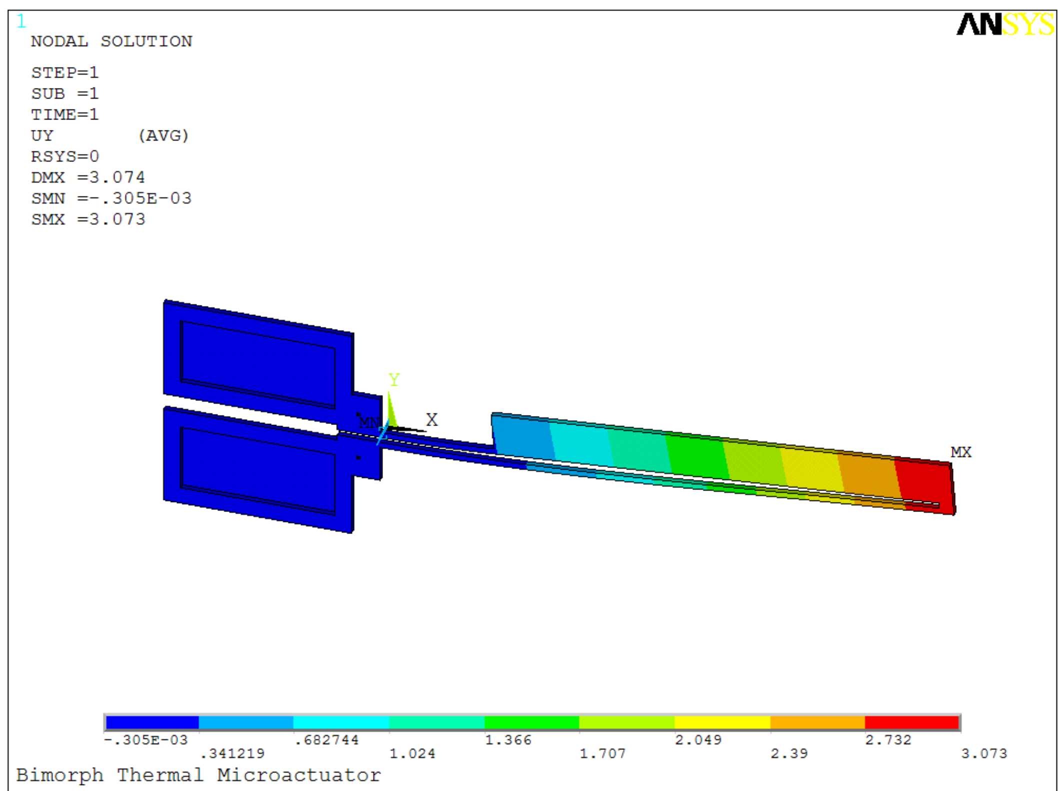

Figure 8.7: Bimorph Thermal Actuator at $T_{max} = 935.8\ °C$ (ANSYS Tutorial)

advantage of the proposed technique, METMA, for microactuation. In other words, applying powerful current pulses, which is introduced in Section 6.4, in the presence of even a weak magnetic field, can make the microactuator operative. Furthermore, the microactuator can also operate for sensing magnetic fields.

Figure 8.5 shows a simulation of the microbridge actuated electrothermomagnetically. In this electromagnetically actuated microbridge, both thermal effects by an applied electrical current and lateral magnetic pressure by an external magnetic field are present. The temperature increase is equal to 445 $^{\circ}K$, and the maximum displacement is equal to 10.231 μm. However, in figure 8.6, the microbridge is subjected to the exact same conditions as shown in figure 8.5, but the effect of lateral magnetic pressure is removed. The maximum displacement is $D = 0.734\ \mu m$, the applied voltage is $V = 2.0\ Volts$, and the temperature is $T = 445\ ^{\circ}K$. These results from the simulations demonstrate the interesting potentials of thermomagnetic microactuation. The significant decrease in the displacement of the bucking microbridge (from $D = 10.231\ \mu m$ to $D = 0.734\ \mu m$), because of removing lateral magnetic pressure, shows the huge sensitivity of this chosen microactuating element to lateral pressure. In fact, lateral pressure on a thermally actuated microbridge dramatically changes the buckling conditions. These conditions include the critical values of temperature and load.

However, a fabricated microbridge is not usually the ideal elastic structure assumed in some analytical computations or simulations. Similar to most other real-fabricated structures, the microbridge can be affected by structural imperfections or nonlinearities produced in the fabrication process. The residual stress alone can cause a significant deviation between experimental results and analytical solutions/simulation results. For example, the predicted eigenvalue buckling strength in a microbridge can be significantly different from the one in an actual fabricated sample because of either residual stress or the end conditions of the microbridge. In fact, the fabricated ends of a microbridge that are developed in PolyMUMPs, for example, facilitate buckling appreciably because of the required design rules and the effects of the lower layer(s) on shaping or deforming upper layer(s).

8.5 Summary

Analytical calculations, simulations, and discussion of the results of this research give a measure of the accuracy of the different steps in the whole approach. Computed critical values in the above sections provide some important design parameters. It is shown that a buckling microbridge can be employed as a microactuating

element. It is further proved that there is significant potential in the proposed microactuating method, METMA, for developing highly controllable and large stroke-force microactuators. The work needed for continuation of this achievement is the outcome of these analytical solutions and simulations. In fact, the above reported computations and simulations give a quantitative as well as a qualitative evaluation of the work. Selected parts of the formulations are used to derive numbers that represent the behavior of the buckling microbridge.

Chapter 9

Conclusions and Future Works

9.1 Introduction

This chapter provides a brief review of the content of the whole thesis. The contributions from this work, limitations of the applied methods, and future plans are outlined. Chapter 1 provides a general view of this work by illuminating the background, motivation, research objectives, and contributions. Chapter 2 highlights the background of the work and illustrates the more relevant prior research. Referenced literature enables readers to better identify the position and the value of the present work. The references also facilitate further investigations. In Chapter 3, readers' attention is drawn to a very crucial issue in microactuation: the way physical phenomena are scaled dramatically differs from the way the dimensions-geometrical sizes of a system are scaled, and also differs from one physical phenomenon to another one in the same scaled system. The emphasis is on the fact that scaling laws are the tools that allow researchers or designers of microactuating systems to predict a system's behavior when the dimensions of the system are scaled down.

Chapter 4 develops an analysis to formulate the temperature distribution over a microbridge. The derived relationship for temperature distribution is inserted in the extended Hooks' law, Duhamel-Neumann equation in Chapter 5, resulting in a model for thermoelastic behavior of a microbridge. For a given input electrical current in the microbridge, the model of the temperature distribution gives a prediction of the elastic behavior of the microbridge. This prediction includes buckling temperature, buckling load, and the maximum deflection. In Chapter 6, actuation of a microbridge carrying electrical current under the effect of an external magnetic

field is modeled. The effect of the magnetic force is formulated as a lateral pressure and proved to be independent of the shape of the microbridge. The microbridge's maximum deflection is computed from the derived magnetoelastic equation. Driving magnetically actuated microactuators by powerful current pulses is a proposed technique with appreciable advantages described in Chapter 6. In Chapter 7, an integrated method of thermal and magnetic microactuation, METMA, is introduced and discussed. The technique is proposed to overcome limitations of either thermal or magnetic microactuation and integrate the capabilities that are present in both methods. Chapter 8 is a report of the analytical computations, simulations, and discussions on the results.

9.2 Contributions

The contributions of this thesis are briefly highlighted in Chapter 1. Here, the most significant contributions are listed based on novelty, uniqueness, and utility of the achievements:

- Proposes a technique to use out-of-plane buckling of a fixed-fixed microbeam as the actuating element being driven electrothermomagnetically
- Initiates and introduces a new series of highly controllable and large force-stroke microactuators by using the proposed microactuating technique, METMA, and microbridges as the actuating elements: single-degree-of-freedom linear microactuators, in-plane and out-of-plane; two-degree-of-freedom linear microactuators, in-plane and out-of-plane; bidirectional, multi-turn, and high torque micromotors
- Introduces a design for a two-layer fixed-fixed microbeam as an actuating element to produce larger stroke-force in comparison to the single fixed-fixed microbeam
- Introduces a unique electrical driving method for generating large force-torque peaks in magnetic and thermomagnetic microactuation by applying powerful current pulses
- Presents electrothermal, thermoelastic, electromagnetic, electrothermomagnetic analysis, and modeling of the proposed microactuation technique; simulation in ANSYS of the introduced technique actuated electrothermally, electromagnetically and electrothermomagnetically

- Effectively applies dimensional analysis in deriving scaling laws, illuminating the aspects of the involved physical effects, which includes highlighting favorable scaled features in magnetic microactuation
  Develops scaling laws on magnetic microactuation showing proper conditions for optimized application of magnetic techniques. This work creates more interest for researchers to adopt the advantages of magnetic microactuation including low voltage driving and higher output forces in comparison with electrostatic methods

- Recognizes mistakes in ANSYS tutorials that need correction
  In ANSYS tutorials, an example of a Bimorph thermal microactuator as a typical problem in the analysis of microelectromechanical systems is described. There are two important mistakes that need correction:

  1. The operating principle of a bimorph actuator is explained. In this explanation, the author has mentioned that the bimorph microactuator's function is the result of the current in the thinner arm being greater than the one in the longer arm. This explanation is wrong. The bimorph microactuator works because the thinner arm has higher resistance than the thicker arm. However, the currents in the two arms, which make two resistors in series, are the same.
  2. In the analysis, the constant value that has been considered as the thermal conductivity of polysilicon is given equal to 150 $(W/m.K)$. However, this value is the thermal conductivity of a single-crystal silicon and not the thermal conductivity of polysilicon. The suggested average value for polysilicon is 32 $(W/m.K)$, which is approximately five times less than the given value in the ANSYS tutorial [50].

- Recognizes that there is a challenge in describing the analysis in heat transfer by conduction in a microbridge
  Masterangelo in his PhD thesis applies a one-dimensional steady-state heat transfer model to represent a fabricated microbridge [50]. A layer of Nitride, chosen for its low thermal conductivity, is used as a thermal insulator to cover a microbridge. He assumes that conduction is the dominant mode of heat transfer. This assumption is justified because of the existing thermal insulating/isolation layer. However, some researchers who have referred to Masterangelo's work have used the same model, although their described microbeams do not have such a thermal insulating layer [77], [58], [56], [57], [78]. In addition, in his analysis and modeling thermal transfer by conduction in the

microbridge, as explained in Section 4.3, Masterangelo has taken the heat conducting area to be equal to the cross section of the microbridge [50]. However, the heat-conducting area in the microbeam must be taken to be twice that of the beam cross-section because the maximum temperature at the mid point of the microbeam results in heat conduction from the midpoint toward the two ends. Therefore, the integrals' limits must be between the minimum and the maximum temperatures and over half of the length of the microbridge that is experiencing these two temperature extremes. Masterangelo's work has been referenced by some other researchers following the same assumption that the heat conducting area is equal to the beam's cross section (Lin et al. [59], [58], [57], Wang [56], Motamedi [60], Amarendra Atre [61]). By assuming that the heat conducting area is equal to the beam cross section rather than twice the microbridge's cross section, the computed value for heat conduction can still result in a correct value if the integral is over the whole length of the microbridge rather than half of its length. However, the assumed heat conducting area in the microbeam equal to the cross section of the microbeam does not seem to be correct because the midpoint has the highest temperature and the end points are kept at the substrate temperature, which dictates the heat flow from the microbridge's midpoint toward both ends at the same time. Therefore, the correct modeling must take double the microbridge's cross-section as the actual heat conducting area.

9.3 The Limitations in this Research

The limitations in this research are recognized in three categories: the proposed microactuating technique, METMA; the investigating methods; the accuracy of the results. The research has been affected by all these factors, which are described briefly.

1. Limitations in the Proposed Microactuating Technique, METMA

    - The method of using METMA proposed in this research requires an external magnetic field. There are many applications in which no limitation exists for incorporating an external magnetic field, an electro-optical switch, for example. However, there are also applications in which limited space exists for incorporating a macroscale external magnetic field. Furthermore, some applications do require a more compact integrated unit of microactuation. Therefore, the proposed way of using METMA

is limited for such applications unless an integrated microscale external magnetic field is incorporated in the designs of METMA.

2. Limitations in the Investigating Methods

   - As in any other research on microactuating techniques, research and development of a microactuator is greatly limited by fabrication technologies.
   - The microfabrication technologies in which polysilicon is used as the structural layer are limited for the fabrication of microactuators that are operating based on the material thermal expansion. The technologies in which metal is the structural material are more appropriate because of the larger thermal expansion coefficient; Nickel's, for example, is about five times more than that of polysilicon.
   - A problem with the design and manufacture of most microactuators, including METMA types, is the electrically biased moving tip of the microactuator. The electrically biased moving tip of a microactuator is not limited to thermal microactuators. Even an electrostatic microactuator, for example, has an electrically biased moving component. The electrically biased tip of the moving component limits the design and development of more than a single degree of freedom microactuator. One solution is in using fabrication technologies that provide extra electrical insulating layers for the moving components.
   - Measuring in-plane displacement of a microstructure in the range of microns is achievable. In comparison, measuring an out-of-plane displacement of a buckling microbridge experimentally is more complicated.
   - Access to appropriate microfabrication equipment could dramatically facilitate design and development of microactuators, especially in a research environment. However, the fabrications run by third parties, CMC, for example, with considerable delay between runs and time-consuming responses, cause a significant overall delay in optimizing designs and advancing research.

3. Limitations in the Accuracy of the Results

   - The significant number of temperature and process dependent parameters that are effective in a microactuator's behavior would suggest that experiments are needed to adjust the developed mathematical models. Therefore, insufficient experiments might cause unexplained deviations

between a mathematical model's predicted behavior for a microactuator and the actual functionality of a fabricated one.

- The results derived from simulations in ANSYS are largely depend on the researcher's skills and familiarity with this sophisticated software. The researcher requires significant skill and experience to effectively incorporate the determining parameters in the models. For example, adjusting the dimensions and geometry of a microbridge model in ANSYS in order for it to be the same as or close to the one that is actually fabricated is a challenging task. As another example, the residual stress, which is naturally inherent in microfabrication, can dramatically modify the buckling condition for a microbridge. Furthermore, it is not straightforward to deposit Poly1 or Poly2 in PolyMUMPs in order to fabricate a microbridge as exactly as the one that is expected in a mathematical model.

9.4 Future Work

The topics covered in this research demand further investigation.

1. Research on the proposed microactuating technique, METMA, should include the following experiments:
   - METMA-based designed microactuators must also be developed in a fabrication technology in which metal structural layers are available, such as MetalMUMPS.
   - Special experimental facilities are needed[1] to measure temperature distribution and out-of-plane buckling of the actuated microbridges.
2. The external magnetic field of a microactuator in METMA can be incorporated in the microstructure, resulting in compaction of the whole device as a microscale microactuation unit.
3. Work on optimizing the proposed microactuating technique could realize the maximum potential of METMA, for example, either increasing the thermal effect by increasing the current passing through the microbridge or increasing the intensity of the applied external magnetic field results in various microactuating options.

[1]Contactless temperature measurement of the microstructure is mentioned by Kovac [108], Serio et al. [109], and Holzer et al. [38].

4. Further investigation of scaling laws for thermomagnetic microactuation is called for. For example, in the case of magnet-magnet interaction, two different conditions are applicable in practical applications. In one of these conditions, the distance between two magnets is scaled, but in another, it is not. In addition, research on scaling laws is also needed to identify the most favorable microactuating techniques and the optimized conditions of their application in a more general extent.

5. Research on developing a thermomagnetic motor that is operated by a non-contacting actuation technique has been proposed for a microscale application, but it seems very practical for microactuation as well [110].

References

[1] Aaron A. Geisberger, Niladri Sarkar, Matthew Ellis, and George D. Skidmore. Electrothermal properties and modeling of polysilicon microthermal actuators. *Journal of Microelectromechanical Systems*, 12(4):513–523, 2003.

[2] K. Tuck, A. Jungen, A. Geisberger, M. Ellis, and G. Skidmore. A study of creep in polysilicon mems devices. *Journal of Engineering Materials and Technology, Transactions of the ASME*, 127(1):90–96, 2005.

[3] Ronald Paul Manginell. Polycrystalline-silicon microbridge combustible gas sensor, 1997. M3: 9813400; M1: Ph.D.

[4] Nilesh Dhananjaya mankame. Modeling of electro-thermal-compliant micromechanisms, 2000.

[5] Y. Okada and Y. Tokumaru. Precise determination of lattice parameter and thermal expansion coefficient of silicon between 300 and 1500k. *Journal of Applied Physics*, 56(2):314–20, 07/15 1984.

[6] John A. Pelesko and David H. Bernstein. *Modeling MEMS and NEMS*. Chapman and Hall/CRC, Boca Raton, Fla. ; London, 2003.

[7] Yong Zhu, Alberto Corigliano, and Horacio D. Espinosa. A thermal actuator for nanoscale in situ microscopy testing: Design and characterization. *Journal of Micromechanics and Microengineering*, 16(2):242–253, 2006.

[8] Clemens Mueller-Falcke, Yong-Ak Song, and Sang-Gook Kim. Tunable stiffness scanning microscope probe. In *Optomechatronic Micro/Nano Components, Devices, and Systems, Oct 27-28 2004*, volume 5604 of *Proceedings of SPIE - The International Society for Optical Engineering*, pages 31–37, Philadelphia, PA, United States, 2004. Micro and Nano Systems Laboratory, Department of Mechanical Engineering, Massachusetts Inst. of Technology,

Cambridge, MA 02139, United States, International Society for Optical Engineering, Bellingham, WA 98227-0010, United States.

[9] M. A. Haque and M. T. A. Saif. A review of mems-based microscale and nanoscale tensile and bending testing. *Proceedings of the Society for Experimental Mechanics, Inc*, 50:248–55, / 2003.

[10] W. S. N. Trimmer. Microrobots and micromechanical systems. *Sensors and Actuators*, 19(3):267–287, 1989.

[11] Marc J. Madou. *Fundamentals of microfabrication : the science of miniaturization*. CRC Press, Boca Raton, Fla. ; London, 2002.

[12] Mohamed Gad el Hak. *MEMS : introduction and fundamentals*. CRC Press/Taylor and Francis Group, Boca Raton, FL, 2006.

[13] Orphee Cugat, Jerome Delamare, and Gilbert Reyne. Magnetic microactuators and systems magmas. *IEEE Transactions on Magnetics*, 39(6):3607–3612, 2003.

[14] Orphec Cugat, Jerome Delamare, and Gilbert Reyne. Magnetic microactuators and systems (magmas). In *Intermag 2003: International Magnetics Conference, Mar 28-Apr 3 2003*, Digests of the Intermag Conference, page 04, Boston, MA, United States, 2003. Lab. d'Electrotechnique de Grenoble, INPG-CNRS, Grenoble, France, Institute of Electrical and Electronics Engineers Inc.

[15] Niladri Sarkar, University of Waterloo. Dept. of Electrical, and Computer Engineering. *MEMS actuation and self-assembly applied to RF and optical devices*. University of Waterloo, Waterloo, Ont., 2004.

[16] Tai-Ran Hsu. *MEMS and Microsystems Design and Manufacture*. McGraw-Hill, United States of America, 2002.

[17] 1948 Elwenspoek, M. (Miko) and 1964 Wiegerink, Remco J. *Mechanical microsensors*. Springer, Berlin ; New York, 2001.

[18] Chang Liu and Y. Bar-Cohen. Scaling laws of microactuators and potential applications of electroactive polymers in mems. *Proceedings of SPIE - The International Society for Optical Engineering*, 3669:345–354, 1999.

[19] Stephen Beeby. *MEMS mechanical sensors*. Artech House, Boston ; London, 2004.

[20] C. C. Lin and Lee A. Segel. *Mathematics applied to deterministic problems in the natural sciences*. Macmillan, New York, 1974.

[21] John F. Douglas. *An Introduction to Dimensional Analysis for Engineers,*. Pitman, London, 1969.

[22] R. C. Pankhurst. *Dimensional Analysis and Scale Factors*. Published on Behalf of the Institute of Physics and the Physical Society by Chapman and Hall, London, 1964.

[23] Edward de St. Quentin Isaacson and joint author Isaacson, M. de St. Quentin. *Dimensional methods in engineering and physics*. Edward Arnold, London, 1975.

[24] G. I. Barenblatt. *Dimensional analysis*. Gordon and Breach Science Publishers, New York, 1987.

[25] S. Deladi, G. Krijnen, and M. C. Elwenspoek. Parallel-beams/lever electrothermal out-of-plane actuator. *Microsystem Technologies*, 10(5):393–399, 2004. Compilation and indexing terms, Copyright 2006 Elsevier Inc. All rights reserved.

[26] W. Szyszkowski, D. Hill, and E. Bordatchev. On modeling and computer simulation of an electro-thermally driven cascaded nickel micro-actuator. *Sensors and Actuators A (Physical)*, 126(1):253–63, 01/26 2006.

[27] C. D. Lott, T. W. McLain, J. N. Harb, and L. L. Howell. Modeling the thermal behavior of a surface-micromachined linear-displacement thermomechanical microactuator. *Sensors and Actuators, A: Physical*, 101(1-2):239–250, 2002.

[28] Eniko T. Enikov, Shantanu S. Kedar, and Kalin V. Lazarov. Analytical model for analysis and design of v-shaped thermal microactuators. *Journal of Microelectromechanical Systems*, 14(4):788–798, 2005.

[29] B. Borovic, F. L. Lewis, D. Agonafer, E. S. Kolesar, M. M. Hossain, and D. O. Popa. Method for determining a dynamical state-space model for control of thermal mems devices. *Journal of Microelectromechanical Systems*, 14(5):961–70, 10/ 2005.

[30] Michael J. Sinclair. High force low area mems thermal actuator. *Thermomechanical Phenomena in Electronic Systems -Proceedings of the Intersociety Conference*, 1:127–132, 2000.

[31] Chi Hsiang Pan, Chia-Lung Chang, and Yi-Kun Chen. Design and fabrication of an electro-thermal microactuator with multidirectional in-plane motion. *Journal of Microlithography, Microfabrication, and Microsystems*, 4(3):33008–1, 07/ 2005.

[32] N. D. Mankame and G. K. Ananthasuresh. Comprehensive thermal modelling and characterization of an electro-thermal-compliant microactuator. *Journal of Micromechanics and Microengineering*, 11(5):452–462, 2001.

[33] R. W. Johnstone and M. Parameswaran. Modelling surface-micromachined electrothermal actuators. *Canadian Journal of Electrical and Computer Engineering*, 29(3):193–202, 2004.

[34] Z. Bai, D. Bindel, J. Clark, J. Demmel, K. S. J. Pister, and N. Zhou. New numerical techniques and tools in sugar for 3d mems simulation. In *2001 International Conference on Modeling and Simulation of Microsystems - MSM 2001, Mar 19-21 2001*, 2001 International Conference on Modeling and Simulation of Microsystems - MSM 2001, pages 31–34, Hilton Head Island, SC, United States, 2001. Department of Computer Science, University of California, Davis, CA, United States, Computational Publications, Cambridge, MA 02139, United States.

[35] D. Hill, W. Szyszkowski, and E. Bordatchev. On modeling and computer simulation of an electro-thermally driven cascaded nickel micro-actuator. *Sensors and Actuators, A: Physical*, 126(1):253–263, 2006.

[36] A. Michael, K. Yu, and C. Y. Kwok. Theoretical analysis of initially buckled, thermally actuated, and snapping bimorph micro bridge. In *Device and Process Technologies for MEMS, Microelectronics, and Photonics III, Dec 10-12 2003*, volume 5276 of *Proceedings of SPIE - The International Society for Optical Engineering*, pages 540–547, Perth, WA, Australia, 2004. Sch. of Elec./Telecom. Engineering, University of New South Wales, Sydney, NSW 2052, Australia, The International Society for Optical Engineering.

[37] Ilene Busch-Vishniac. Case for magnetically driven micro-actuators. In *Winter Annual Meeting of the American Society of Mechanical Engineers, Dec 1-6 1991*, volume 32 of *American Society of Mechanical Engineers, Dynamic Systems and Control Division (Publication) DSC*, pages 287–302, Atlanta, GA, USA, 1991. Univ of Texas, Austin, TX, USA, Publ by ASME, New York, NY, USA.

[38] Raphael Holzer, Isao Shimoyama, and Hirofumi Miura. Lorentz force actuation of flexible thin-film aluminum microstructures. In *Proceedings of the 1995 IEEE/RSJ International Conference on Intelligent Robots and Systems. Part 2 (of 3), Aug 5-9 1995*, volume 2 of *IEEE International Conference on Intelligent Robots and Systems*, pages 156–161, Pittsburgh, PA, USA, 1995. Univ of Tokyo, Tokyo, Jpn, IEEE, Piscataway, NJ, USA.

[39] Jong Soo Ko, Myung Lae Lee, Dae-Sik Lee, Chang Auck Choi, and Youn Tae Kim. Development and application of a laterally driven electromagnetic microactuator. *Applied Physics Letters*, 81(3):547–9, 07/15 2002.

[40] Jeong Sam Han, Jong Soo Ko, and Jan G. Korvink. Structural optimization of a large-displacement electromagnetic lorentz force microactuator for optical switching applications. *Journal of Micromechanics and Microengineering*, 14(11):1585–1596, 2004.

[41] Z. Nami, C. H. Ahn, and M. G. Allen. Energy-based design criterion for magnetic microactuators. *Journal of Micromechanics and Microengineering*, 6(3):337–344, 1996.

[42] Raanan A. Miller, Geoffrey W. Burr, Yu-Chong Tai, and Demetri Psaltis. Magnetically actuated mems scanning mirror. In *Miniaturized Systems with Micro-Optics and Micromechanics, Jan 30-31 96*, volume 2687 of *Proceedings of SPIE - The International Society for Optical Engineering*, pages 47–52, San Jose, CA, USA, 1996. California Inst. of Technology, Pasadena, CA, USA, Society of Photo-Optical Instrumentation Engineers, Bellingham, WA, USA.

[43] Yong Yi and Chang Liu. High-yield assembly of hinged 3-d optical mems devices using magnetic actuation. In *Micromachining and Microfabrication Process Technology IV, 21-22 Sept. 1998*, volume 3511 of *Proc. SPIE - Int. Soc. Opt. Eng. (USA)*, pages 125–34, Santa Clara, CA, USA, / 1998. Micro-Actuators, Sensors and Syst. Group, Illinois Univ., Urbana, IL, USA, SPIE-Int. Soc. Opt. Eng.

[44] J. W. Judy and R. S. Muller. Magnetically actuated, addressable microstructures. *Journal of Microelectromechanical Systems*, 6(3):249–56, 1997.

[45] J. W. Judy and R. S. Muller. Fabrication processes for magnetic microactuators with polysilicon flexures. In *Proceedings of the Fourth International Symposium on Magnetic Materials, Processes, and Devices. Applications to

Storage and Microelectromechanical Systems (MEMS), 9-12 Oct. 1995, Proceedings of the Fourth International Symposium on Magnetic Materials, Processes, and Devices. Applications to Storage and Microelectromechanical Systems (MEMS), pages 451–60, Chicago, IL, USA, / 1996. Dept. of Electr. Eng. and Comput. Sci., California Univ., Berkeley, CA, USA, Eletrochem. Sco.

[46] Yael Nemirovsky, I. Zelniker, Ofir Degani, and Gilaad Sarusi. A methodology and model for the pull-in parameters of magnetostatic actuators. *Journal of Microelectromechanical Systems*, 14(6):1253–1264, 2005. Compilation and indexing terms, Copyright 2006 Elsevier Inc. All rights reserved.

[47] H. Guckel, J. Klein, T. Christenson, K. Skrobis, M. Laudon, and E. G. Lovell. Thermo-magnetic metal flexure actuators. In *Proceedings of the 5th IEEE Solid-State Sensor and Actuator Workshop, Jun 22-25 1992*, pages 73–75, Hilton Head Island, SC, USA, 1992. Univ of Wisconsin, Madison, WI, USA, Publ by IEEE, Piscataway, NJ, USA.

[48] Andrew Cao, Jong Baeg Kim, Tony Tsao, and Lin Liwei. A bi-directional electrothermal electromagnetic actuator. In *17th IEEE International Conference on Micro Electro Mechanical Systems (MEMS): Maastricht MEMS 2004 Technical Digest, Jan 25-29 2004*, Proceedings of the IEEE International Conference on Micro Electro Mechanical Systems (MEMS), pages 450–453, Maastricht, Netherlands, 2004. Berkeley Sensor and Actuator Center, Department of Mechanical Engineering, University of California at Berkeley, Berkeley, CA 94720-1740, United States, Institute of Electrical and Electronics Engineers Inc., Piscataway, United States.

[49] B. Bahreyni and C. Shafai. A micromachined magnetometer with frequency modulation at the output. In *2005 IEEE Sensors, 30 Oct.-3 Nov. 2005*, 2005 IEEE Sensors (IEEE Cat. No.05CH37665C), page 4, Irvine, CA, USA, / 2005. Dept. of Electr. and Comput. Eng., Manitoba Univ., Winnipeg, Man., Canada, IEEE.

[50] Carlos Horacio Mastrangelo. Thermal applications of microbridges, 1991.

[51] Y. C. Tai, C. H. Mastrangelo, and R. S. Muller. Thermal conductivity of heavily doped lpcvd polysilicon. In *Technical Digest - International Electron Devices Meeting 1987.*, Technical Digest - International Electron Devices Meeting, pages 278–281, Washington, DC, USA, 1987. Univ of California, Berkeley, CA, USA, IEEE, New York, NY, USA.

[52] Carlos H. Mastrangelo, Yeh Hsi-Jen, and Richard S. Muller. Electrical and optical characterististics of vacuum-sealed polysilicon microlamps. *IEEE TRANSACTION ON ELECTRON DEVICES*, 39(6):1363–1375, 1992, June.

[53] Carlos H. Mastrangelo, Yu-Chong Tai, and Richard S. Muller. Thermophysical properties of low-residual stress, silicon-rich, lpcvd silicon nitride films. *Sensors and Actuators, A: Physical*, 23(1-3):856–860, 1990.

[54] Y. C. Tai, C. H. Mastrangelo, and R. S. Muller. Thermal conductivity of heavily doped low-pressure chemical vapor deposited polycrystalline silicon films. *Journal of Applied Physics*, 63(5):1442–7, 03/01 1988.

[55] Qing-An Huang, Yuxing Zhang, Ren-Gang Li, and Weihua Li. Macromodeling for polysilicon cascaded bent beam electrothermal microactuators. *Sensors and Actuators A (Physical)*, 128(1):165–75, 03/31 2006.

[56] Ming-Wen Wang. The experimental studies for micro thermal vapor film incipience on a micro wire. pages 1–6, June 3-5 2003.

[57] Liwei Lin and Mu Chiao. Electrothermal responses of lineshape microstructures. *Sensors and Actuators, A: Physical*, 55(1):35–41, 1996.

[58] Liwei Lin and Albert P. Pisano. Bubble forming on a micro line heater. In *Winter Annual Meeting of the American Society of Mechanical Engineers, Dec 1-6 1991*, volume 32 of *American Society of Mechanical Engineers, Dynamic Systems and Control Division (Publication) DSC*, pages 147–163, Atlanta, GA, USA, 1991. Univ of California, Berkeley, CA, USA, Publ by ASME, New York, NY, USA.

[59] Liwei Lin, Kent S. Udell, and Albert P. Pisano. Vapor bubble formation on a micro heater in confined and unconfined micro channels. In *29th National Heat Transfer Conference, Aug 8-11 1993*, volume 253 of *American Society of Mechanical Engineers, Heat Transfer Division, (Publication) HTD*, pages 85–93, Atlanta, GA, USA, 1993. Univ of California, Berkeley, Berkeley, CA, USA, Publ by ASME, New York, NY, USA.

[60] M. Edward Motamedi. *MOEMS : micro-opto-electro-mechanical systems*. SPIE Press, Bellingham, Wash., 2005.

[61] Amarendra Atre. Analysis of out-of-plane thermal microactuators. *Journal of Micromechanics and Microengineering*, 16(2):205–213, 2006.

[62] Stephen Timoshenko. *Strength of materials.* Van Nostrand 1947, New York, 1940.

[63] Stephen Timoshenko. *Theory of elastic stability.* McGraw-Hill book companyinc, New York and London, 1936.

[64] Stephen Timoshenko and Joint Author Gere, James M. *Mechanics of Materials.* New YorkVan Nostrand Reinhold Co, 1972.

[65] Chi teh Wang. *Applied elasticity.* McGraw-Hill, New York, 1953.

[66] James M. Gere. *Mechanics of materials.* Thomson, Toronto, 2006.

[67] Ferdinand Pierre Beer, E. Russell Johnston, and John T. DeWolf. *Mechanics of materials.* McGraw-Hill Higher Education, Boston, 2006.

[68] Raymond J. Roark and Warren C. Young. *Roark's formulas for stress and strain.* McGraw-Hill, New York ; Montreal, 1989.

[69] O. T. Bruhns. *Advanced mechanics of solids.* Springer, Berlin ; New York, 2003.

[70] John W. Brewer. *Engineering analysis in applied mechanics.* Taylor and Francis, New York, NY, 2002.

[71] B. A. Samuel, A. V. Desai, and M. A. Haque. Design and modeling of a mems pico-newton loading/sensing device. *Sensors and Actuators, A: Physical*, 127(1):155–162, 2006.

[72] Harry Wilfred Reddick and Frederic H. Miller. *Advanced mathematics for engineers.* Wiley, New York, 1957.

[73] Wai-Fah Chen 1936-. *Theory of beam columns.* McGraw-Hill, New York, 1976-1977.

[74] 1940 Senturia, Stephen D. *Microsystem design.* Boston : Kluwer Academic Publishers, United States of America, 2001.

[75] Nicolae Lobontiu and Ephrahim Garcia. *Mechanics of Microelectromechanical Systems.* Kluwer Academic Publishers, United States of America, 2005.

[76] M. Ichiki, R. R. A. Syms, and I. R. Young. A micromechanical expanding coil mechanism for in vivo magnetic resonance imaging. *Journal of Micromechanics and Microengineering*, 15(4):771–777, 2005.

[77] Mu Chiao and Liwei Lin. Self-buckling of micromachined beams under resistive heating. *Journal of Microelectromechanical Systems*, 9(1):146–151, 2000.

[78] Liwei Lin and Mu Chiao. Electro, thermal and elastic characterizations of suspended micro beams. *Microelectronics Journal*, 29(4-5):269–276, 1998.

[79] Yogesh B. Gianchandani and Khalil Najafi. Bent-beam strain sensors. *Journal of Microelectromechanical Systems*, 5(1):52–58, 1996.

[80] Bruno A. Boley and Jerome Harris Weiner. *Theory of thermal stresses*. Wiley, New York, 1960.

[81] Y. C. Fung. *Foundations of solid mechanics*. Prentice-Hall, Englewood Cliffs, N.J., 1965.

[82] S. P. Timoshenko and J. N. Goodier. *Theory of elasticity*. McGraw-Hill, New York, 1970.

[83] Stephen Timoshenko. *Theory of elasticity*. McGraw-Hill, New York, 1951.

[84] Michael J. Sinclair and Kerwin Wang. Thermal actuator improvements: Tapering and folding. In *Smart Sensors, Actuators, and MEMS, May 19-21 2003*, volume 5116 I of *Proceedings of SPIE - The International Society for Optical Engineering*, pages 237–251, Maspalonas, Gran Canaria, Spain, 2003. Microsoft Research, Microsoft Corporation, Redmond, WA 98052-6399125, United States, The International Society for Optical Engineering.

[85] Emre Ozlu, Jiang Zhe, Santanu Chandra, Jin Cheng, and Xingtao Wu. Feasibility study of a smart motion generator utilizing electromagnetic microactuator arrays. *Smart Materials and Structures*, 15(3):859–868, 2006. Compilation and indexing terms, Copyright 2006 Elsevier Inc. All rights reserved.

[86] Munir H. Nayfeh and Morton K. Brussel. *Electricity and Magnetism*. John Willey and Sons, New York; Toronto, 1985.

[87] Matthew N. O. Sadiku. *Elements of electromagnetics*. Oxford University Press, New York ; Oxford, 2001.

[88] Herbert Christopher Roters. *Electromagnetic devices*. J. Wiley and sonsinc.; LondonChapman and Hall limited 1955, New York, 1941.

[89] Malcolm McCaig and Alan G. Clegg. *Permanent magnets in theory and practice.* -. Pentech, London, 1987.

[90] Mohamed Gad el Hak. *The MEMS handbook.* CRC Press, Boca Raton, FL, 2002.

[91] O. Madelung. *Semiconductors : data handbook.* Springer, Berlin ; New York, 2004.

[92] Polymumps design handbook.

[93] Frank P. Incropera and David P. DeWitt. *Introduction to heat transfer.* Wiley, New York, 1996.

[94] Nikolai Valerianovich TSederberg. *Thermal conductivity of gases and liquids. Translation.* M.I.T. Press, Cambridge, 1965.

[95] M. Necati zisik. *Basic heat transfer.* McGraw-Hill, New York, 1977.

[96] David A. LaVan and Thomas E. Buchheit. Strength of polysilicon for mems devices. *Proceedings of SPIE - The International Society for Optical Engineering*, 3880:40–44, 1999.

[97] Brian H. Stark. Thin film technologies for hermetic and vacuum packaging of mems, 2004. M3: 3122050; M1: Ph.D.

[98] William N. Jr Sharpe, Bin Yuan, Ranji Vaidyanathan, and Richard L. Edwards. Measurements of young's modulus, poisson's ratio, and tensile strength of polysilicon. In *Proceedings of the 1997 10th Annual International Workshop on Micro Electro Mechanical Systems, MEMS, Jan 26-30 1997*, Proceedings of the IEEE Micro Electro Mechanical Systems (MEMS), pages 424–429, Nagoya, Jpn, 1997. Johns Hopkins Univ, Baltimore, MD, USA, IEEE, Piscataway, NJ, USA. Compilation and indexing terms, Copyright 2006 Elsevier Inc. All rights reserved.

[99] W. N. Sharpe Jr and J. Bagdahn. Fatigue testing of polysilicon-a review. *Mechanics of Materials*, 36(1-2):3–11, 01/ 2004.

[100] Bin Yuan. Mechanical testing of microsamples from weldments and mems materials, 1997.

[101] W. N. Sharpe Jr, R. Vaidyanathan, Yuan Bin, Bao Gang, and R. L. Edwards. Effect of etch holes on the mechanical properties of polysilicon. *Journal of Vacuum Science and Technology B (Microelectronics and Nanometer Structures)*, 15(5):1599–603, 1997.

[102] W. N. Sharpe Jr., J. Bagdahn, K. Jackson, and G. Coles. Tensile testing of mems materials-recent progress. *Journal of Materials Science*, 38(20):4075–4079, 2003. Compilation and indexing terms, Copyright 2006 Elsevier Inc. All rights reserved.

[103] George C. Rybicki and P. Pirouz. Indentation plasticity and fracture in silicon. Technical report, Nasa Lewis Research Cent, 1988. Compilation and indexing terms, Copyright 2006 Elsevier Inc. All rights reserved.

[104] S. Molokov and J. E. Allen. Fragmentation of wires carrying electric current. *Journal of Physics D: Applied Physics*, 30(22):3131–3141, 1997.

[105] W. N. Jr Sharpe, Bin Yuan, and R. L. Edwards. New technique for measuring the mechanical properties of thin films. *Journal of Microelectromechanical Systems*, 6(3):193–199, 1997. Compilation and indexing terms, Copyright 2006 Elsevier Inc. All rights reserved.

[106] K. Mackay, M. Bonfim, D. Givord, and A. Fontaine. 50 t pulsed magnetic fields in microcoils. *Journal of Applied Physics*, 87(4):1996–2002, 2000. Compilation and indexing terms, Copyright 2006 Elsevier Inc. All rights reserved.

[107] Saeed Moaveni. *Finite element analysis : theory and application with ANSYS*. Prentice Hall, Upper Saddle River, N.J., 1999.

[108] Gregory T. A. Kovacs. *Micromachined transducers sourcebook*. WCB-McGraw-Hill, Boston ; London, 1998.

[109] B. Serio, J. J. Hunsinger, F. Conseil, P. Derderian, D. Collard, L. Buchaillot, and M. F. Ravat. Close infrared thermography using an intensified ccd camera: Application in nondestructive high resolution evaluation of electrothermally actuated mems. In *Optical Measurement Systems for Industrial Inspection IV, Jun 13-17 2005*, volume 5856 PART II of *Proceedings of SPIE - The International Society for Optical Engineering*, pages 819–829, Munich, Germany, 2005. FEMTO-ST, CNRS UMR 6174, LPMO Department, 25044 Besancon Cedex, France, International Society for Optical Engineering, Bellingham WA, WA 98227-0010, United States.

[110] Takashi Kenjo. *Electric motors and their controls, an introduction*. Oxford ; Toronto : Oxford University Press, 1991.

Appendix A

A.1 Derivation of Heat Equation Discussed in Section 4.2

Outlined in section 4.1, the heat equation is derived by applying conservation laws of energy and principles of heat transfer. At a fixed point of time, the thermal energy per unit volume of an arbitrary control volume along the length of a fixed-fixed beam, $\Delta V = wz\Delta x$, 4.4, is $\rho_m cT$ [6]. The change of energy is equal to

$$\frac{dQ_{Total}}{dt} = \frac{d}{dt}\int_V \rho_m cTdV \Rightarrow \text{Flux through surface} - \int_S \vec{Q}\,.ndS \tag{A.1}$$

$$\frac{d}{dt}\int_V \rho_m cTdV = -\int_S \vec{Q}\,.ndS \tag{A.2}$$

From Divergence theorem $\Rightarrow$

$$\frac{d}{dt}\int_V \rho_m cTdV = -\int_V \nabla.\vec{Q}\,dV \tag{A.3}$$

By exchanging the order of integration and differentiation on the above left $\Rightarrow$

$$\int_V (\rho_m c\frac{\partial T}{\partial t} + \nabla.\vec{Q})dV = 0 \tag{A.4}$$

The integrand must be zero because the volume was chosen arbitrarily $\Rightarrow$

$$\Rightarrow \rho_m c\frac{\partial T}{\partial t} + \nabla.\vec{Q} = 0 \tag{A.5}$$

By assuming that the heat flux is proportional to the temperature gradient $\Rightarrow$

$$\vec{Q} = -k\nabla T \Rightarrow \rho_m c\frac{\partial T}{\partial t} = \nabla.k\nabla T \tag{A.6}$$

A.2 Designs of Microactuators without a Buckling Microbridge as the Actuating Element

Figure A.1 shows a design of a bi-directional limited-angle rotating actuator for micromirror positioning. This design is developed to be fabricated by EFAB technology[1].

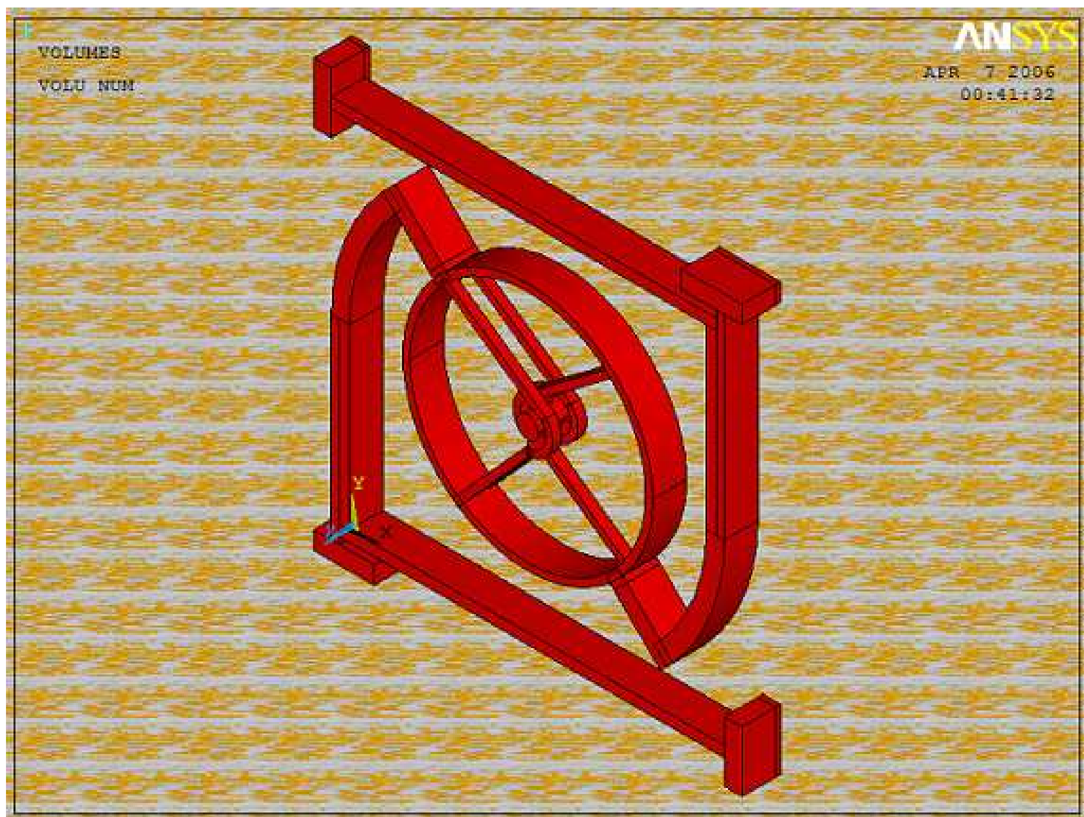

Figure A.1: Limited-Angle Rotating Actuator, ±45°, by EFAB Technology

[1]EFAB is a microstructure fabrication technology developed and employed by Microfabrica. EFAB is a twenty-layer fabrication technology with a maximum thickness of 140. microns. The technology has some unique capabilities for microactuator design: greater thickness, considerable number of layers, and independent layer formation, for example.

A.3 A Typical PolyMUMPs Fabrication Process

In a PolyMUMPs fabrication Process, seven successive layers are deposited, patterned, and etched. An example of a fabrication process in PolyMUMPs is demonstrated as follows. Figure A.7 shows part of a design of a microactuator for which the PolyMUMPs fabrication process and side views are outlined. This fabrication process is accomplished in 21 steps beginning with the substrate and continuing with the following steps: one Nitride layer, three structural layers (Poly0, Poly1, and Poly2), two sacrificial layers, and one metal layer. These layers are deposited and processed with the specific masks. However, there are some intermediate steps that are implemented regardless of the pattern or design. Deposits of 200.0 nm Oxide layers above polysilicon layers, for example, are done for two reasons: to increase the masks' strength and better consequent patterning/etching and to improve the electrical property of the polysilicon.

The twenty-one steps of the process are as follows, and ilustrated in figures, A.2, A.3, A.4, A.5, and A.6.

1. Step one: Wafer
2. Step Two: Deposit Nitride
3. Step Three: Deposit Polysilicon
4. Step Four: Etch Polysilicon
5. Step Five: Etch Polysilicon (Hole 0)
6. Step Six: Deposit Oxide
7. Step Seven: Etch Dimple
8. Step Eight: Etch Anchor 1
9. Step Nine: Deposit Polysilicon
10. Step Ten: Etch Polysilicon
11. Step Eleven: Etch Polysilicon (Hole 1)
12. Step Twelve: Deposit Oxide
13. Step Thirteen: Etch Poly1-Poly2-Via
14. Step Fourteen: Etch Anchor 2
15. Step Fifteen: Deposit Polysilicon
16. Step Sixteen: Etch Polysilicon
17. Step Seventeen: Etch Polysilicon (Hole 2)
18. Step Eighteen: Sputter Metal
19. Step Nineteen: Metal Liftoff
20. Step Twenty: Etch Hole Metal
21. Step Twenty-one: Sacrificial Etch

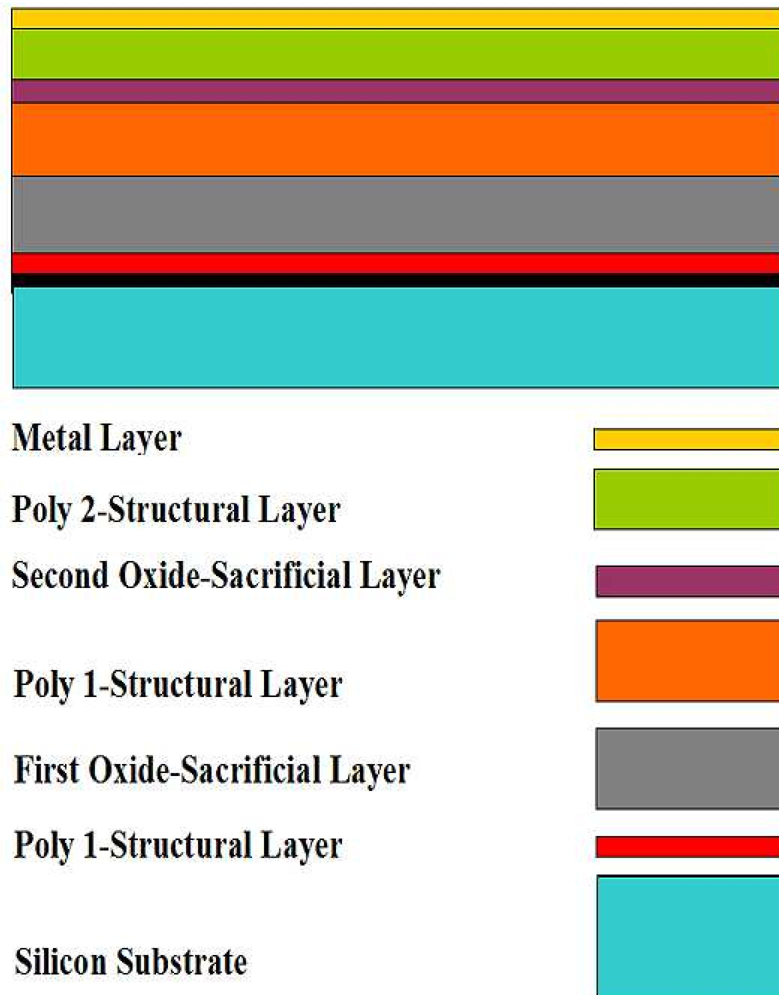

Figure A.2: PolyMUMPs Fabrication Process

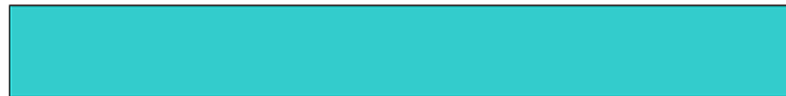

Step 1: Wafer

Step 2: Deposit Nitride

Step 3: Deposit Polysilicon

Step 4: Etch Polysilicon

Figure A.3: PolyMUMPs Fabrication Process, Step 1 to Step 4

Step 5: Deposit Oxide

Step 6: Deposit Polysilicon

Step 7: Etch Polysilicon

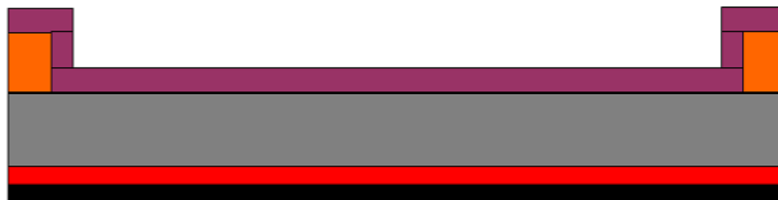

Step 8: Deposit Oxide

Figure A.4: PolyMUMPs Fabrication Process, Step 5 to Step 8

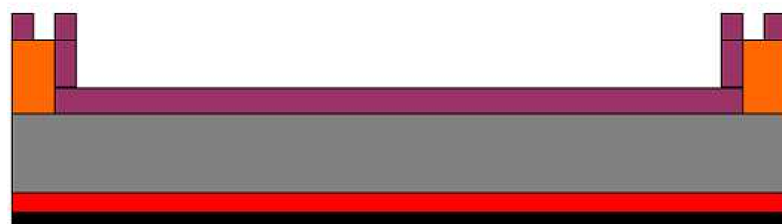

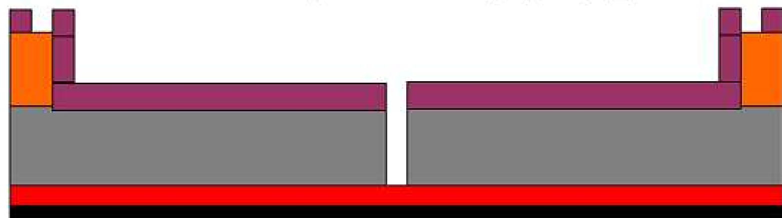

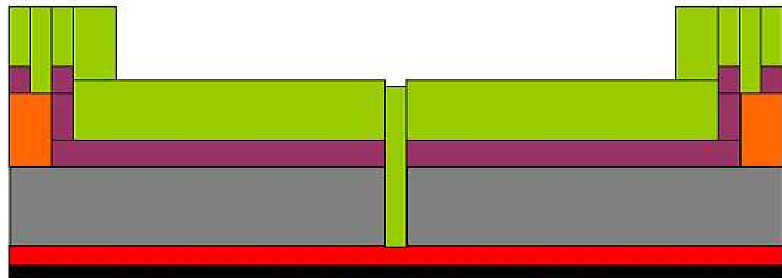

Figure A.5: PolyMUMPs Fabrication Process, Step 9 to Step 11

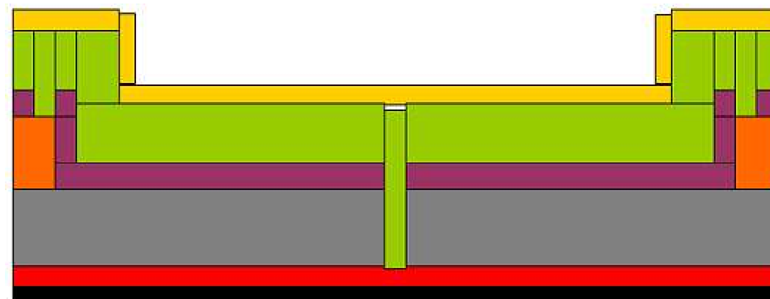

Step 12: Sputter Metal

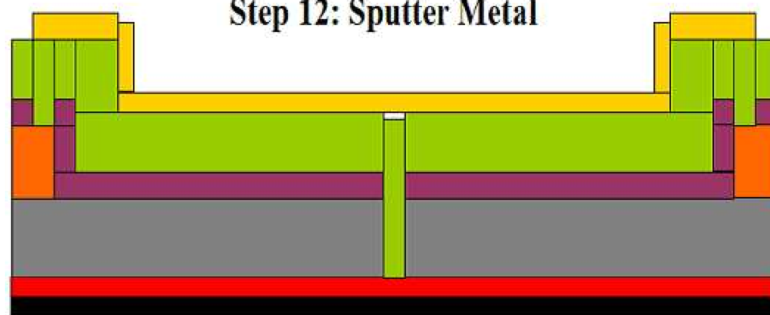

Step 13: Metal Liftoff

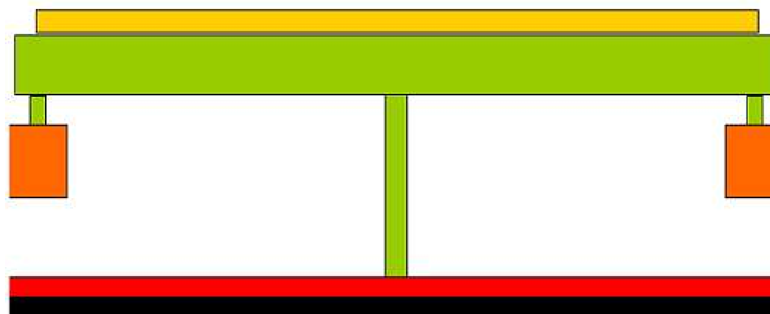

Step 14: Sacrificial etch

Figure A.6: PolyMUMPs Fabrication Process, Step 12 to Step 14

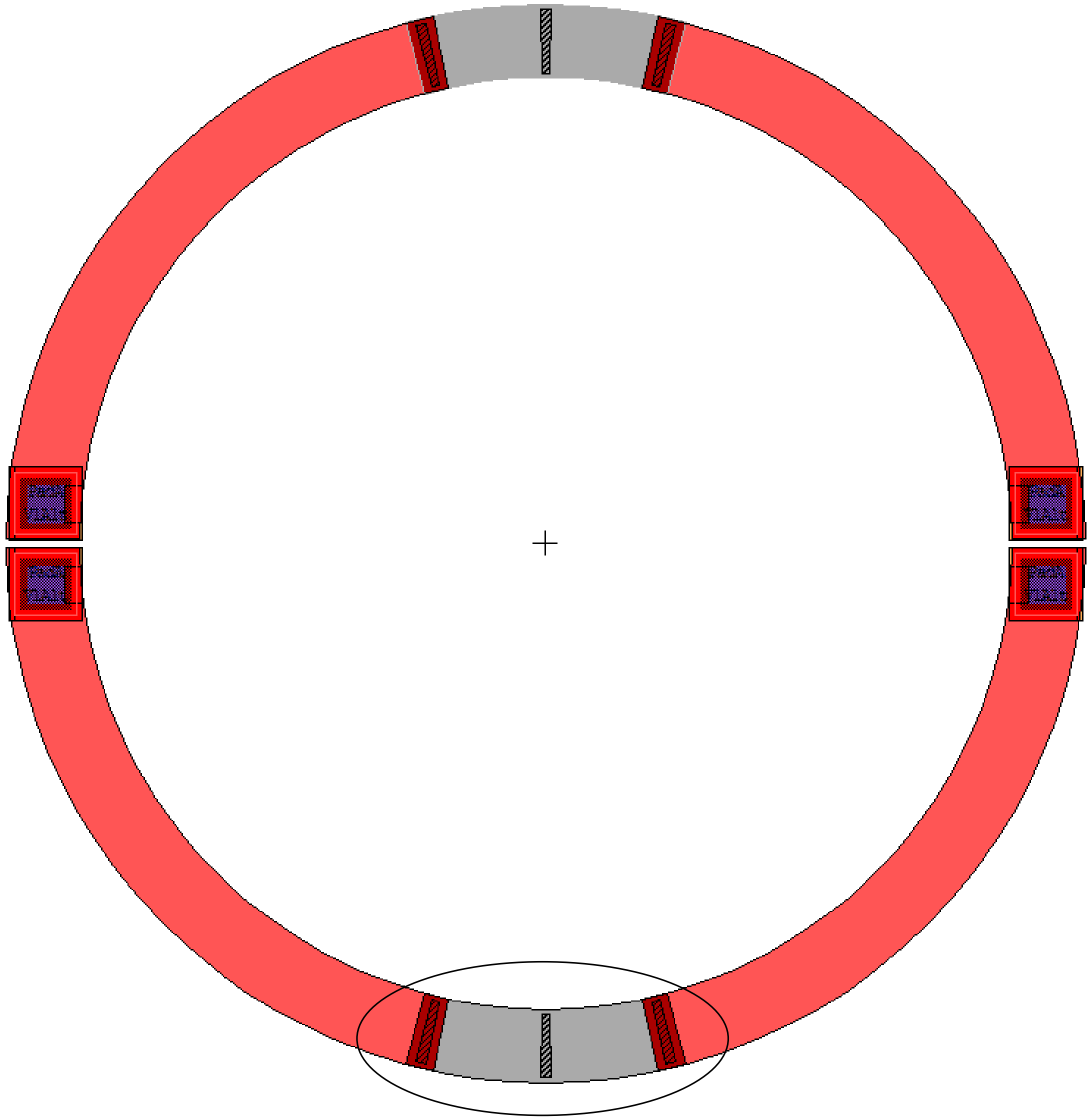

Figure A.7: Part of a Microactuator Design Used to Show the PolyMUMPs Fabrication Process Outlined in Figures, A.2, A.3, A.4, A.5, and A.6

Appendix B

B.1 Animated Simulations in ANSYS, Discussed in Section 8.2

If you accessed this thesis from a source other than the University of Waterloo, you may not have access to these files. You may access it by searching for this thesis at http://uwspace.uwaterloo.ca.

This Appendix includes "avi" files, animated simulations in ANSYS of buckling microbridges, which are actuated electrothermally, electromagnetically, and electrothermomagnetically. An animation of a bimorph thermal microactuator's simulation, which is taken from ANSYS tutorial, is also included for comparion[1].

1. Electrothermally actuated microbridge:
   - $TD2235T1049w.avi$
     Displacement (Applied voltage 2.1 ($Volts$); maximum deflection of 2.234 (μm); maximum temperature 1049 ($^{\circ}K$))
   - $TT1049D2235w.avi$
     Temperature distribution over the microbridge (Applied voltage 2.1 ($Volts$); maximum deflection of 2.234 (μm); maximum temperature 1049 ($^{\circ}K$))
   - $TDT850V1.8.avi$
     Displacement (Applied voltage 1.8 ($Volts$); maximum deflection of 1.877(μm); maximum temperature 850 ($^{\circ}K$))

[1] In this simulation, the microactuator, shown in figure 8.7, is driven to higher temperatures beyond 1200 ($^{\circ}K$), which is not advised based on the results in this research because polysilicon above 1050 ($^{\circ}K$) begin to experience plasticity and permanent deformation.

- $TDT682V1.5.avi$
  Displacement (Applied voltage 1.5 ($Volts$); maximum deflection of 1.574(μm); maximum temperature 682 ($^{\circ}K$))
- $TDT438V0.9.avi$
  Displacement (Applied voltage .9 ($Volts$); maximum deflection of 1.135(μm); maximum temperature 438 ($^{\circ}K$))

2. Electromagnetically actuated microbridge:

   - $MP0353w.avi$
     Displacement (Applied magnetic pressure $IB = 0.0353$ ($\frac{\mu N}{\mu m}$); maximum displacement, 8.355 (μm))
   - $MP0706w.avi$
     Displacement (Applied magnetic pressure $IB = 0.0706$ ($\frac{\mu N}{\mu m}$); maximum displacement, 16.71 (μm))
   - $MP137w.avi$
     Displacement (Applied magnetic pressure $IB = 0.137$ ($\frac{\mu N}{\mu m}$); maximum displacement, 32.426 (μm))

3. Electrothermomagnetically actuated microbridge:

   - $TMT445D1023w.avi$
     Temperature distribution (applied lateral pressure 0.001 ($\frac{\mu N}{\mu m}$); maximum deflection of 10.23 (μm); maximum temperature 445 ($^{\circ}K$))
   - $TMD1023T445w.avi$
     Displacement (applied lateral pressure 0.001 ($\frac{\mu N}{\mu m}$); maximum deflection of 10.23 (μm); maximum temperature 445 ($^{\circ}K$))
   - $TwoMT445D735w.avi$
     Temperature distribution (applied lateral pressure 0.0 ($\frac{\mu N}{\mu m}$); maximum deflection of 0.735 (μm); maximum temperature 445 ($^{\circ}K$))
   - $TwoMD735T445w.avi$
     Displacement (applied lateral pressure 0.0 ($\frac{\mu N}{\mu m}$); maximum deflection of 0.735 (μm); maximum temperature 445 ($^{\circ}K$))

4. Bimorph thermal microactuator, taken from ANSYS Tutorial for comparison:

   - *Bimorph.avi*
     Displacement (maximum deflection of 3.074 (μm); maximum temperature 1209 ($^{\circ}K$))